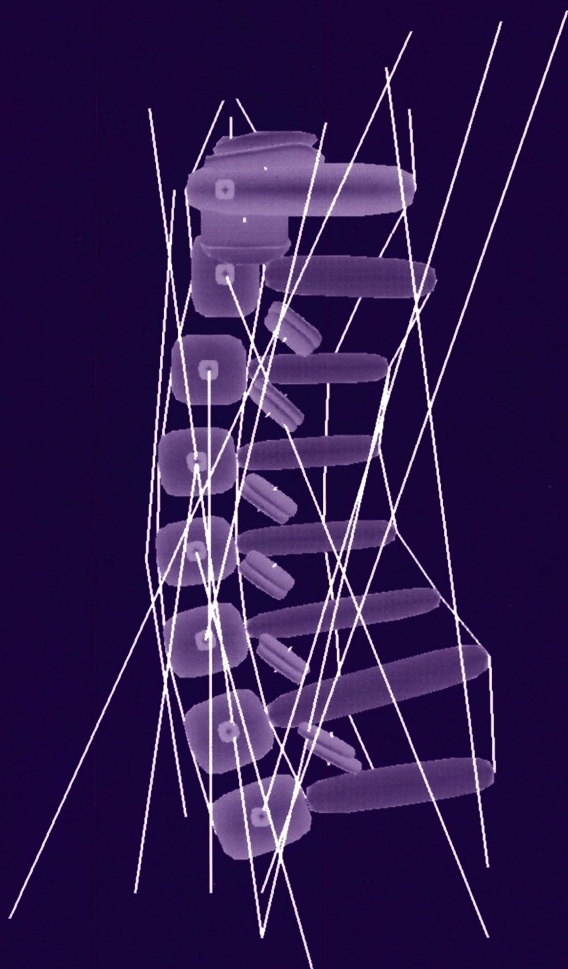# Mathematical Head-Neck Models for Acceleration Impacts

Marko de Jager

Mathematical Head-Neck Models

for Acceleration Impacts

Mathematical Head-Neck Models

for Acceleration Impacts

Proefschrift

ter verkrijging van de graad van doctor
aan de Technische Universiteit Eindhoven,
op gezag van de Rector Magnificus,
prof.dr. J.H. van Lint, voor een commissie
aangewezen door het College van Dekanen
in het openbaar te verdedigen op
donderdag 30 mei 1996 om 16.00 uur

door

Marinus Karel Johannes de Jager

geboren te Zwijndrecht

Dit proefschrift is goedgekeurd door de promotoren

prof.dr.ir. J.S.H.M. Wismans
en
prof.dr.ir. J.D. Janssen

en de copromotor

dr.ir. A.A.H.J. Sauren

Highway: Michigan

Here from the field's edge we survey
The progress of the jaded. Mile
On mile of traffic from the town
Rides by, for at the end of day
The time of workers is their own.

They jockey for position on
The strip reserved for passing only.
The drivers from production lines
Hold to advantage dearly won.
They toy with death and traffic fines.

Acceleration is their need:
A mania keeps them on the move
Until the toughest nerves are frayed.
They are the prisoners of speed
Who flee in what their hands have made.

The pavement smokes when two cars meet
And steel rips through conflicting steel.
We shiver at the siren's blast
One driver, pinned beneath the seat,
Escapes from the machine at last.

—Theodore Roethke

Voor Charlotte

Summary

The human neck is vulnerable. In car accidents, inertia forces of the head can load or deform the tissues of the neck beyond tolerable limits, resulting in injury. Most neck injuries are minor injuries (whiplash), but they may lead to long-lasting complaints. Severe neck injuries are disabling or fatal. Knowledge of the mechanisms through which loads cause injuries to the neck (injury mechanisms) is incomplete, especially for minor injuries, for which usually no clearly identifiable damage in the neck can be found. Mathematical modelling will aid to understand neck injury mechanisms better. The objective of this research is to develop a detailed three-dimensional mathematical model describing the dynamic behaviour of the human head and neck in accident situations without head contact. It was chosen to proceed from a relatively simple model, for gaining insight into head-neck dynamics, towards a more complex model, which includes sufficient details to assess the loads and deformations of the tissues of the neck. This thesis presents these models.

The anatomy, biomechanics and injury mechanisms of the human neck (or cervical spine) were reviewed. Emphasis was on the mechanical characteristics of the cervical spine and its tissues, which were compiled from the literature and used to construct the models. It appeared that sufficient data were available to create a model, even though the characteristics are incomplete, especially for dynamic loading.

First, a relatively simple model with few anatomical details was developed. This *global head-neck model* comprises a rigid head and rigid vertebrae, connected through three-dimensional nonlinear viscoelastic elements for the intervertebral joints. These joints describe the lumped mechanical behaviour of the intervertebral disc, ligaments and facet joints. Joint characteristics were derived from the behaviour of motion segments of the lower and upper cervical spine. Because these *in vitro* characteristics result in a too flexible model, the characteristics can be scaled to incorporate the stiffening effect of muscle tensioning on the neck, and to allow for calibration of the model response to impacts. The model was calibrated to match the response of human volunteers to frontal impacts and a reasonable agreement could be obtained. The linear and angular accelerations of the head and the neck rotation agreed satisfactorily, but head rotation was too large. This was ascribed to the too large rotation of the head relative to the neck due to the absence of active muscle behaviour. A parametric study was performed using a fractional factorial design to quantify the effect of parameter changes on the model response.

Second, detailed segment models of the upper and lower cervical spine were developed as an intermediate step. These models comprise rigid bodies for the vertebrae, three-dimensional linear viscoelastic elements for the intervertebral disc, nonlinear viscoelastic line elements for the ligaments, and frictionless contact interactions between almost rigid bodies for the facet joints. Models of lower cervical motion segments C3-C4 and C5-C6 were in good agreement with experiments for small loads (20 N, 1.8 Nm) and showed a similar response to large loads (500 N, 20 Nm) as the intervertebral joints of the global model. Their centres of rotation agreed favourably with experiments. The upper cervical spine model C0-C1-C2 showed smaller displacements than experiments for small loads (1.5 Nm) and larger displacements than the joints of the global model for larger loads (500 N, 15 Nm). The centres of rotation compared well with experiments. Parametric studies were performed with the C3-C4 and C0-C1-C2 models.

Finally, the *detailed head-neck model* was formed by joining the segment models and adding muscle elements. This model comprises a rigid head and rigid vertebrae, linear viscoelastic discs, frictionless facet joints, nonlinear viscoelastic ligaments and contractile Hill-type muscles. Human volunteer responses were used to validate the model. In the lateral impact, the model agreed excellently with the volunteers for the linear and angular accelerations of the head, the trajectories of the occipital condyles and centre of gravity of the head, and the lateral head rotation. Axial head rotation was too large as were the lateral rotations of the lowest intervertebral joints. In the frontal impact, the linear and angular head accelerations agreed reasonably with the volunteer responses, but head and neck rotation were too large. Rotation of the head relative to the neck, however, was accurately reflected due to muscle tensioning. The trajectories also reflected that the model was too flexible. This was mainly attributed to the incapability of the muscle elements to curve around the vertebrae: their straight lines of action became unrealistic for large neck rotations, such that the muscles failed to effectively constrain the head-neck motion and stiffen the joints. Further, the lowest joints appeared too flexible compared with the *in vivo* ranges of motion. Qualitatively, most joint rotations were described accurately, as reflected by their centres of rotation resembling those found for human volunteers performing slow flexion-extension movements. Tissue loads were compared with (tentative) failure limits and also showed that the deformations were too large for the frontal impact, while they were tolerable for the lateral impact. A parametric study was performed to estimate the effect of parameter changes on the model response.

Main conclusions are: active muscle behaviour is essential to accurately describe the human head-neck response to impacts; the global model is a computationally efficient model and, therefore, especially suited for car safety improvement and dummy neck development; the detailed model is suitable for studying neck injury mechanisms and neck injury criteria, since it reveals the loads and deformations of individual tissues of the neck. Recommendations are given for additional experiments, model enhancements, and further validation.

Contents

1

Introduction

The research described in this thesis is concerned with neck injuries due to automotive accidents. Neck injuries occur frequently in car crashes, especially in rear-end collisions. Most neck injuries are minor, but they can result in long-lasting complaints. These injuries are usually referred to as whiplash injuries. Severe neck injuries may lead to permanent disability, or even death. It is not well understood how an accident can result in an injury to the neck. Experimental and numerical research aid to understand the cause of neck injuries better.

In this thesis, mathematical models are described which have been developed to study the dynamic behaviour of the human head and neck in car crashes. These models give insight into the head-neck motion and the deformations and loads within the neck to enhance the understanding of the cause of neck injuries. Published data of experimental research on the neck and its tissues were used to construct the head-neck models. The models were validated with published data on simulated car crashes with human volunteers for frontal and lateral impacts. Although amenable to enhancements, the models can be used to improve car safety and dummy necks, and to study neck injuries.

This chapter provides background information on and the rationale for the research. The first section deals with the epidemiology of neck injuries. Section 1.2 states the research objectives, Section 1.3 the research strategy, and Section 1.4 the thesis outline.

1.1   Epidemiology of Neck Injuries

The human neck (or cervical spine) is a mechanically complex structure allowing for a considerable amount of motion of the head. The cervical spine consists of seven vertebrae, the bony elements, which are connected to each other and to the head and torso through various tissues, including intervertebral discs, ligaments and muscles. In an accident, the head and neck are exposed to inertia and contact forces, which may load and deform the tissues in the neck beyond recoverable limits, resulting in injury.

Severe neck injuries can result in serious damage of the nervous tissues and lead to permanent disability, or even death. Neck injuries are responsible for one third of all automotive injuries leading to permanent disability [41]. Most neck injuries, however, are minor injuries with a low threat to life. These injuries are often referred to as whiplash injuries. Whiplash patients suffer from irritating complaints like neck pain, headache, dizziness, cognitive function loss and numbness of the upper limbs. The onset of these symptoms may not occur until several hours or days after the accident [13]. Although classified as a minor injury, the whiplash injury can have serious consequences for the patient's professional and personal life, due to the often long-lasting symptoms. As a result, whiplash patients may no longer be able to work or function normally in everyday life.

An important concept in injury studies is the injury mechanism. A neck injury mechanism is the process through which a load applied to the neck leads to deformation of tissues within the neck beyond a recoverable limit, resulting in injury of these tissues [120]. Because severe neck injuries are often easily identified, for example, by a fractured or displaced vertebra, their injury mechanisms are usually well understood qualitatively, but the causative load or deformation remains to be quantified. Whiplash injuries, on the contrary, are diagnostically difficult to define: medical professionals seldom find a clear sign of structural changes (injuries) of tissues within the neck. Consequently, whiplash injuries and their injury mechanisms are not well understood.

In the literature, whiplash has been used for the injury and its symptoms as well as for its assumed injury mechanism. Historically, whiplash refers to the motion the head and neck make in rear-end collisions: an extreme rearward bending of the head and neck (hyperextension) followed by forward bending. Indeed, rear-end collisions are the most common cause for whiplash injury but, nowadays, it is recognized that whiplash injuries may also follow from other loading conditions. Therefore, 'whiplash' should not be used to identify an injury mechanism. In this thesis, 'whiplash' or 'whiplash injury' refers to minor neck injuries, and 'whiplash symptoms' to the symptoms that may follow from these injuries.

Neck Injury Incidence   Neck injuries seem to occur frequently in automotive accidents, although the reported incidences vary widely from one study to another. These differences may be due, among other factors, to regional influences (population density, traffic intensity, motorway or city traffic) and database selection. Databases commonly

used to determine injury incidences are those of the police, hospitals and motor vehicle insurance companies, and none of those is fully representative. In police databases, severe and fatal accidents are over-represented [30, 101] since police intervention is not always necessary or called for in minor or moderate accidents. Furthermore, a victim is not always recognized to have sustained a neck injury, due to the delayed onset of symptoms of minor neck injuries. Hospital databases may be incomplete, as treatment and nursing at a hospital is seldom required for minor neck injuries. Patients may directly visit a general practitioner and other health-care providers without affiliation to a hospital. Databases of motor vehicle insurance companies may not be representative since the need, motivation and possibility to claim may differ from one person to another, and because of differences in insurance systems in various countries [5, 100].

Most studies fail to clearly define the regional and database characteristics, as well as other relevant factors, which makes it difficult to judge the validity and representativeness of the reported (neck) injury incidences. Furthermore, large differences in reported incidences are found in the literature. At one extreme, Ono and Kanno [70], using insurance data, found that as much as half of all injuries resulting from car-to-car impacts were neck injuries. At the other extreme, Otte and Rether [71] reported for an in-depth accident investigation study that only 2% of the injured car occupants sustained neck injuries. Faverjon *et al.* [22] found neck injuries for 10% of *all* front seat car occupants involved in an accident, whereas Bunketorp *et al.* [9] reported that 25% of the *injured* car occupants had neck injuries. Consistent findings, though, are that the majority (70 to 90%) of neck injuries are rated as minor (AIS 1)[1] and that neck injury is the most common injury in rear-end collisions. In rear-end collisions, the neck is more easily injured than in other collisions and this may already happen at low speeds, typically less than 20 km/h [9, 22, 41, 42, 70, 71].

Deutscher [16] analyzed 10,740 car-to-car crashes, representative for the German traffic situation in 1990. The crashes were taken from a database of a German motor vehicle insurance company in 1990. Almost 84% of the collisions resulted in minor injuries (MAIS 1)[2] of at least one of the occupants, and fatal injuries were found in 2.2% of all collisions. Deutscher found that half of all collisions resulting in injuries are rear-end collisions and that more then 90% of all front seat occupants with a MAIS 1 injury sustained a neck injury.

For Quebec (Canada), Spitzer *et al.* [100] recently reported that whiplash cases form 20% of the traffic injury insurance claims and that the incidence of compensated whiplash cases is 0.7 per 1000 inhabitants (in 1987). About 50% of the whiplash victims recovered within a month after the accident, and 97% within one year. They noted that care and compensation result in high and increasing economical losses.

In a recent Dutch study, Wismans and Huijskens [121] found that 23% of all claims to motor vehicle insurance companies was for whiplash. They estimated that car and other traffic accidents cause 15,000 to 30,000 new whiplash patients annually,

---

1. AIS stands for Abbreviated Injury Scale which ranges injuries according to their threat to life from AIS 0 for 'no injury' to AIS 6 for a 'fatal injury' [3].
2. MAIS is the maximum of all AIS scores in case more than one body region is injured.

on a population of 16 million (in 1994).

Based on an extensive literature review, Barnsley *et al.* [5] estimated an annual incidence of 1 whiplash injury per 1000 inhabitants in western countries. They found that most patients recovered within 2 to 3 months after the accident, but about 25% of the patients developed chronic pain and 10% constant, severe pain. They estimated the prevalence of whiplash symptoms in the entire population at roughly 1% for chronic pain and 0.4% for severe pain.

1.2   Rationale and Research Objective

The rationale for this research is that a mathematical model of the human head and neck can aid to a better understanding of neck injury mechanisms and can be used in injury prevention research. To understand how an accident can lead to neck injury, it is necessary to understand how the loads imposed on the neck are transferred to loads and deformations of individual tissues of the neck, and how these loads and deformations result in injury of the tissues. In experimental research, these tissue loads are often impracticable if not impossible to determine. With a mathematical model, however, the loads applied to the head and neck can be converted into loads and deformations of the tissues which can be compared with failure limits of these tissues to check whether injury took place or not.

Objective   The objective of this research is to develop and validate a detailed three-dimensional mathematical model that describes the dynamic behaviour of the human head and neck in accident situations in which no head contact occurs. Thus, the head and neck are loaded through inertial forces only. The model has to provide insight into the motion of the head relative to the torso, and into the deformations and loads that occur within the cervical spine. Then, the model will contribute to a better understanding of injury mechanisms.

Applications   The model, if well validated, can be used for various purposes. It can be applied to improve car safety by optimizing the restraint systems, car structure and such. In computer-aided car design, realistic models of the human body are needed to accurately predict the behaviour of occupants involved in car crashes. A realistic neck model is needed, for example, to assess the ability of different seat-belt configurations or head rests to reduce neck injuries.

The model may be used to develop more realistic mechanical necks for dummies. The Hybrid III dummy is the most frequently used dummy to evaluate car safety in full-scale crash tests. It has been shown that the neck of this dummy lacks humanlike behaviour since it is too stiff in comparison with the human neck, especially for frontal and rear-end collisions [94, 95, 105].

If injury mechanisms and criteria are sufficiently understood, the model may be used for injury diagnosis of persons with neck injury symptoms following a car crash.

With the model, the impact can be reconstructed to reveal the loading condition that may have occurred and what injuries are likely to be found.

1.3 Research Strategy

The strategy in this study is to proceed from a relatively simple model to a much more complex one. From a literature review, it was found that precise data on the mechanical behaviour of the cervical spine and its anatomical components are sparse. Data are either not available or show large variations across different studies. This will necessitate the introduction of numerous assumptions if a highly detailed model with many parameters is constructed from the beginning. Such a detailed model is more difficult to validate than a simple model, as more unknown parameters are present which can all be modified when trying to obtain the desired, humanlike behaviour of the model.

The three types of models that have been used to describe head-neck dynamics are two-pivot, discrete parameter and finite element models [34, 126]. Two-pivot models are the simplest models in which head and torso are modelled as rigid bodies connected by a rigid or extensible neck-link. The mechanical behaviour of the neck is lumped into the head-neck and neck-torso pivots, usually as rotational spring-damper elements. Pivot models have been developed by Bosio and Bowman [8], Seemann *et al.* [95] and Wismans and co-workers [105, 118, 119] to analyze the response of human volunteers and cadavers in sled acceleration impacts. Discrete parameter models have more anatomic details than pivot models. They include head and vertebrae as rigid bodies which are connected by massless spring-damper elements representing the intervertebral soft tissues. Muscles may be represented as passive spring-damper or active force-generating elements. These models have been developed, among others, by Huston *et al.* [33], Tien and Huston [106] and Deng and Goldsmith [15]. Finite element models are the most complex models, as they allow for highly detailed representations of geometry and material behaviour of the cervical spine. Each tissue may be represented in detail by numerous deformable elements with the same mechanical characteristics as the tissue. These models have been developed by Williams and Belytschko [112] and, recently, by Kleinberger [40] and Dauvilliers *et al.* [12].

Although two-pivot models can adequately describe the motion of the head and neck relative to the torso, discrete parameter and finite element models are needed to represent vertebral motions and tissue deformations. Finite element models are more difficult to develop and validate than discrete parameter models, since they include many parameters for which realistic values are difficult to retrieve from the sparse experimental data. Because discrete parameter models are mathematically less complex than finite element models, they are computationally more efficient, which will enhance their practical usefulness. Because models of the car and its occupants are used together in car safety studies, simple but efficient models are more feasible to rapidly evaluate occupant safety.

To limit model complexity, it was chosen to start with a discrete parameter model that had few anatomical details and was easy to validate with the data available. The model includes the cervical vertebrae as separate elements and is, thus, complex enough to describe how loads applied to the head and neck are transferred to loads on the vertebrae. The model is simple enough to understand how certain modelling choices and model parameters affect the model behaviour. After more knowledge and insight was gained, the complexity of the model was increased by including extra details to obtain an anatomically more realistic head-neck model. This model is detailed enough to describe the loads and deformations of the tissues and can be used to assess injury mechanisms.

1.4 Thesis Outline

Chapter 2 describes the biomechanics of the human cervical spine. A brief review is given of the anatomy, kinematics and injury mechanisms of the human neck. The mechanical characteristics are presented in more detail, as these characteristics are used to develop the mathematical models.

Discrete parameter models of increasing complexity have been developed according to the strategy outlined in Section 1.3. First, a head-neck model including few anatomical details has been developed and validated for a frontal impact (Chapter 3). This global model includes the head and cervical vertebrae as rigid bodies which are given the inertia properties of the head and neck. The bodies are connected by massless joints representing the compound behaviour of the soft tissues between two adjacent vertebrae and of the muscles.

Second, a detailed head-neck model has been developed which has more anatomical details. To that end, detailed models of segments of the upper and lower cervical spine were developed and validated separately (Chapter 4). These segment models include separate mathematical representations for the intervertebral discs, ligaments and facet joints. These models were then transformed into a complete model of the cervical spine, including the major neck muscles as active force-generating elements (Chapter 5). This detailed model was validated for frontal and lateral impacts using sled acceleration test data with human volunteers. Furthermore, vertebral motions were compared with those found for human volunteers performing slow flexion-extension movements.

Chapter 6 concludes this thesis by summarizing the main findings of this research. Furthermore, the global and the detailed head-neck model are compared with each other, and recommendations to enhance the models and their validation are given. Finally, possible applications are outlined.

Biomechanics of the Human Cervical Spine
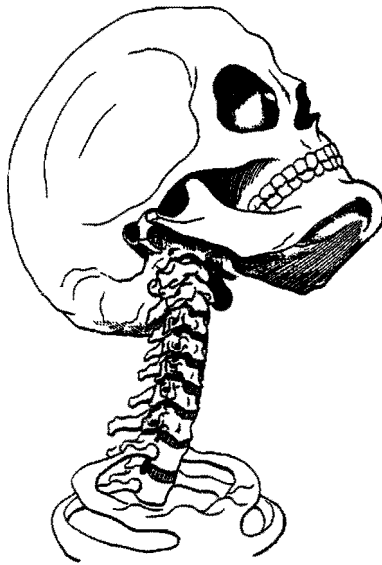
This chapter reviews the biomechanics of the human neck or cervical spine. Section 2.1 summarizes the functional anatomy of the cervical spine. Section 2.2 gives definitions of concepts that are used throughout this thesis to describe the biomechanical behaviour of the cervical spine. Section 2.3 presents its kinematic characteristics, which may be used to validate mathematical neck models. Section 2.4 discusses the mechanical characteristics of the neck and its tissues in detail and provides a synthesis of these characteristics as derived from numerous references presented in the literature. These characteristics are used as input for the mathematical models developed in this study. Further, injury mechanisms and criteria are briefly discussed in Section 2.5 as they are also a relevant aspect of this study. Finally, a discussion and conclusions are presented.

2.1 Functional Anatomy

The human cervical spine is the upper part of the spine. It supports the head and protects the spinal cord. It is an articulate structure made up of joints allowing for motion of the head relative to the torso. The four basic motions of head and neck are flexion (forward bending), extension (rearward bending), lateral (sideward) bending and axial rotation. In this section, the anatomy of the human cervical spine is summarized. More detailed information can be found in [31, 37, 38, 39, 51, 110].

The cervical spine comprises seven bony elements, called vertebrae, which are joined by soft tissues. Of these tissues, intervertebral discs, ligaments, uncovertebral joints, facet joints and muscles are relevant to the biomechanics of the neck as they control motion between vertebrae. In this thesis, the cervical spine is assumed symmetrical with respect to the midsagittal plane.

Vertebrae   The cervical spine comprises seven vertebrae, numbered C1 through C7 (see Figure on previous page; adapted from Kapandji [38]). The first and second vertebra, atlas and axis, are distinct from each other and from the lower five vertebrae, which are basically the same. Due to these differences, the cervical spine can be divided into the lower and upper cervical spine.

The lower cervical spine comprises vertebrae C3 through C7, each of which consists of a cylindrically shaped body and an arch (Fig. 2.1). The lower end of the body is concave from front to back, whereas its upper end is concave from side to side and has an uncinate process on each side. The upper and lower ends of the body are covered by a thin layer of hyaline cartilage, the endplates. The arch includes two pairs of articular facets, a spinous process and two transverse processes. The articular facets are almost flat and covered with cartilage, and have a backward inclination of about 45 degrees in the horizontal plane. The transverse and spinous processes constitute attachment points for muscles and ligaments. The arch and body enclose the vertebral foramen to form the spinal canal through which the spinal cord and associated structures run.
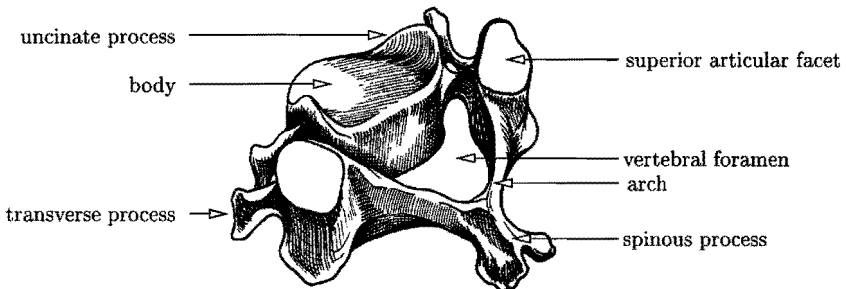
Figure 2.1: A typical vertebra from the lower cervical spine (Adapted from Kapandji [38]).
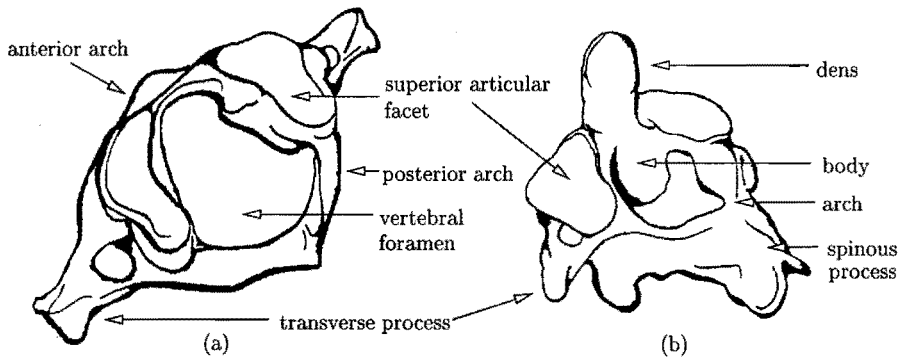
Figure 2.2: Axis (a) and atlas (b), the first and the second cervical vertebra (Adapted from Huelke [31]).

The upper cervical spine comprises axis, atlas and occiput, and is also called the occipito-atlanto-axial region. The occiput (C0) is the base of the skull and articulates with the atlas through the occipital condyles which are convex in shape. The atlas (C1) has no vertebral body, but consists of a bony ring with anterior and posterior arches on which the articular facets and transverse processes are situated (Fig. 2.2a). The upper facets are large, concave and oval. Like the lower vertebrae, the axis (C2) comprises a body and an arch, but it has an additional element, the odontoid process or dens (Fig. 2.2b). The dens points out upwards from the body of C2 and is the missing body of the atlas fused to the axis.

Joints The joints between two adjacent vertebrae are the intervertebral disc, the facet joints and the uncovertebral joints. The disc allows for motion between vertebrae in all directions, and the uncovertebral and facet joints guide and constrain these motions. The intervertebral disc is a fibrocartilaginous joint between the endplates of each two adjacent vertebral bodies, but there are no discs between axis, atlas and occiput. Because discs are thicker anterior than posterior, the cervical spine has an anteriorly convex curve, known as cervical lordosis. Uncovertebral joints, situated on either side of the disc, are small synovial joints between the uncinate processes of the lower vertebra and the lower endplate of the upper vertebra. Facet joints are synovial joints formed by the corresponding articular facets of adjacent vertebrae and enclosed by capsular ligaments. Usually, synovial joints allow for sliding movements only, but within the facet joints other movements are also possible due to the laxity of the capsular ligaments. The facet joints between the superior facets of the atlas and the occipital condyles allow little axial rotation and much flexion/extension. Atlas and axis articulate through the facet joints and a synovial joint between the dens and the anterior arch of the atlas, which together allow much axial rotation.
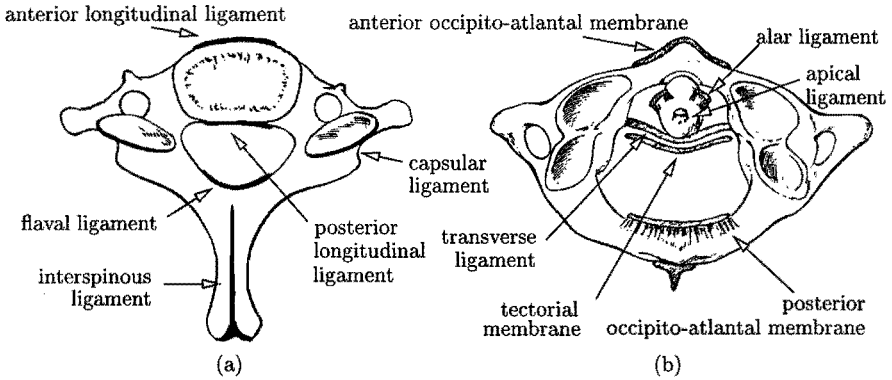
Figure 2.3: Lower (a) and upper (b) cervical ligaments (Adapted from Sances *et al.* [90]).

Ligaments Ligaments allow spinal motion within physiologic limits and prevent excessive motion to protect the spinal cord. They connect adjacent vertebrae or extend over several vertebrae. Ligaments resist tension and fold in compression.

Figure 2.3a depicts the ligaments of the lower cervical spine. The anterior and posterior longitudinal ligaments are strong ligaments attached to the anterior and posterior parts of the vertebral bodies and intervertebral discs. The interspinous ligament is a thin, tough membrane between adjacent spinous processes and the flaval ligament is a strong band between adjacent laminae. The capsular ligaments enclose the facet joints. The nuchal ligament (not shown) is a thin and weak triangular membrane joining all cervical spinous processes and interspinous ligaments to the posterior midline of the occiput; its posterior edge runs from the occiput to the spinous process of C7. The anterior longitudinal ligament limits extension of the spine. The other ligaments are all posterior ligaments and limit flexion.

The most important ligaments of the upper cervical spine are shown in Figure 2.3b. The tectorial membrane is a broad and strong band which extends the posterior longitudinal ligament from the axis to the occiput. The anterior and posterior occipito-atlantal and atlanto-axial membranes are continuations of the anterior longitudinal and flaval ligament, respectively. The transverse ligament is a strong horizontal ligament of the atlas, which holds the dens against the anterior arch of the atlas to constrain the dens posteriorly. The dens is held anteriorly by the apical and alar ligaments. The apical ligament runs from the top of the dens to the occiput. The alar ligaments extend from the dens on each side of the apical ligament to the medial side of the occipital condyles and the atlas. Apical and alar ligaments limit rotation of the upper cervical spine.

Neck Muscles Neck muscles are needed to maintain the head and neck in a given posture and to produce movements of the head and neck.

The muscular anatomy of the human cervical spine is extremely complex. Numerous muscles can be identified, many of which originate from or insert on several vertebrae. Due to midsagittal symmetry, muscles appear twice, one to the left and one to the right of the cervical spine. When paired muscles contract simultaneously (bilaterally), they either flex or extend the neck and head. In unilateral contraction, the muscle may also cause lateral bending and axial rotation. Only a brief description of muscular anatomy is given here, since a detailed treatment goes beyond the scope of this thesis. Detailed descriptions of the functional anatomy of the muscles may be found in Kapandji [38] and anatomy textbooks, such as Jenkins [37].

The neck muscles can be divided into superficial, intermediate and deep muscles. Superficial muscles have no attachments to the cervical spine, but run directly from the skull to the thoracic region, like the sternocleidomastoid and trapezius. Intermediate muscles have several attachments to the cervical vertebrae. They run from the cervical vertebrae to the thorax, like the scalenus muscles, or link the skull with the spine, like the semispinalis capitis, splenius capitis, longus capitis and longissimus capitis. Deep muscles lie close to the cervical vertebrae. Some join one vertebra to another, like the suboccipital muscles or the transversospinalis cervicis, which run between the spinous and transverse processes of adjacent vertebrae. Others span several vertebrae, like the longus colli, longissimus cervicis and splenius cervicis.

Motion Segment A motion segment comprises two adjacent vertebrae with the surrounding soft tissues: intervertebral disc, uncovertebral joints, facet joints and ligaments. Its biomechanical behaviour is similar to that of the entire spinal column, which may be considered as a series connection of motion segments. A motion segment is also referred to as functional spinal unit or intervertebral joint. The upper cervical spine is usually treated as a single biomechanical unit due to its functional arrangement. Upper and lower cervical segments are used to study the biomechanics of the cervical spine.

2.2 Definitions and General Remarks

This section presents the definitions that are used in this thesis to characterize the biomechanical behaviour of the human cervical spine and its anatomical components.

Coordinate System, Loads and Displacements Figure 2.4 shows the general experimental set-up to determine the mechanical behaviour of motion segments. The lower vertebra is fixed to the test frame, whereas the upper vertebra is free to move in all directions in response to the loads applied to it. The origin of a right-handed orthogonal coordinate system is placed at the geometric centre of the upper vertebral body. The *geometric centre* is assumed to lie in the midsagittal plane at the intersection of the diagonals connecting the corners of the body in this plane. The x, y, z-axes of the coordinate system point forwards, to the left and upwards. Figure 2.4 also defines the positive directions for the loads (forces F and moments M) and the corresponding
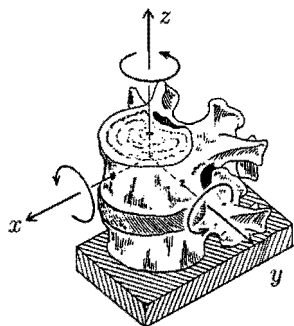
load	displ.	name	abbr.
$+F_x$	$+t_x$	anterior shear	AS
$-F_x$	$-t_x$	posterior shear	PS
$\pm F_y$	$\pm t_y$	lateral shear	LS
$+F_z$	$+t_z$	tension	TNS
$-F_z$	$-t_z$	compression	CMP
$\pm M_x$	$\pm \phi_x$	lateral bending	LB
$+M_y$	$+\phi_y$	flexion	FLX
$-M_y$	$-\phi_y$	extension	EXT
$\pm M_z$	$\pm \phi_z$	axial rotation	AR

Figure 2.4: Definition of coordinate system, loads and displacements. Drawing adapted from White and Panjabi [110].

displacements (translations t and rotations ϕ). The names assigned to the loads and displacements reflect that the mechanical behaviour may differ for positive and negative displacements about or along the same axis. Assuming midsagittal symmetry, the behaviour in left and right lateral shear, left and right lateral bending, or left and right axial rotation is identical.

Main and Coupled Displacements, Coupling   When a load is applied to the specimen in one direction, it will generate displacements in all six directions. The displacement in the same direction as the applied load is called the *main displacement*, the other displacements are referred to as *coupled displacements*. Coupled displacements are often much smaller than the main displacement, although some significant consistent couplings between motions are present in the cervical spine. In the literature on spine biomechanics, *coupling* is used to indicate that a (main) rotation about or translation along one axis of a body is consistently associated with a simultaneous (coupled) rotation about or translation along another axis [110], see Section 2.3.

Centre of Rotation and Helical Axis of Motion   Two useful concepts to characterize the motion of a vertebra are the centre of rotation and the helical axis of motion. The *centre of rotation* (COR) characterizes the two-dimensional displacement of a body from one position to another as a single rotation about this centre (Fig. 2.5a). The displacement is fully described by the position of the COR and the magnitude of rotation. The COR depends on the two positions of the body that are used to determine the COR (Fig. 2.5b): it has a fixed position for circular motions only. The *helical axis of motion* (HAM) is the three-dimensional equivalent of the COR. The three-dimensional displacement of a body from one position to another can be characterized as a superposition of a rotation about and a translation along an axis, the helical axis of motion. The motion is fully described by the orientation of the axis and the amount of translation and rotation.
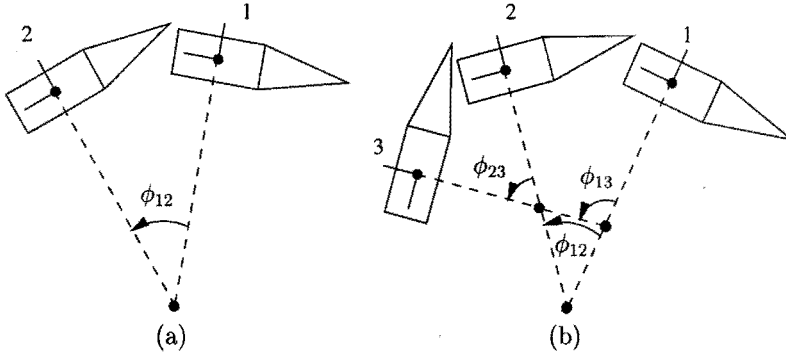
Figure 2.5: (a) The displacement of a body from position 1 to position 2 described as a single rotation ϕ_{12} about the centre of rotation (COR). (b) The position of the COR depends on the body positions used to determine the COR.

Load-displacement Behaviour   Load-displacement curves for biomechanical structures as motion segments or ligaments typically have the nonlinear, sigmoidal shape shown in Figure 2.6a. The curve is divided into a physiologic and a traumatic range. The *physiologic range* starts with the *neutral zone* (NZ) in which little load is needed to deform the structure. The transition from the neutral to the *elastic zone* (EZ) is characterized by a substantial increase in load. Throughout the elastic zone, the curve is usually fairly linear. The name 'elastic zone' reflects that, on release of the load, the specimen will return to the state it had before being loaded. The physiologic *range of motion* (ROM) is the sum of the neutral and the elastic zone, and represents the total amount of displacement that the biomechanical structure can sustain without being damaged. Because it is difficult to identify precisely when damage (microtrauma) starts and the ROM ends, the ROM should be specified together with the load that caused it, to enable the comparison of ROMs reported in different studies. The *traumatic range* starts when microtrauma occurs within the structure and ends with failure of the structure, which is characterized as a substantial drop in load. Load and displacement at failure define the *failure strength* of the structure.

For motion segments, the NZ represents the region where ligaments are lax such that small loads produce large displacements. In the EZ, the ligaments are stretched and their resistance to deformation increases, resulting in increased motion segment stiffness.

In most experimental studies on motion segments, loads are applied statically: load is increased in small increments after which the specimen is given time to relax before the displacements are measured. Consequently, viscous effects are minimized and elastic characteristics are obtained. In few cases, loads are applied quasi-statically or dynamically: load is continuously increased at a relatively low, respectively, high rate, and viscoelastic characteristics are measured.
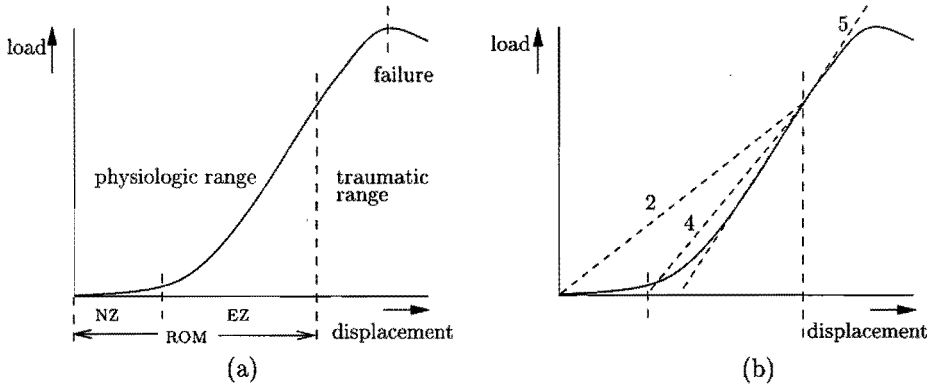
Figure 2.6: (a) Typical load-displacement curve for biomechanical structures. (b) Different stiffness calculations used to characterize the load-displacement curve, see text.

Stiffness and Flexibility Stiffness and flexibility are used to characterize load-displacement behaviour. Stiffness is defined as the slope of the tangent to the curve at a certain load or displacement (tangent stiffness). Thus, stiffness varies along a nonlinear curve. Flexibility is defined as the reciprocal of stiffness.

In most publications, the experimentally obtained load-displacement curves are not reproduced but represented by one or more stiffness (or flexibility) coefficients. Unfortunately, up to five different stiffness calculations have been used by different authors (Fig. 2.6b). 1) Tangent stiffness (not shown). 2) Stiffness as the ratio of load to displacement for a point on the curve. This point is usually the point of maximum applied load or failure. 3) Stiffness derived from linear regression analysis of the curve (not shown). 4) Stiffness as the ratio of load to displacement minus neutral zone displacement for a point on the curve. 5) Stiffness as the slope of the most linear part of the curve. Stiffnesses 2 and 3 measure the average stiffness of the specimen up to the point chosen, whereas 4 and 5 represent the stiffness of the elastic zone of the curve. Stiffness 1 may be used to approximate a complete curve, if stiffnesses are given for a sufficient number of points. For all definitions, the range of load and displacement for which the stiffnesses were calculated should be given.

2.3   Kinematics

Several authors have characterized the kinematics of the cervical spine, using concepts introduced in the preceding section: range of motion, coupling, centre of rotation and helical axis of motion. These data are useful in understanding the biomechanics of the cervical spine and for validation of mathematical models.

Range of Motion White and Panjabi [110] presented representative values for the ranges of rotation of the cervical joints based on various studies (Table 2.1). In most of

Table 2.1: Representative ranges of motion for *in vivo* rotation of the cervical joints [110].

motion	C0-C1	C1-C2	C2-C3	C3-C4	C4-C5	C5-C6	C6-C7	C7-T1
					deg			
one side lateral bending	5	5	10	11	11	8	7	4
combined flexion/extension	25	20	10	15	20	20	17	9
one side axial rotation	5	40	3	7	7	7	6	2

these studies, measurements were derived from radiographic examination of volunteers and, therefore, represent *in vivo* ROMs. The load magnitudes that produced the motions are not known. The atlanto-axial joint (C1-C2) allows for much axial rotation, due to the unique shapes of the vertebrae and articulations: roughly half of the axial rotation of the neck occurs at this joint. The occipito-atlantal joint (C0-C1) allows for much flexion/extension and only little axial rotation. Both C0-C1 and C1-C2 allow for little lateral bending compared with the lower joints. C7-T1, at the transition of the cervical and thoracic spine, allows for the least rotation in all directions.

White and Panjabi [110] state that there is almost no translation between C0-C1, and no lateral translation and 2–3 mm of vertical and anterior/posterior translation between C1-C2. The vertical translation of C1 is coupled with axial rotation of C1. Ranges of translation for the lower joints can be deduced from the motion segment studies presented in Section 2.4.1.

Coupling In the lower cervical spine, two characteristic couplings are present due to the spatial orientation of the facet joints and the uncovertebral joints [56]. First, flexion is coupled with anterior translation and extension with posterior translation. This coupling is reflected by the position of the centre of rotation. Second, lateral bending is associated with axial rotation such that the spinous processes move to the left when head and neck are bent to the right. This coupling is reflected by the helical axis of motion. In the upper cervical spine, axial rotation of the atlas is coupled with vertical translation of the atlas due to the shape of the C1-C2 articulations [110].

Centre of Rotation The centre of rotation (COR) is used to describe the motion of a vertebra relative to its adjacent lower one. According to Penning [82], the position of the COR is largely determined by the facet joints: the spaces between adjacent facets form part of a circle with the COR as midpoint (Fig. 2.7a). Regional differences in the shape and orientation of the facet joints are reflected in differences in COR locations with vertebral level.

For flexion/extension, the COR of a vertebra relative to its lower adjacent vertebra has been determined by various researchers. Penning[82], Dvorak *et al.* [19] and Amevo *et al.* [2] determined the position of the CORs using lateral X-rays of the cervical spine of humans who held their head in full flexion and full extension. These CORs reflect the apparent centre of rotation for vertebral motions from full flexion to full extension

(a)   (b)
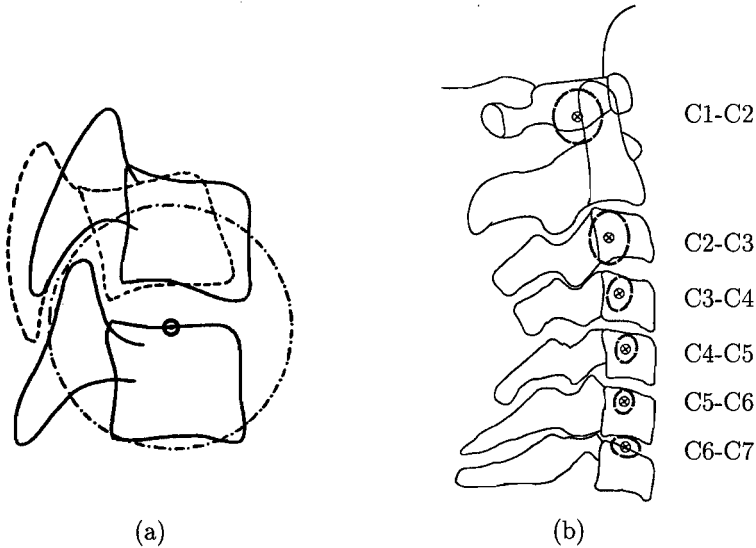
Figure 2.7: (a) Position of the centre of rotation (COR) as determined by facet joint anatomy. Shown are the bodies and articular facets of two adjacent vertebrae. The upper vertebra rotates relative to the lower one around the COR, the midpoint of the circle through the spaces formed by adjacent facets [82]. (b) Average positions (⊗) and SD (large ellipses) of CORs for flexion/extension of each cervical vertebra relative to adjacent lower vertebra [19].

(and vice versa), but do not reflect the centre of rotation for positions in between these two extremes. Van Mameren *et al.* [43] monitored voluntary flexion/extension motions using lateral X-ray recordings at 4 frames/s to determine the CORs for positions in between these two extremes. They found that the positions of the CORs varied little during the motion and that the average positions compared well with the positions found from static X-rays in full flexion and full extension.

    The positions of the CORs found by Amevo, Dvorak, Van Mameren and Penning agree well with each other. Figure 2.7b shows the average positions of the CORs found by Dvorak. At the C6-C7 level, the COR is located at the middle of the upper endplate of the C7 vertebral body. The CORs move gradually downwards and backwards with each higher vertebral level, such that at C2-C3 the COR is located halfway the height of the vertebral body of C3 and close to its posterior margin [2, 19, 43, 82]. For C1-C2, the COR is at the posterior margin of the dens near the transverse ligament [19, 43]. For C0-C1, the COR shows the largest variations, but it is consistently located above the occipital condyles [43].

Helical Axis of Motion   Milne [57] determined the position and orientation of the helical axis of motion (HAM) for each cervical joint of cervical spine specimens (C2-T3;

third thoracic vertebra) which were loaded at C2 in either lateral bending or axial rotation. Milne found that the HAM lies in the midsagittal plane only for symmetrical bilateral movements (left to right or vice versa). For unilateral motion (from neutral position to the left or to the right), the HAM makes an angle with the midsagittal plane. For the projection of the HAM onto the midsagittal plane, Milne noted that the orientation of the HAM tends to be in line with the axis about which the moment is applied; that is, about the x-axis for lateral bending and about the z-axis for axial rotation. For combined axial rotation and lateral bending, the orientation of the HAM in the midsagittal plane is more or less perpendicular to the plane of the facet joints, which was also suggested by Penning [82] based on anatomical observations. Thus, the orientation of the HAM describing the motion of a vertebra relative to its lower one was found to vary with the type (lateral bending or axial rotation) and amount of motion (unilateral or bilateral).

2.4 Mechanical Characteristics

The mechanical behaviour of the human cervical spine is quantified by its physical properties. These properties include the geometric, inertial and mechanical characteristics of the complete cervical spine, of motion segments and of individual tissues. This section deals with the mechanical characteristics as they are the most difficult characteristics to obtain experimentally. Consequently, large variations between different studies are found. Geometric and inertial characteristics can usually be obtained more easily and smaller differences between studies are noted. Therefore, these characteristics are dealt with in Chapters 3, 4 and 5 which describe the construction of the mathematical models.

In this section, only average data are presented for clarity and brevity. A general observation from all referenced studies is that the variation in the data, quantified by the standard deviation, is large. Standard deviations may be as large as 80% of the reported average stiffness or ROM, and are seldom less than 10%. This reflects not only the large variability, which is typical for biological structures, but also the limited accuracy and errors involved in these experiments, as they are extremely difficult to perform.

Another aspect that is not considered here is coupling. In most studies, both main and coupled displacements were measured. Within the same study, the coupled motions were generally much smaller than the main motions and of the same magnitude as the standard deviations. Between studies, large differences were noted in magnitude and direction of coupled motions for the same applied load. Coupled motions are even more sensitive than main motions to differences in experimental set-up. Furthermore, the amount and direction of coupled motion depend on the (initial) relative position of adjacent vertebrae in a cervical spine specimen as was found by Panjabi *et al.* [77].

2.4.1 Mechanical Characteristics of Lower Cervical Spine Segments

Few studies quantify the mechanical behaviour of segments of the lower cervical spine. Goel *et al.* [27, 26], Moroney *et al.* [61] and Panjabi *et al.* [79, 76] measured static characteristics, whereas Shea *et al.* [97] measured quasi-static characteristics of cervical segments. Below, a brief review is given of the used experimental set-ups as well as a summary and comparison of the reported mechanical characteristics.

Experimental Set-ups Goel, Moroney and Panjabi all used a similar experimental set-up (described in Section 2.2) to test segments of the lower cervical spine. The main differences are the size of the specimens and the application of loads to the specimens. Specimen size ranges from motion segments comprising two vertebrae to C2-T2 segments comprising eight vertebrae. Panjabi [79] and Moroney [61] used motion segments ranging from C2-C3 down to C7-T1. Moroney also used disc segments comprising two vertebral bodies, the intervertebral disc and both longitudinal ligaments. These studies were designed purely to measure the mechanical characteristics of the specimens. Panjabi [76] and Goel [27, 26] used longer specimens (C4-C7 respectively C2-T2) as their studies were also designed to measure the stabilizing effects of fixation devices on artificially injured specimens.

In all studies, forces or moments were applied to the upper vertebra of the specimen, while the lowest vertebra was rigidly attached to the test apparatus. Displacements were measured at the geometric centre of the vertebral bodies. The maximum applied loads differ widely from one study to another. Panjabi [79] used a maximum force of 50 N, and Moroney used maximum forces of 10–40 N for motion segments and 4–16 N for disc segments. Maximum moments vary from 0.3 Nm for Goel up to 2.2 Nm for Moroney. Furthermore, Panjabi and Moroney used axial preloads of 10 N and 49 N, respectively. Another difference is that Panjabi applied the load at the geometric centre of the upper vertebral body, whereas Moroney applied the load in effect at the centre of the disc using a special construct ('crown piece').

Shea *et al.* [97] used a different set-up. They used segments comprising three vertebrae and the interconnecting tissues from the C2-C5 or C5-T1 region, and prescribed the displacement of the lowest vertebra, while measuring the displacements and the loads at the geometric centre of the middle, respectively, upper vertebral body. The maximum prescribed displacements were 17 deg for flexion, 5 deg for extension, 2 mm for tension/compression, and 1.5 mm for anterior/posterior shear. Displacement rates were 5 deg/s and 5 mm/s. They stated that results obtained at these rates were not significantly different from results obtained at rates as low as 0.05 deg/s and 0.05 mm/s. Since Shea measured the displacement at the middle vertebra and loads at the upper one, the measured load-displacement behaviour represents single motion segment behaviour (and not three-vertebrae segment behaviour as stated incorrectly by Shea).

Summary of Reported Mechanical Characteristics Table 2.2 lists average values for the NZ and ROMs, which were reported or derived from the reported results. Table 2.3

Table 2.2: Neutral zone (NZ) and range of motion (ROM) for motion segments of the lower cervical spine for the loading directions defined in Figure 2.4.

author et al.	motion	AS	PS	LS	TNS	CMP	LB	FLX	EXT	AR	
				mm				deg			
Panjabi [79]	NZ	0.8	0.8	0.7	0.3	0.3					
	ROM	1.9	1.6	1.5	1.1	0.7					*a*
Moroney [61]	ROM	0.2	0.1	0.4		0.1	4.7	5.6	3.5	1.9	*b*
Goel [27]	ROM						2.5	7.3	1.4	1.6	*c*
Goel [26]	ROM						2.5	2.7	2.4	2.0	*d*
Panjabi [76]	NZ						2.7	3.2	3.2	1.7	
	ROM						10.2	16.7	13.5	9.0	*e*

a reported average NZ and ROM at 50 N for all cervical spinal levels
b reported average ROM at 20 N or 1.8 Nm for all cervical spinal levels
c average of reported ROM at 0.3 Nm for spinal levels C4-C5 and C5-C6
d average of reported ROM at 0.3 Nm for spinal levels C3-C4 – C7-T1
e average of reported NZ and ROM at 1.5 Nm for spinal levels C4-C5 – C6-C7

Table 2.3: Stiffnesses for motion segments of the lower cervical spine for the loading directions defined in Figure 2.4.

author et al.	spinal level	n	AS	PS	LS	TNS	CMP	LB	FLX	EXT	AR	
							direction of load					
				N/mm					Nm/deg			
static stiffness disc segments												
Moroney [61]	C2–T1	30	62	50	73		492	0.33	0.21	0.32	0.42	*b*
static stiffness motion segments												
Panjabi [79]	C2–T1	18	34	53	53	53	141					*a*
Moroney [61]	C2–T1	16	131	49	119		1318	0.68	0.43	0.73	1.16	*b*
Goel [27]	C4–C6	4–6						0.12	0.04	0.22	0.19	*c*
Goel [26]	C3–T1	9						0.12	0.11	0.12	0.15	*c*
Panjabi [76]	C4–C7	10						0.20	0.11	0.15	0.21	*d*
quasi-static stiffness motion segments												
Shea [97]	C2–T1	27	183	162		433	718		1.13	1.88		*e*
	C2–T1	16	123	114		193	957		1.13	1.74		*f*
	C2–C5	8	110	115		229	1114		1.44	2.29		*f*
	C5–T1	8	136	112		157	800		0.83	1.19		*f*

n: number of specimens
a reciprocal of reported average flexibility at 25 N
b reported stiffness obtained from linear regression
c calculated from average of reported ROM at 0.3 Nm: load/ROM
d calculated from average of reported NZ and ROM at 1.5 Nm: load/(ROM-NZ)
e reported average stiffness at 300 N TNS, CMP; 150 N AS, PS; 5 Nm FLX, EXT
f idem at 500 N CMP; 100 N TNS, AS, PS; 5 Nm FLX; 3.5 Nm EXT

gives the average stiffnesses together with the number of specimens and the spinal level of the motion segments used in each study.

Panjabi *et al.* [79] found no significant variation in mechanical characteristics with vertebral level and, therefore, reported average results for the NZ, ROM and flexibility of the main and coupled motions. Flexibility was calculated as the slope of the load-displacement curves between 13 and 37 N (first and third load increment). Moroney *et al.* [61] also did not find a variation of the mechanical characteristics with vertebral level and presented, for motion and disc segments, average results for the ROM of the main and coupled motions and for the stiffnesses of the main motions. Stiffnesses were derived from linear regression of the load-displacement curves.

The load-displacement curves measured by Shea *et al.* [97] were highly nonlinear showing a progressive increase in load with increasing deformation. They used third-order polynomials to fit the experimental load-deformation curves. Stiffnesses were calculated in linear regions of the fitted curve for various load magnitudes. They averaged the stiffnesses for all specimens and for specimens from either the C2-C5 or C5-T1 region, and found that specimens from the C2-C5 region were significantly stiffer in compression and extension. Unfortunately, they did not report average displacements at which the load-stiffness pairs were derived, which makes it impossible to reconstruct an average load-displacement curve from their data.

Comparison of Reported Characteristics   As all experimental set-ups differ, the results can not easily be compared. Nevertheless, some conclusions can be drawn from the results presented in Tables 2.2 and 2.3.

The ranges of motion are difficult to compare as they depend on the maximum applied load. Only Panjabi [79, 76] reported NZ-displacements and these are found, by definition, for very small loads. If these NZs are compared with the ROMs reported by others, it is observed that the NZs of Panjabi are larger than the translational ROMs reported by Moroney [61] for 20 N and similar to the rotational ROMs of Goel [27, 26] for 0.3 Nm. The differences between Panjabi and Moroney may be caused by differences in load application, see below.

Although the experiments of Panjabi [79] and Moroney [61] are almost similar, the stiffnesses differ to a large extent except for posterior shear. The main differences in the experimental set-ups are the point where the load is applied to the upper vertebra and the magnitude of the axial preload. Both aspects may have contributed to the differing results. Panjabi applied the load at the geometric centre of the upper vertebral body, and Moroney at the centre of the disc, resulting in a different loading situation. To obtain the same loading situation in shear, an additional bending moment should be applied to the upper vertebra in Moroney's set-up. But even if the translation coupled with this bending moment is taken into account, Moroney's data still represents stiffer motion segment behaviour than Panjabi's data. A further explanation is the axial preload (10 N for Panjabi, 49 N for Moroney): a large preload may stiffen the motion segment and result in smaller displacements. Indeed, Janevic *et al.* [36] found that compressive preloads significantly stiffen lumbar motion segments, probably due

to impingement of the facet joints and stiffening of the intervertebral disc. Similar findings were reported by Wilke et al. [111], who found that simulated muscle loads could significantly decrease the NZs and ROMs of lumbar segments in comparison with the unloaded situation.

Although the quasi-static stiffnesses of Shea [97] were obtained for much larger loads than the static stiffnesses of Moroney, they agree remarkably well for anterior shear and compression, but differ largely for posterior shear. The stiffnesses of Panjabi are much smaller.

Combining the results of Panjabi, Moroney and Shea, it may be concluded that a motion segment of the lower cervical spine is stiffest in compression and least stiff in shear.

The rotational stiffnesses reported by Panjabi [76] and Goel [27, 26] are almost all in the range 0.1–0.2 Nm/deg. They agree reasonably well, especially compared with the larger stiffnesses of Moroney ranging from 0.4 to 1.2 Nm/deg. This supports the suggestion that an axial preload stiffens a motion segment, since only Moroney applied a significant preload. The stiffnesses of Shea [97] are larger than the other stiffnesses and reflect an increased stiffness of specimens at larger load levels. All studies consistently show that a motion segment is most flexible in flexion and stiffest in axial rotation.

2.4.2 Mechanical Characteristics of the Upper Cervical Spine

The moment-rotation characteristics of the upper cervical spine are well documented for static loads. Quasi-static and dynamic characteristics have been reported only for axial rotation across C0-C2. Force-displacement characteristics of C0-C1-C2 have not been reported.

Static Experiments   Static characteristics were determined by Goel et al. [25], using C0-C5 specimens, and Panjabi and co-workers [68, 72, 73, 75], using C0-C3 or C0-C7 specimens. The lowest vertebra was fixed, while the upper most vertebra was loaded incrementally up to a maximum moment of 1.5 Nm for Panjabi, and 0.3 Nm for Goel. Pure moments were applied in flexion/extension, lateral bending and axial rotation. The three-dimensional displacements were measured to determine the NZs and ROMs for relative rotations between C0-C1, C1-C2 and C0-C2. Table 2.4 shows the average NZs, ROMs and stiffnesses for the main rotations compiled from these studies.

According to Panjabi et al. [75], a maximum moment of 1.5 Nm is sufficient to determine the physiologic range of motion: they found that a further increase in load with 1.0 Nm increased the maximum rotation with less than 5 deg, on the average. Forced by limitations in the experimental set-up, Goel et al. kept the maximum moments as small as 0.3 Nm. Consequently, their rotations do not represent the physiologic ROM. Therefore, their results were not used to compute stiffnesses. Because Oda et al. [68] and Panjabi et al. [72, 73, 75] used a similar experimental set-up and a maximum moment of 1.5 Nm to determine the ROM, their data may be pooled and averaged. The average data was used to calculate the stiffnesses.

Table 2.4: Neutral zone (NZ), range of motion (ROM) and elastic-zone stiffnesses for upper cervical spine specimens loaded in lateral bending (LB), flexion (FLX), extension (EXT) and axial rotation (AR).

spinal level	author et al.	n	LB NZ	LB ROM	FLX NZ	FLX ROM	EXT NZ	EXT ROM	AR NZ	AR ROM
							deg			
C0-C1	Goel [25]	8		3.4		6.5		16.5		2.4
	Oda [68]	5	1.4	3.9	6.7	12.7	8.3	13.5	1.5	6.4
	Panjabi [72]	10	1.5	5.5	1.1	3.5	1.1	21.0	1.6	7.3
	Panjabi [73, 75]	10	3.6	5.4	10.5	14.4	10.4	14.4	0.9	4.7
	average[a]	25	2.2	4.9	6.1	10.2	6.6	16.3	1.3	6.1
C1-C2	Goel [25]	8		4.2		4.9		5.2		23.3
	Oda [68]	5	6.4	10.8	3.6	10.9	3.3	7.3	16.4	31.4
	Panjabi [72]	10	1.2	6.7	3.2	11.5	3.2	10.9	29.6	38.9
	Panjabi [73, 75]	10	7.4	10.5	7.6	12.7	8.1	10.5	27.5	35.7
	average[a]	25	5.0	9.3	4.8	11.7	4.9	9.6	24.5	35.3
C0-C2	Goel [25]	8		7.6		11.4		21.7		25.7
	average[a]	25	7.2	14.2	10.9	21.9	11.5	25.9	25.8	41.4

			LB		FLX		EXT		AR	
						stiffness[b]				
						Nm/deg				
C0-C1	average[a]	25	0.55		0.37		0.16		0.32	
C1-C2	average[a]	25	0.35		0.22		0.32		0.14	
C0-C2	average[a]	25	0.21		0.14		0.10		0.10	

All ROM are for 1.5 Nm except Goel *et al.* [25] which are for 0.3 Nm
n: number of specimens
a average of Oda *et al.* [68] and Panjabi *et al.* [72, 73, 75]
b EZ-stiffness = load/EZ

For C0-C1, the NZ and ROM are small in lateral bending and axial rotation. The data of Panjabi *et al.* [72] for flexion and extension do not agree well with the other data, but the combined ROM flexion/extension is similar. The stiffness (of the elastic zone) is least in extension and largest in lateral bending. For C1-C2, the NZ and ROM are similar in lateral bending, flexion and extension. Axial rotation is the predominant motion. The stiffness is largest in extension and lateral bending and smallest in axial rotation. For C0-C2, the NZ and ROM are similar in flexion and extension, much larger in axial rotation, and smallest in lateral bending. Stiffness is largest in lateral bending and least in axial rotation and extension.

Quasi-static and Dynamic Experiments   Chang *et al.* [10] determined quasi-static and dynamic characteristics of C0-C2 specimens in axial rotation. They prescribed the axial rotation of C2 at rates of 4, 50, 100 and 400 deg/s up to failure of the specimens. The
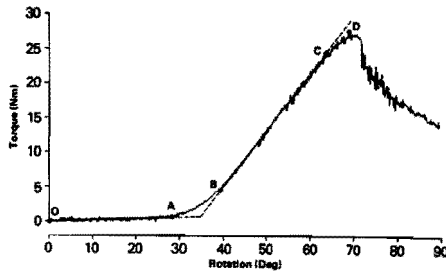
Figure 2.8: Typical moment-rotation curve for axial rotation of C0-C2 specimens measured by Chang et al. [10].

resulting moment was measured at C0 of which only axial rotation was constrained. Thus, motion of C1 was not measured. Figure 2.8 shows a typical moment-rotation curve that was obtained. Chang et al. determined average values for the points A, B, C and D on the curve and for the stiffnesses of the parts OA and BC for all loading rates (Table 2.5).

For the quasi-static rate of 4 deg/s, viscous effects are smaller than for the higher dynamic rates. Therefore, the quasi-static data can be compared with the static data, for which viscous effects are absent. The points A at 0.5 Nm and B at 2.0 Nm match more or less with the NZ at 0 Nm and ROM at 1.5 Nm found in the static tests, although the rotations are smaller than in the static tests. The static stiffness of the elastic zone lies in between the quasi-static OA- and BC-stiffnesses. Thus, the OA-stiffness may be considered to reflect the stiffness of the neutral zone for quasi-static (and dynamic) loading, and the BC-stiffness to reflect the stiffness of the structure beyond the static, physiologic range of motion. The transition from physiologic to traumatic zone, then, should take place somewhere along this part of the curve; compare Figures 2.6a and 2.8.

Table 2.5: Moment-rotation curves and stiffnesses for C0-C2 specimens in quasi-static and dynamic axial rotation (From Chang et al. [10]).

load	no. of	points on moment-rotation curve								stiffness	
rate	spec.	A		B		C		D		OA	BC
deg/s		deg	Nm	deg	Nm	deg	Nm	deg	Nm	Nm/deg	
4	12	20.7	0.5	29.9	2.0	57.8	11.9	68.1	13.6	0.028	0.383
50	4	27.7	0.6	37.4	3.0	56.5	13.0	67.8	14.3	0.027	0.528
100	6	29.2	1.0	40.1	4.6	65.9	23.7	77.7	27.8	0.035	0.733
400	5	30.0	1.5	30.0	1.5	57.8	20.3	64.7	23.2	0.053	0.669

2.4.3 Mechanical Characteristics of Cervical Components

Little is known about the mechanical behaviour of cervical vertebrae, intervertebral discs, facet joints and uncovertebral joints. Substantial data are available for the cervical ligaments.

Vertebrae   Yamada [125] reported the force and relative deformation at failure for wet cervical vertebrae. Vertebrae failed at 1000 N and 0.75% shortening in compression and at 3090 N and 6.6% elongation in tension. Thus, vertebrae do not deform much.

Intervertebral Discs   Few data are available for the mechanical behaviour of cervical intervertebral discs. Pintar *et al.* [83] measured load-displacement curves for quasi-static tension at a rate of 1 cm/s. Stiffness was defined as the slope of the most linear part of the sigmoidal-shaped curve and averaged 68 N/mm for 20 specimens (C2-C3 to C7-T1). This is about the same as the average of the ratios of force to displacement at failure (64 N/mm) which reflects the average linear stiffness for the complete curve. For the other load directions, the data for disc segments reported by Moroney *et al.* [61] may be used (Table 2.3), although these segments also comprise the longitudinal ligaments and uncovertebral joints. Furthermore, axial preloads were applied which may have resulted in stiffening of the discs.

Facet and Uncovertebral Joints   No quantitative data on the mechanics of facet and uncovertebral joints are known for the cervical spine. The articular facets and uncinate processes of these synovial joints are covered with a thin layer of hyaline cartilage allowing for gliding motion with almost no friction, due to the lubrication with synovial fluid [24]. Thus, little deformation of the thin cartilage layer and stiff vertebra is expected in compression, and resistance is offered through capsular ligaments in tension and shear.

Ligaments   The mechanical characteristics of (cervical) spinal ligaments have been determined by Chazal *et al.* [11], Dvorak *et al.* [20], Myklebust *et al.* [64] and Yoganandan *et al.* [127]. They all used bone-ligament-bone specimens to preserve the insertions of the ligaments into the bone. Ligaments were loaded to failure using a constant loading rate ranging from 1/60 up to 2500 mm/s. The load-displacement curves typically had a sigmoidal shape with a fairly linear elastic zone.

Chazal *et al.* presented the load and deformation at the start and end of the elastic zone as well as at failure for 39 ligaments from C2-C3 down to L5-S1 loaded at 1/60 mm/s. For one cervical anterior and three posterior longitudinal ligaments, they found failure forces and displacements of 140 N and 2.4 mm, respectively, 185 N and 2.4 mm. Dvorak *et al.* reported only average failure forces of 214 N and 354 N for 11 alar and 7 transverse ligaments loaded at 1.5 mm/s. Myklebust *et al.* tested 402 spinal ligaments (C2-C3 to L5-S1) at a rate of 1 cm/s. For almost all upper and lower cervical ligaments, the average force and displacement at failure are given for

each spinal level. For the lower cervical spine, average failure forces range from 34 N
(at 7.3 mm elongation) for the interspinous ligament to 215 N (at 8.7 mm) for both
joint capsules. Yoganandan *et al.* loaded 54 cervical anterior longitudinal and flaval
ligaments at rates of 9, 25, 250 and 2500 mm/s. They found that failure force and
stiffness increased with increasing loading rate, but that the displacement at failure
varied little with loading rate. Averaged for both ligaments, failure force increased
from 127 N at 9 mm/s to 343 N at 2500 mm/s. Stiffness, defined as the slope of
the linear region of the load-displacement curve, increased accordingly from 19 to 87
N/mm.

Average forces and displacements at failure have been reported for most cervical
ligaments. Stiffnesses are reported only by Yoganandan *et al.* and average 15 and 22
N/mm for the anterior longitudinal and flaval ligament loaded at 9 mm/s. In contrast,
much larger EZ-stiffnesses of 71 and 104 N/mm are estimated from the data of Chazal *et
al.* for the anterior and posterior longitudinal ligaments loaded as slowly as 1/60 mm/s.
The reason for this difference is not clear, but seems to originate from differences in
measured displacements: the failure displacements of Yoganandan are three to four
times as large as the displacements of Chazal, whereas the failure forces are of similar
magnitude.

2.5   Injury Mechanisms

Cervical spinal injuries may result from direct impact to or inertial loading of the head
and neck. A neck *injury mechanism* is the process through which a load applied to
the neck leads to deformation or loading of tissues within the neck beyond recoverable
limits, resulting in injuries of these tissues [120]. In practise, injury criteria are used
to determine whether an injury took place. An *injury criterion* is a physical parameter
or a function of several physical parameters that correlates well with a specific injury.
It is related to quantities that can be measured relatively easily, like the (maximum)
acceleration of the head. The *tolerance level* is the level of the injury criterion beyond
which the risk of sustaining an injury becomes too large. The determination of injury
mechanisms, injury criteria and tolerance levels is extremely difficult because of the bi-
ological variability, the nonlinear viscoelastic behaviour of tissues, and the wide variety
of loading conditions that are involved.

To determine neck injury mechanisms in detail, it is necessary to determine, first,
how the loads that are imposed on the cervical spine are transferred to loads on and
deformations of individual tissues, and, second, how these tissue loads and deformations
result in injury of the tissues. Thus, the load applied to the neck needs to be related
to injuries through loads and deformations of individual tissues to describe neck injury
mechanisms. In experimental research, these tissue loads and deformations are often
impracticable if not impossible to determine, but a mathematical model may be able to
provide them. Consequently, the experimental and numerical approach to neck injury
mechanisms differ.

In the experimental approach, injury mechanisms are basically determined as follows. A cervical spine specimen is subjected to loads representing a certain (postulated) injury mechanism. Load and deformation of the specimen are measured until failure of the specimen. Examination of the specimen, then, reveals the injured tissues so that the applied load or injury mechanism can be related to possible injuries. Information about the loads and deformations of the tissues is usually not obtained.

In the numerical approach, a sufficiently detailed mathematical model is used to convert the loads applied to the specimen into tissue loads and deformations, which are compared with injury criteria of these tissues to determine whether injury took place. Predicted injuries of the tissues and predicted failure strength of the specimen may then be correlated with experimental results to validate the model. If valid, the model provides a detailed description of the injury mechanism. A valid model can be used to extend experimental data to loading conditions for which experiments are not feasible and it can provide data that cannot be measured experimentally. Then, the model can be used to define (new) injury criteria.

In the literature on spinal injuries, injury mechanisms are often defined as equivalent to a loading condition. Of all loads the neck is exposed to in an accident, the injury mechanism may be thought of as the most important load or combination of loads that actually causes the injury. The injury mechanism has been referred to as the major injuring vector (White and Panjabi [110]) or the principal applied load (McElhaney and Myers [48]) and is used, in practice, to classify injuries. For example, Table 2.6 shows a part of the classification used by McElhaney and Myers: only injuries that may result from compression alone, or from compression in combination with flexion or extension are given here. Clearly, different injuries may result from the same loading situation due, among other factors, to differences in the load magnitude. Allen *et al.* [1] used the load magnitude to range injuries of the lower cervical spine from minor to severe within a given injury mechanism. For example, facet dislocation will occur secondary to hyperflexion sprain for sufficiently large compression-flexion loads. In reality, injury mechanisms are more complex due to other, minor loads that modify the principal load.

For whiplash, there is not a single injury mechanism. The loading condition most

Table 2.6: Partial classification of injury mechanisms (principal applied load) and injuries of the cervical spine (Adapted from McElhaney and Myers [48]).

principal applied load	possible injuries
compression	multi-part atlas fracture
	vertebral body compression fracture
	burst fracture
compression-flexion	vertebral body wedge compression fracture
	hyperflexion sprain
	unilateral or bilateral facet dislocation
compression-extension	posterior element fractures

often identified with whiplash is hyperextension, such as is caused by rear-end impacts. Nowadays, it is recognized that whiplash may follow from other loading conditions as well, although the rear-end impact is still the most common cause of whiplash. Recently, Barnsley *et al.* [5] extensively reviewed the literature on the etiology and pathology of whiplash and concluded that in whiplash injuries the "cervical facet joints, intervertebral discs, ligaments and muscles can be seriously injured without necessarily producing clinical or radiological signs". They stated that tears and sprains of muscles and ligaments are likely to heal within several weeks with loss of pain, but injured discs and joints do not heal completely and will result in chronic symptoms. They could not identify a specific injury mechanism as all these injuries can be caused by bending as well as shear loads.

The injury mechanisms of most cervical injuries seem to be known according to classifications presented in the literature [1, 29, 39, 110], which resemble the one given in Table 2.6. However, the use of such a classification in experimentally and numerically simulated crashes is limited, since it is a qualitative description which does not consider tissue loads and deformations. To be useful, injury criteria need to be known for each mechanism and injury. Numerous experimental studies have been presented that deal with injury mechanisms and criteria [4, 32, 48, 90]. Apart from biological variability, a major problem is that injury criteria depend on the type of specimen used: it may make a difference whether the specimen is an isolated tissue, a motion segment, a head-neck complex, or even an intact cadaver. Despite numerous efforts, few neck injury criteria have been proposed to date. Mertz [55] presents neck injury criteria which are used for Hybrid III dummies; tolerance levels ('injury assessment reference values') are given for the loads measured at the occipital condyles of the dummy. McElhaney and Myers [48] summarize data, obtained from several studies, which may be used to define neck injury tolerance levels. A mathematical head-neck model can be a useful tool to integrate and extend the vast amount of experimental data such that reliable criteria can be defined that can easily be measured in experiments.

2.6 Conclusions

The anatomy of the human cervical spine is complex. Mechanically relevant tissues are the vertebrae, the intervertebral discs, the ligaments, the facet and uncovertebral joints, and the muscles. The soft tissues allow for motion between the individual vertebrae and, consequently, for the high mobility of the head relative to the torso. Neck muscles are needed to stabilize and move the head and neck.

Mechanical characteristics have been determined for most tissues and for motion segments of the upper and lower cervical spine. Vertebrae may be treated as rigid as they do not deform much under load in comparison with the soft tissues. Ligaments have been tested extensively for quasi-static and dynamic loading, but mostly the force and elongation at failure are reported only. Cervical intervertebral discs have been examined only in quasi-static tension, although the static disc-segment experiments of

Moroney *et al.* [61] provide data for the other loads. The facet and uncovertebral joints are stiff in compression only; for the other load directions, the mechanics of these joints are largely determined by their capsular ligaments.

The mechanics of lower cervical motion segments have been determined for static, physiologic loads in all directions, and for quasi-static loads in the midsagittal directions only. Results of experiments with dynamic loading have not been reported to date. The results obtained in these studies differ largely, which is most likely due to differences in the experimental set-ups, and due to the nonlinear behaviour of tissues, as was pointed out in Section 2.4. Stiffness increases with increasing load, and may be influenced by the axial compressive preloads used in some studies. Additional experiments are needed to clarify these differences.

For the upper cervical spine, only moment-rotation characteristics, and no force-translation characteristics, have been determined for static, physiologic loads. This is not a real limitation as the upper cervical spine does not easily allow for translational deformations. Nevertheless, force-displacements characteristics should be determined to quantify this. Quasi-static and dynamic loading have only been applied in axial rotation up to failure of C0-C2 specimens.

In conclusion, the *in vitro* mechanical characteristics are fairly complete, except for dynamic loading. Missing characteristics may be estimated through comparison with other segments, tissues, and loading directions or magnitudes for which characteristics have been quantified. Then, a complete data set for the mechanical behaviour may be obtained that can be used to model the cervical spine. Additional experiments will be needed to fill the gaps and provide data for dynamic loading conditions similar to those experienced in car crashes.

The injury mechanisms of most cervical injuries seem to be known qualitatively. No well-established neck injury criteria have been presented in the literature, despite numerous experimental efforts to quantify the loading conditions that may lead to a specific injury. A mathematical model will be useful to integrate the experimental data such that injury criteria can be defined. To this end, the model must describe soft tissue loads and deformations and should, therefore, include separate representations of the individual soft tissues. Vertebrae may be treated as rigid bodies.

To gain insight and limit model complexity, a relatively simple model will be developed first in which the behaviour of the intervertebral soft tissues is lumped into a single element representing motion segment behaviour (Chapter 3). This intervertebral joint model will have less parameters, and the parameters can be obtained directly from the experiments on cervical motion segments reviewed in this chapter. Then, a more detailed model will be developed, starting with detailed models of segments of the upper and lower cervical spine in which disc, ligaments and facet joints are modelled separately (Chapter 4). Finally, the segment models will be assembled into a detailed head-neck model, which will also include active muscle elements (Chapter 5).

Global Head-Neck Model
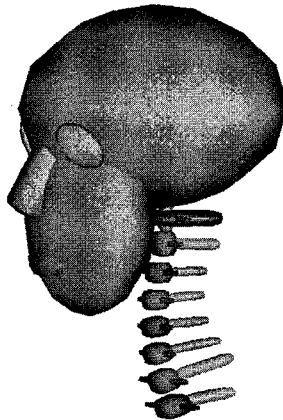
The modelling strategy adopted in this research is to proceed from a simple model to a more detailed one. Two simple models were developed. The first one was based on the model presented by Deng and Goldsmith in 1985 [14, 15]. This model was chosen because its simplicity would enable a clear insight into its behaviour, and because all input data could be extracted from the original publications. The model was modified to remove inaccuracies, and validated for frontal and lateral impacts, as was described in detail by De Jager et al. [35]. The Deng-model proved to be a good starting point, as validation and a sensitivity analysis revealed the capabilities and insufficiencies of, and possible enhancements to the model. The second model that was developed is the subject of this chapter. This new model, which will be referred to as the global model, comprises head and vertebrae as rigid bodies and the intervertebral joints as nonlinear viscoelastic elements. Section 3.1 describes the global model and summarizes the differences with the Deng-model. Section 3.2 compares the model response with human volunteer responses to frontal impacts. Section 3.3 gives the results of a systematic parametric study. Section 3.4 concludes this chapter with a discussion.

3.1 Model Description

The global model comprises nine rigid bodies for the head, the seven cervical vertebrae and the first thoracic vertebra (T1). The bodies are connected by nonlinear viscoelastic elements with load-displacement characteristics derived from recent (1986-1994) experimental data on cervical motion segment behaviour. The lower joints have basically the same characteristics and the upper cervical joints have unique characteristics. For simplicity, muscle behaviour is lumped into the intervertebral joint stiffnesses. The model was implemented using the multi-body part of the integrated multi-body/finite-element package MADYMO, version 5.1.1, of the TNO Crash-Safety Research Centre [107]. Theoretical backgrounds on multi-body dynamics are provided, among others, by Roberson and Schwertassek [89] and Wittenburg [122].

3.1.1 Rigid Head and Vertebrae

Nine rigid bodies represent the head, the seven cervical vertebrae and the first thoracic vertebra (T1). Table 3.1 shows the numbering of the bodies, in which body 1 for T1 serves as the base of the head-neck model. The motion of T1 is prescribed to simulate impacts. Below, the configuration and inertial properties of the model are presented.

Configuration The position and the orientation of a body are described relative to its adjacent lower numbered body. Therefore, a local right-handed coordinate system was assigned to each body (see Section 2.2). The local coordinate system of T1 is the reference coordinate system with the x, y, z-axes pointing forwards, to the left and upwards. The origin of the local coordinate system of body j is defined relative to the

Table 3.1: Inertial and geometric data used for the rigid bodies in the global model. Body 1 for T1 serves as the base of the model; its body local coordinate system is the reference coordinate system. Data for C0 includes correction for instrumentation with a mass of 0.53 kg [105]. Due to midsagittal symmetry, $s_y = g_y = 0.0$.

no.	name	mass	moments of inertia				origin of coordinate system		position of centre of gravity		initial orientation
			I_{xx}	I_{yy}	I_{zz}	I_{xz}	s_x	s_z	g_x	g_z	ϕ_y
		kg	kg·cm^2				mm		mm		deg
1	T1	–	–	–	–	–	0.0	0.0	–	–	0.0
2	C7	0.22	2.2	2.2	4.3	–	6.4	16.8	−8.2	0.0	20.8
3	C6	0.24	2.4	2.4	4.7	–	−2.0	18.4	−8.3	0.0	−5.6
4	C5	0.23	2.3	2.3	4.5	–	−2.8	17.4	−8.1	0.0	−5.2
5	C4	0.23	2.3	2.3	4.4	–	−3.3	17.2	−7.9	0.0	−4.7
6	C3	0.24	2.4	2.4	4.6	–	−4.0	17.8	−7.8	0.0	−5.3
7	C2	0.25	2.5	2.5	4.8	–	−3.3	18.7	−7.7	0.0	0.0
8	C1	0.22	2.2	2.2	4.2	–	0.0	16.5	−7.7	0.0	0.0
9	C0	4.69	181.0	236.0	173.0	71.0	−4.0	20.0	27.0	43.0	0.0
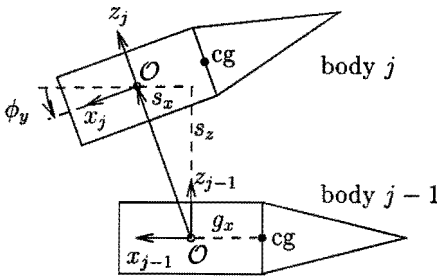
Figure 3.1: Definition of the position of the origins ($\mathcal{O}$) of the local coordinate systems and the centres of gravity (cg) of the bodies.
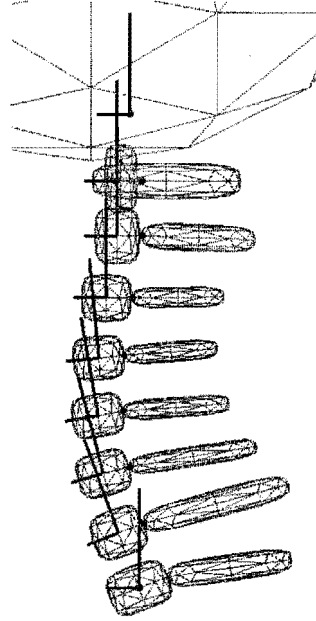
Figure 3.2: Lateral view of the global model; shown are the vertebrae and base of the skull with their body local coordinate systems.

coordinate system origin of the lower body $j-1$ by the coordinates s_x, s_y, s_z expressed in the lower body coordinate system (Fig. 3.1, Table 3.1). The coordinate system origins were positioned at the geometric centre of the vertebral bodies of vertebrae T1 through C2. The coordinate system of C1 originates in the upper part of the dens as C1 has no body. The coordinate system of C0 was placed above and slightly posterior to the occipital condyles at the apparent centre of rotation of the head relative to C1 [38, 43]. The relative orientation of a body is given by the angle ϕ_y about the y-axis of the lower body; the initial orientation of the bodies represents the cervical lordotic curve. Simple geometric shapes are used to visualize the head and vertebrae (Fig. 3.2), between which contact was not defined.

The initial configuration of the rigid bodies were derived from experimental data, see Appendix A. The relative positions and orientations of the lower cervical vertebrae were derived from the data presented by Nissan and Gilad [67] which were based on lateral X-rays of young males standing erect. The average length and weight of these volunteers compare well with those of the (NBDL-)volunteers who were subjected to frontal impacts and whose head-neck motions are used to validate the model (see

Section 3.2). Further, the reconstructed orientation of C2 relative to C7 is 20.8 deg for the model, which compares favourably with the orientation of 21.6 deg measured by Gore *et al.* [28] from lateral X-rays of males standing erect. Thus, the rigid body configuration of the model can be considered to represent the head and neck of an average young male of about 170 cm length and 70 kg weight.

Inertial Properties   The inertial properties of head and neck are lumped into the rigid bodies. The position of the centre of gravity of body j is given in the local coordinate system of body j by the coordinates g_x, g_y, g_z (Fig. 3.1, Table 3.1). The (principal) moments of inertia are defined with respect to a coordinate system originating at the centre of gravity and parallel to the local coordinate system. The inertial properties of the head and the position of the head centre of gravity match the average properties of the NBDL-volunteers given by Thunnissen *et al.* [105]. Their inertial data were converted to express them in the inertial coordinate system used here. The head mass includes the mass of the instrumentation (0.53 kg) worn by the volunteers.

The inertial properties assigned to the vertebrae represent the inertia of segments of the neck including the vertebrae and surrounding soft tissues. The properties were estimated assuming that the straightened neck is a cylinder formed by seven neck segments with heights simply set equal to s_z, the vertical distance between the origins of adjacent body local coordinate systems (Table 3.1). The volume and radius of the cylinder can be calculated using a total neck mass of 1.63 kg and an average density of 1170 kg/m³ as derived from Walker *et al.* [109]. Calculating mass and moments of inertia of individual segments, then, is straightforward. Following Merrill *et al.* [54], the centre of gravity of each neck segment was assumed to lie at the posterior margin of the vertebral bodies at the same height as the geometric centre of the body. Rough estimates for the inertial data of the vertebrae are allowed, as it was found that changes in these data hardly influenced the response of the Deng-model to impacts [35].

3.1.2 Nonlinear Viscoelastic Intervertebral Joints

The rigid bodies are connected by intervertebral joints that represent the compound behaviour of intervertebral disc, ligaments, facet joints and muscles. The nonlinear elastic characteristics of the joints are based on experimental data representing the *in vitro* mechanics of segments of the upper and lower cervical spine (presented in Chapter 2). A scale factor was introduced with which the joint stiffnesses can be modified to include the effect of muscle behaviour on the head-neck response.

Joint Model   Intervertebral joint behaviour is modelled as a parallel connection of a spring and a damper, for each degree of freedom. Thus, joint loads are given by

$$
\begin{aligned}
F_i &= k_{ti}(t_i) \cdot t_i + b_{ti} \cdot v_i, \\
M_i &= k_{\phi i}(\phi_i) \cdot \phi_i + b_{\phi i} \cdot \omega_i \quad (i = x, y, z),
\end{aligned}
$$

in which F_i and M_i are the components of the forces and moments with respect to the i-axis of the lower body, t_i and ϕ_i the relative translations and rotations, and v_i and ω_i

moment   force
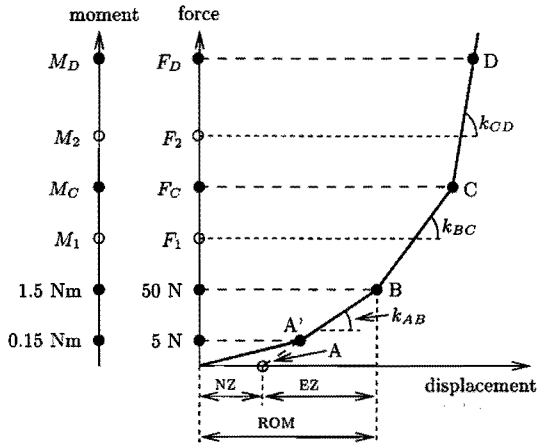
Figure 3.3: Determination of the load-displacement curves for the intervertebral joints from experimental data. See text for details. Graph is not to scale.

the relative translational and rotational velocities. Elastic behaviour is modelled with nonlinear stiffnesses k that depend on the relative displacements; they are prescribed using load-displacement curves. Viscous behaviour is represented by constant damping coefficients b. No reliable data were available to estimate the damping coefficients; therefore, the coefficients were determined such that a satisfactory model response was obtained, see Section 3.2.

The definition of the relative translations and rotations, and the application of the loads to the vertebrae were chosen in agreement with the experimental set-ups from which the results were used to define the load-displacement data. The translation of the upper body is defined as the translation of its coordinate system origin relative to the lower body coordinate system. Bryant angles (in the order x, y, z) are used to resolve the relative three-dimensional orientation of the bodies into three rotations. The joint loads are applied to both the upper and lower vertebrae at the coordinate system origin of the upper body; that is, at the geometric centre of the upper vertebral body. This point is fixed to the upper body and moves relative to the lower body.

Lower Cervical Joint Stiffness Figure 3.3 schematically presents the method used to derive the load-displacement curves for the lower cervical joints from the experimental data presented in Section 2.4.1. Points A and B represent the neutral zone (NZ) at zero load and the range of motion (ROM) at maximum applied load (50 N, 1.5 Nm) as given by Panjabi et al. [79, 76], see Table 2.2. Stiffness k_{AB} of the elastic zone (EZ) was calculated as the maximum applied load divided by the displacement from A to B. Point A' along the curve at 10% of the maximum load was used instead of A to have a well-defined reference position (equilibrium) for the joints. The data of Panjabi et al. [79, 76] were used, as these data accurately describe the nonlinear behaviour for loads
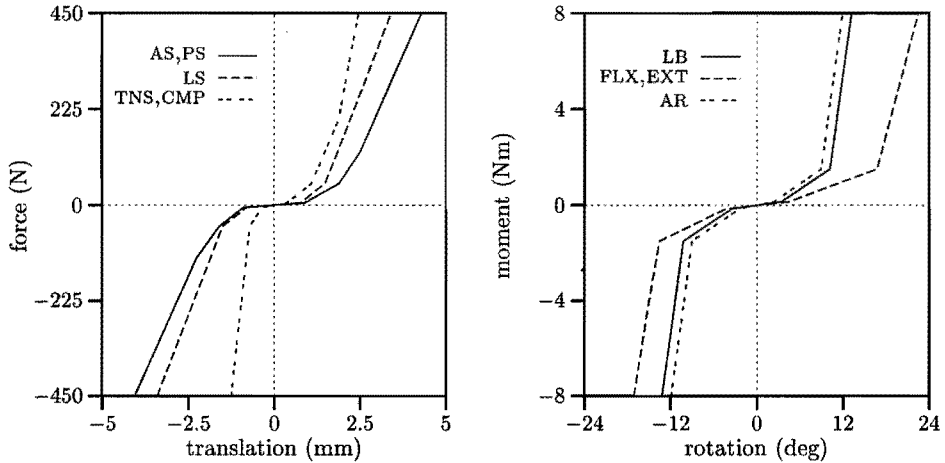
Figure 3.4: Load-displacement curves for the intervertebral joints of the lower cervical spine. Data are given in Table 3.2

that are large enough to quantify the *in vitro* range of motion; the data of Moroney *et al.* [61] and Goel *et al.* [27, 26] only give linear behaviour and were mostly obtained for very small loads (20 N, 0.3 Nm) compared with Panjabi *et al.* (50 N, 1.5 Nm).

Points C and D were derived from the data of Shea *et al.* [97], who reported two stiffnesses (k_{BC}, k_{CD}) at two different load magnitudes $(F_1, F_2$ or $M_1, M_2)$; the corresponding displacements were not reported. Stiffnesses k_{BC} and k_{CD} are used to extend the curve from B to C, respectively, C to D, where the load at C is the average of loads F_1 and F_2 (or M_1 and M_2) and the load at D is sufficiently large. For k_{BC} and k_{CD}, the average stiffnesses for all vertebral levels (C2-T1) were used, see Table 2.3. Although these stiffnesses were obtained for quasi-static (viscoelastic) loading, they can be used to represent static (elastic) behaviour, since Shea *et al.* pointed out that the stiffnesses did not significantly differ from the stiffnesses obtained at much lower loading rates.

No stiffnesses beyond point B were available for lateral shear, lateral bending and axial rotation as Shea *et al.* only used midsagittal loads. For these loads, characteristics were determined by appropriate scaling: stiffness k_{BC} was obtained by multiplying stiffness k_{AB} with the average of the ratios k_{BC}/k_{AB} for the midsagittal loads. This resulted in $k_{BC} = 212$ N/m in lateral shear, 2.20 Nm/deg in lateral bending and 2.40 Nm/deg in axial rotation. Point C was chosen at a sufficiently large load and D is not used.

Figure 3.4 shows the resulting load-displacement curves for all six degrees of freedom. The curves for lateral shear, lateral bending and axial rotation are symmetrical. Table 3.2 gives the load-displacement data, which are the same for all joints. These curves describe the *in vitro* elastic behaviour of motion segments of the lower cervical

Table 3.2: Coordinates of points of the load-displacement curves shown in Figure 3.4.

force-translation data		A'		B		C		D	
		mm	N	mm	N	mm	N	mm	N
AS	anterior shear	0.9	5	1.9	50	2.5	125	12.8	2000
PS	posterior shear	−0.9	−5	−1.6	−50	−2.3	−125	−13.8	−2000
LS	lateral shear	0.8	5	1.5	50	10.8	2000		
TNS	tension	0.4	5	1.1	50	1.9	200	6.0	2000
CMP	compression	−0.3	−5	−0.7	−50	−1.2	−400	−2.9	−2000

moment-rotation data		A'		B		C		D	
		deg	Nm	deg	Nm	deg	Nm	deg	Nm
LB	lateral bending	3.5	0.15	10.2	1.5	23.3	30.0		
FLX	flexion	4.5	0.15	16.7	1.5	41.9	30.0		
EXT	extension	−4.2	−0.15	−13.5	−1.5	−15.1	−4.3	−28.8	−30.0
AR	axial rotation	2.4	0.15	9.0	1.5	21.8	30.0		

spine. A difference with *in vivo* behaviour is seen when comparing the average *in vitro* ROMs (at 1.5 Nm) with the average *in vivo* ROMs reported by White and Panjabi [110], see Table 3.3. Clearly, the *in vitro* ROMs are much larger than the *in vivo* ROMs for rotation. Thus, using the *in vitro* data will result in an unrealistic model that is much too flexible. To prevent this, the data were modified for each joint separately by multiplying the rotations with the ratio of the *in vivo* ROM for that joint to the average *in vitro* ROM. Thus, the rotation axis of the moment-rotation curves is linearly scaled such that at 1.5 Nm the *in vivo* ROM is found. Consequently, the modified moment-rotation curves are now different for each joint and reflect the regional differences found *in vivo*. For translational ROMs, no correction was applied because no *in vivo* data were available.

Table 3.3: Differences in the *in vitro* and *in vivo* ranges of motion for the lower joints. Data taken from Tables 2.1 and 2.2. The ratio 16.7/13.5 of the *in vitro* ROMs for flexion and extension is used to divide the *in vivo* ROMs for combined flexion/extension into separate ROMs.

	in vitro	*in vivo*						
motion	average C2–T1	average C2–T1	C2-C3	C3-C4	C4-C5	C5-C6	C6-C7	C7-T1
	deg				deg			
lateral bending	10.2	8.5	10	11	11	8	7	4
flexion	16.7	8.4	5.5	8.3	11.1	11.1	9.4	5.0
extension	13.5	6.8	4.5	6.7	8.9	8.9	7.6	4.0
axial rotation	9.0	5.3	3	7	7	7	6	2

Upper Cervical Joint Stiffness   Static moment-rotation characteristics are available for the C0-C1 and C1-C2 joints separately, whereas quasi-static and dynamic data are available only for rotation of C0 relative to C2 (Section 2.4). To obtain the moment-rotation curves for the upper cervical joints, a similar procedure as above was used for the first part of the curves. Points A and B represent the NZ and ROM at 1.5 Nm, which were averaged from the results of Panjabi and co-workers [68, 73, 75, 72], see Table 2.4. Averaging is justified since the experimental procedures used in these studies are alike (Section 2.4). Point A' ensures a well-defined reference position for the joints.

To extend the curves beyond 1.5 Nm, stiffness k_{BC} was estimated by scaling the EZ-stiffness using the quasi-static data for axial rotation of C0-C2 given by Chang *et al.* [10]. They reported a stiffness of 0.383 Nm/deg for the linear part of the curve starting at [30 deg, 2.0 Nm]. This stiffness represents the combined stiffness of C0-C1 and C1-C2. For a series connection of two springs with stiffnesses k^{01} and k^{12}, the combined stiffness k^{02} follows from $1/k^{02} = 1/k^{01} + 1/k^{12}$. Stiffness k_{AB}^{02} was calculated using the known stiffnesses k_{AB}^{01} for C0-C1 and k_{AB}^{12} for C1-C2. For the part of the curve after point B, only stiffness k_{BC}^{02} of C0-C2 is known for axial rotation. Because the ratio $k_{BC}^{02}/k_{AB}^{02} = 4.0$ of the combined spring holds also for the individual springs, stiffness k_{BC} could be calculated for axial rotation of C0-C1 and C1-C2. For flexion, extension and lateral bending, it was assumed that the increase in stiffness from the AB-part to the BC-part of the curve is the same as for axial rotation.

Figure 3.5 shows the resulting moment-rotation curves that represent the *in vitro* elastic behaviour of the C0-C1 and C1-C2 joints, and Table 3.4 gives the corresponding data. When the ROMs at 1.5 Nm are compared with the *in vivo* ROMs presented in Table 2.4, it is observed that they agree very well. Therefore, no correction for the *in vivo*
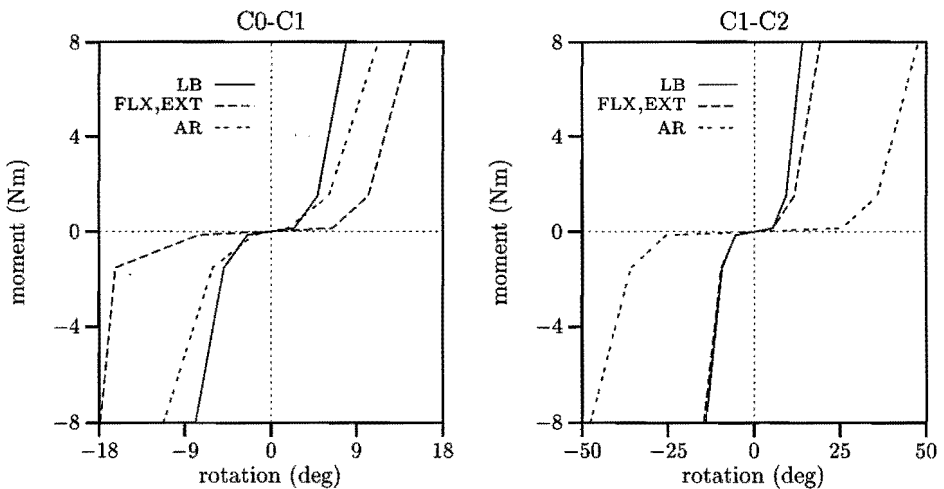
Figure 3.5: Moment-rotation curves for the upper cervical joints C0-C1 and C1-C2. Data are given in Table 3.4.

Table 3.4: Coordinates of points of the moment-rotation curves shown in Figure 3.5.

| | C0-C1 | | | | | | C1-C2 | | | | | |
| | A' | | B | | C | | A' | | B | | C | |
	deg	Nm	deg	Nm	deg	Nm	deg	Nm	deg	Nm	deg	Nm
LB	2.5	0.15	4.9	1.5	13.4	20.0	5.4	0.15	9.3	1.5	22.7	20.0
FLX	6.5	0.15	10.2	1.5	36.6	40.0	5.5	0.15	11.7	1.5	33.1	20.0
EXT	−7.6	−0.15	−16.3	−1.5	−78.7	−40.0	−5.3	−0.15	−9.6	−1.5	−24.1	−20.0
AR	1.8	0.15	6.1	1.5	20.8	20.0	25.6	0.15	35.8	1.5	69.4	20.0

ROMs was introduced for these joints. Because no force-translation data were available, these characteristics are simply modelled by assuming a relatively large stiffness of 500 N/mm. This stiffness results in little translational motion under normal physiologic loads which agrees with observations for these joints (Section 2.3).

Scale Factor for Joint Stiffness Preliminary simulations showed that the model was much too flexible compared with human volunteers subjected to frontal impacts. A factor was introduced to scale the joint stiffnesses, such that the model response can be calibrated with experimental responses. This factor can be considered to represent the difference in stiffness between *in vitro* and *in vivo* joint behaviour as well as the increased neck stiffness due to muscle tensioning. Muscle tensioning leads to larger axial compression forces on the joints, which may result in larger joint stiffnesses, similar as was found for lumbar intervertebral joints [36, 111]. Furthermore, muscle forces will counteract (involuntary) head motion and, thus, increase the overall neck stiffness.

The factor scales the *displacement* axis of the load-displacement curves of the joints, since Wilke *et al.* [111] found that simulated muscle loads could reduce the NZs and ROMs of lumbar motion segments to 10–50% of the NZs and ROMs in the unloaded situation. (The maximum load at which the ROMs were measured, were the same in both situations.) It is, thus, assumed that the ROMs of cervical motion segments are also reduced through muscle tensioning. In the model, joint stiffness increases for a factor less than 1 and it decreases for a factor larger than 1. A separate factor was introduced for each of the nine relevant motions: tension, compression, lateral shear, anterior shear, posterior shear, flexion, extension, lateral bending and axial rotation. Due to the lack of data, it was assumed that muscle loads affect the joint stiffnesses to the same extent at each vertebral level: each scale factor is the same for all joint levels.

3.1.3 Differences between the Global Model and the Deng-model

The global model has improved characteristics compared to the model of Deng and Goldsmith. The main differences between the Deng-model and the global model are the modelling of the intervertebral joints and of the muscles. The global model comprises rigid head and vertebrae and nonlinear viscoelastic intervertebral joints, which also include muscle behaviour. The Deng-model comprises rigid head and vertebrae, linear viscoelastic intervertebral joints and nonlinear elastic muscle elements.

In the global model, *nonlinear* elastic characteristics are used that are based on *cervical* motion segment behaviour, whereas in the Deng-model, *linear* elastic characteristics are used that were mainly based on *thoracic* motion segment behaviour. The global model, however, does not include coupling behaviour as opposed to the Deng-model, since no reliable experimental data were found to quantify this coupling accurately (as was pointed out in Chapter 2). Moreover, it was found that the coupling present in the Deng-model had only a small effect on the model response [35].

The global model uses *unique* load-displacement characteristics for the upper cervical joints to account for the unique and different structural properties of these joints. The moment-rotation characteristics of its lower cervical joints reflect the *experimentally found* variation in mechanical behaviour with vertebral level. The Deng-model, in contrast, applies the *same* stiffnesses to all (upper and lower) joints, and scales the joint loads proportional to the cross-sectional area of the intervertebral disc to incorporate an *assumed* variation in mechanical behaviour with vertebral level.

In the global model, muscle behaviour is lumped into the joint characteristics through scale factors with which joint stiffnesses can be increased to account for increased neck stiffness due to muscle tensioning. The Deng-model has nonlinear springs to represent passive muscle behaviour, but these muscle elements only moderately influenced the response of the model [35].

3.2   Model Response to Frontal Impacts

This section presents the verification of the model response to frontal impacts, which can be considered as a first step towards a complete model validation. The model has to be validated to check its capability to predict the dynamic response of the human head and neck to impacts. An accurate validation is achieved by correlating model responses with experimentally obtained head-neck responses to various impacts. In the present study, response corridors are used that are based on sled acceleration tests performed with human volunteers in frontal impacts. These corridors specify the responses that a valid model has to meet. Only the response to frontal impacts is considered as it was found that joint parameters had to be modified to *calibrate* the model response with the corridors. First, the volunteer tests and response corridors are described. Second, the calibration of the model response is presented.

3.2.1 Response Corridors

The corridors are based on the head-neck responses obtained from sled acceleration tests performed with human volunteers at the Naval Biodynamics Laboratory (NBDL), see Ewing and Thomas [21]. At the NBDL, an extensive series of impact tests has been performed with male human volunteers to obtain head-neck responses for various levels and directions of impact. Impacts have been conducted for frontal, lateral and oblique directions. In these tests, the volunteer was seated on a sled and straps were used to prevent torso motion adequately. Head and neck could move freely in response to
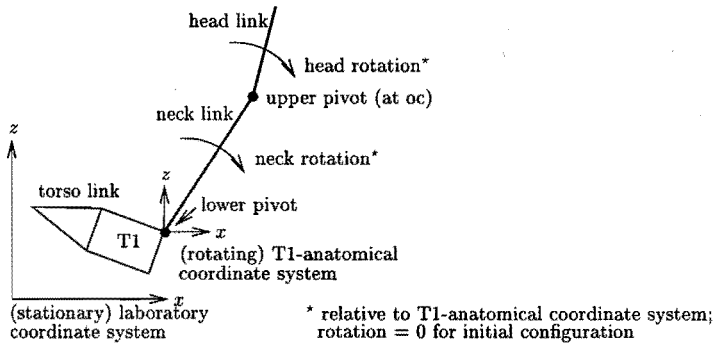
Figure 3.6: The two-pivot head-neck model used by Thunnissen *et al.* [105] to analyze the head-neck motions of the NBDL-volunteers subjected to acceleration impacts.

the impact applied by accelerating the sled from zero velocity. The three-dimensional accelerations and displacements of the head and vertebra T1 were monitored using accelerometers and high speed film.

Recently, a new analysis of the most severe *frontal* impacts was made by Thunnissen *et al.* [105], the results of which are used in the present study; therefore, a brief summary is given. More details about the tests and results can be found in Thunnissen *et al.* [105] and references cited therein. Results for the lateral and oblique impacts were presented by Wismans *et al.* [118].

Thunnissen *et al.* analyzed frontal tests in which the peak sled acceleration was $14g$ ($g = 9.81$ m/s^2) or higher (nine tests with five volunteers). The tests were analyzed using a two-pivot model of the head-neck system, which comprises three links for the head, neck and torso (T1), connected by two pivots allowing only for rotation in the plane of impact (Fig. 3.6). The neck link is flexible in axial direction. The upper pivot is located at the occipital condyles and the lower pivot at the origin of the so-called T1-anatomical coordinate system, which is positioned at the upper anterior corner of the T1-vertebral body[1]. This coordinate system is initially oriented parallel to the non-moving laboratory coordinate system (of which the x, y, z-axes point forwards, to the left and upwards) and it rotates together with T1 during the impact. Head and neck rotation are defined as the rotation of the head and neck link relative to the T1-anatomical coordinate system; both rotations are zero in the initial configuration. Neck length is defined as the length of the (flexible) neck link and equals the linear distance between the occipital condyles and the origin of the T1-anatomical coordinate system.

It was observed that the measured horizontal T1-acceleration differed from the acceleration applied to the sled due to the flexibility of straps and thorax: the peak T1-accelerations were twice the peak sled accelerations. The effect of vertical T1-accelerations was considered small enough to be neglected. The maximum rotation

---

1. In the global model, the T1-anatomical coordinate system originates at the coordinates $x = 11, z = 3$ mm in the local coordinate system of body T1 (Appendix A).

of T1 about the y-axis averaged about 22 deg. To simulate the frontal impact, the average horizontal T1-acceleration (in impact direction) is used as input to the model, since this circumvents the modelling of the straps and thorax flexibility (Fig. 3.7a). This acceleration is prescribed relative to the laboratory coordinate system. It is not needed to prescribe the rotation of T1, because it was accounted for in the analysis [105]. Measured responses for the nine tests were averaged and standard deviations were calculated. The response corridors were defined as the responses at plus and minus one standard deviation of the average response. The model response should be close to the corridors to have a sufficiently accurate model. The following corridors are used:

- The linear acceleration (resultant and x, z-components) of the centre of gravity of the head relative to the laboratory coordinate system. This implies that the sled acceleration is included in the corridors as well.

- The angular acceleration (y-component) of the head relative to the laboratory coordinate system.

- The trajectory of the occipital condyles and the centre of gravity of the head in the midsagittal plane relative to the T1-anatomical coordinate system (Fig. 3.7b). The corridor is specified for the loading phase only (up to maximum flexion).

- The rotation of head and neck versus time.

- The neck rotation versus head rotation (Fig. 3.7c). This corridor reflects two important phenomena observed for the volunteer responses in frontal impacts. Head lag: initially head rotation lags considerably behind neck rotation, as the head first translates forwards, due to its inertia, before it is forced to rotate and follow the stretched neck. Locking: starting at 30 deg head rotation, head and neck rotation increase uniformly, reflecting that head and neck move more or less as one unit; that is, the head appears to be locked to the neck preventing it to rotate relative to the neck.

- The neck length versus time.
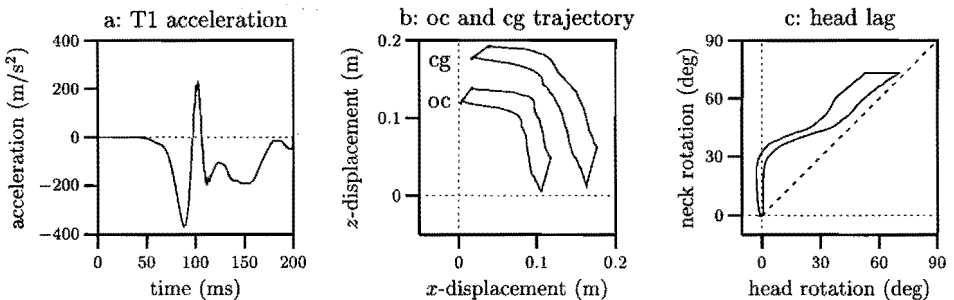
Figure 3.7: (a) Average forward T1-acceleration used as input to the model to simulate the frontal impact. (b) Response corridors for the trajectory of the occipital condyles (oc) and centre of gravity (cg) of the head in the midsagittal plane. (c) Response corridor for the head lag: neck rotation versus head rotation.

3.2.2 Calibrating the Model Response

Both scale factors and joint damping coefficients were modified to obtain a model response resembling the human volunteer response. This calibration also served to obtain a realistic starting point for a parametric study quantifying the effect of parameter changes on the model response. A simulation of a frontal impact of 200 ms typically takes about 40 CPU-seconds on an SG Indigo 2 R4400 workstation using MADYMO with a fifth order Runge-Kutta-Merson method with variable time step.

First, the scale factors were estimated with the damping coefficients set at 300 Ns/m for translational damping and 1.0 Nms/rad for rotational damping, which were taken from the Deng-model. The scale factors were found by setting them all at the same arbitrary value. For the value 0.6, a reasonable response was obtained: the major deviations between model and volunteer response were found for the peak values of the linear and angular acceleration and the maximum rotation of the head. Second, the damping coefficients were increased to 1000 Ns/m and 2 Nms/rad to obtain a better attenuation of the maximum linear and angular accelerations of the head. Note that there may exist other combinations for the values of the scale factors and damping coefficients that will result in a similar model response.

Figure 3.8 illustrates the model configurations in 10 ms intervals starting at 60 ms. Figure 3.9 shows the resulting model responses together with the response corridors. Overall, the model response is satisfactory, except for head rotation. The trajectories of the occipital condyles and the centre of gravity of the head accurately follow the corridors, but, eventually, the downward displacements become too large, especially for the centre of gravity. The neck length response is fairly accurate and shows that the head oscillates slightly too much in axial direction, suggesting that the damping coefficients may still be too small. The linear accelerations of the head centre of gravity agree qualitatively with the corridors, although the peaks outweigh the corridors. The linear accelerations of the model lag slightly behind the corridors. The
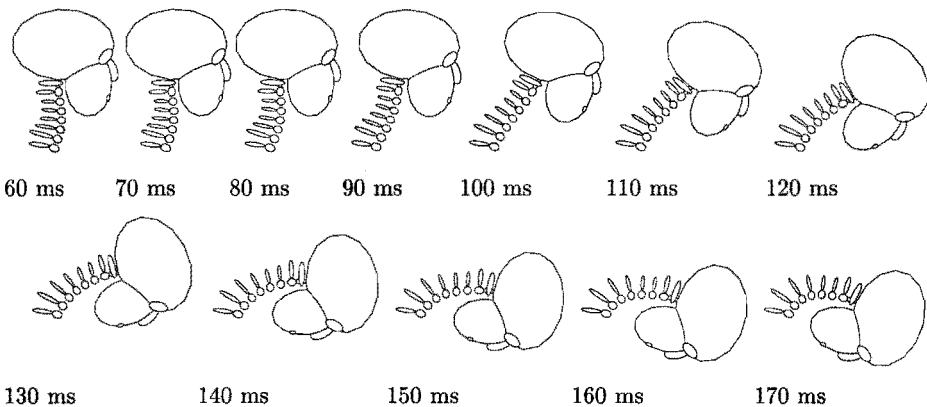
Figure 3.8: Configuration of the model for the frontal impact at 10 ms intervals.
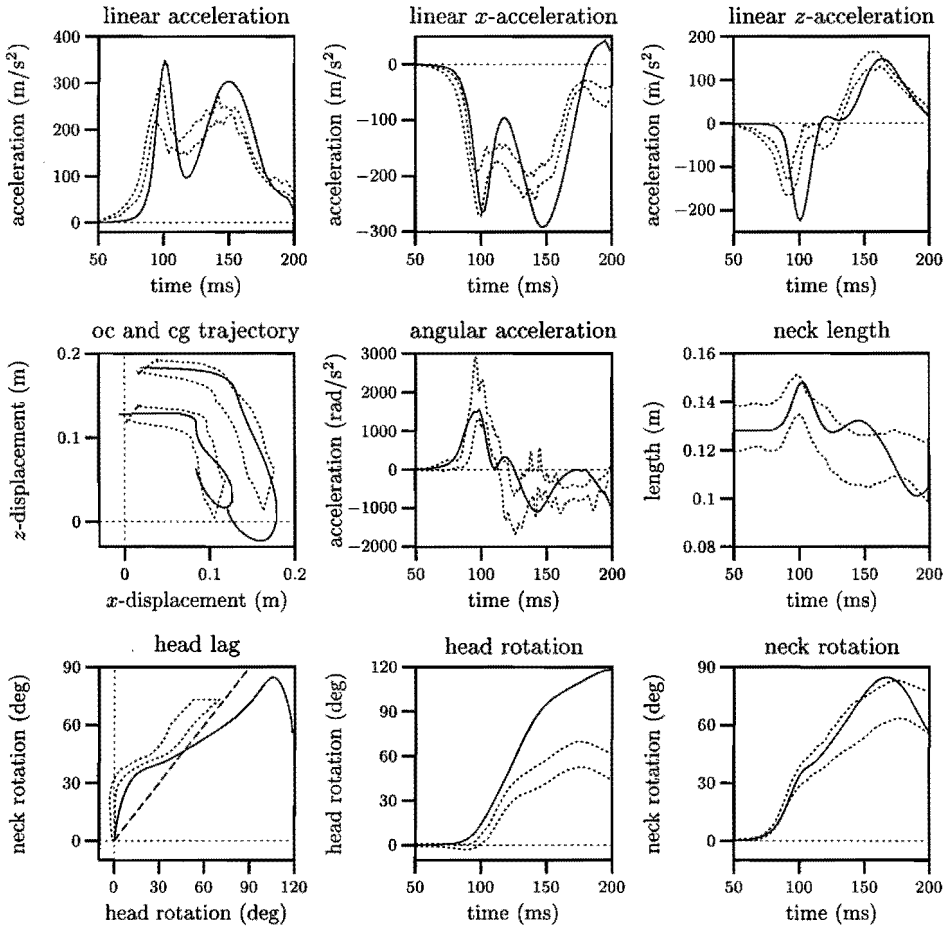
Figure 3.9: Response of the calibrated model (solid line) together with the response corridors (dotted lines) defined previously (see text).

head angular acceleration corresponds reasonably with the corridors and the maximum is well reflected. The angular acceleration increases somewhat too early as does the head rotation. Neck rotation falls well inside the corridors, while head rotation agrees poorly with the volunteer responses. The head lag response reflects that head rotation lags well behind neck rotation, although it deviates a little due to the early rise of head rotation. Eventually, head rotation exceeds the neck rotation for the model (overtipping) in contrast to the volunteers, of whom head and neck rotation increase uniformly (locking).

Figure 3.10 depicts the intervertebral joint rotations with the *in vivo* ranges of motion for static flexion/extension. These rotations clearly reflect the scenario of head-neck motion for this impact. Initially, the pure translation of the head forces the
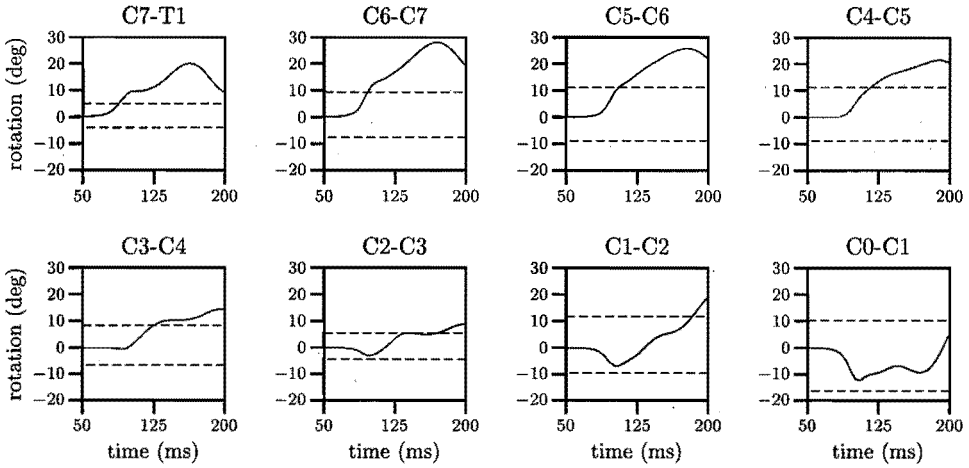
Figure 3.10: Intervertebral joint rotations for the frontal impact (solid line) and corresponding *in vivo* ranges of motion for flexion/extension from Tables 3.3 and 3.4 (dashed lines).

upper three joints into extension and the lower joints into flexion, up to the moment of maximum neck length at about 100 ms. Then, the neck forces the head to move downwards and to rotate, which increases the flexion of the lower joints and decreases the extension of the upper joints. In the end, all joints are flexed.

The magnitude of the rotations of the upper four joints appear accurate compared with the ranges of motion. The maximum rotations of the lowest four joints are at least twice as large as the ranges of motion. It appears that the *overall* neck response is described accurately, since the oc-trajectory and, consequently, the neck rotation lie well within the corridors. The joint rotations, however, reflect that the *segmental* neck response is not yet accurate, indicating that the neck is curved too strongly, and that the large head rotation is not caused by a too weak coupling between occiput and atlas, but primarily by too much rotation of the lower joints.

Clearly, head rotation is unrealistically large. If chin-torso contact had been incorporated into the model, head rotation might have been limited, but would still be too large as chin-torso contact did not occur for the volunteers. The model responses can also be compared with human cadaver responses. Wismans *et al.* [119] presented the responses of human cadavers subjected to similar sled tests and compared their responses with the same volunteer responses used here. The neck muscles of the cadavers were artificially stiffened to represent muscular tension. Main differences in response were that the cadavers had a smaller head lag, had a maximum head rotation that was about 20 deg larger, and showed overtipping of head rotation. Thus, the cadavers show a similar difference in response with the volunteers as the model, indicating that muscle tensioning limits head rotation and prevents overtipping for the volunteers.

It was found that the (maximum) head rotation could hardly be reduced without

severely deteriorating the other responses. For example, a drastic decrease of the flexion factor to 0.2 decreased not only the head rotation but also the neck rotation, such that the trajectories of the occipital condyles and centre of gravity became unrealistic. Furthermore, the head lag disappeared and overtipping occurred sooner. It was found that the minimum resultant and x-component of the linear acceleration at 120 ms was difficult to influence by small adjustments of scale factors and damping coefficients.

3.3   Parametric Study for Frontal Impacts

In the previous section, parameters were adjusted to improve the model response, but no experimental data were available to verify the resulting values for the scale factors and damping coefficients. This section describes the parametric study performed to quantify the influence of model parameters on model response. First, the selected parameters, model responses and experimental design are presented. Second, the results are summarized.

Experimental Design   Twelve parameters relevant to the model response in frontal impacts were selected (Table 3.5). For each parameter, a high (+) and a low (−) level were arbitrarily chosen such that the parameter values of the calibrated model lie in between the high and low levels. Scale factors (joint stiffness) and joint damping coefficients were chosen as these parameters were modified to calibrate the model response (Section 3.2). Head mass and moment of inertia were selected since it was found that head mass had a relatively large influence on the response of the Deng-model, see De Jager *et al.* [35]. Vertebral masses were not considered since, in the same study, it was found that the mass of a vertebra had only a small influence on the response. Finally, the initial configuration (the relative orientation) of the vertebrae were changed to represent a more curved and a more straightened neck.

Five discrete responses were defined as characteristic quantifiers of the continuous model response to frontal impacts:

- R1, the maximum resultant linear acceleration of the head (first peak);
- R2, the maximum angular acceleration of the head;
- R3, the maximum neck rotation;
- R4, the maximum head rotation; and
- R5, the rotation of the head when the neck rotation equals 25 deg — this response quantifies the head lag.

As experimental design, a fractional factorial [59] was chosen that required 32 numerical simulations (runs). This is an efficient and effective design to estimate the effect of a single parameter independently of any other parameter and of any interaction of two parameters[2]. In each run, the level of several parameters was changed such that each parameter was run 16 times at its high level and 16 times at its low level. The

---

2. This is called a Resolution IV design, for which main effects are not aliased with other main effects and with two-parameter interactions [59].

Table 3.5: Selected parameters, their levels and their effect on the model responses R1–R5; see text for definition of the responses.

parameter		level			effect on response[a]				
		−	+	[unit]	R1	R2	R3	R4	R5
scale factor									
A	anterior shear	0.4	0.8	[−]	0	0	0	0	−
B	posterior shear	0.4	0.8	[−]	0	0	0	0	0
C	tension	0.4	0.8	[−]	−	0	0	0	0
D	compression	0.4	0.8	[−]	0	0	0	0	0
E	flexion	0.4	0.8	[−]	0	0	+	+	0
F	extension	0.4	0.8	[−]	0	−	0	0	0
damping coefficient									
G	anterior/posterior shear	750	1250	[Ns/m]	0	0	0	0	0
H	tension/compression	750	1250	[Ns/m]	0	0	0	0	0
I	flexion/extension	1.5	2.5	[Nms/rad]	0	0	0	0	+
inertia of head									
K	mass	4.2	5.2	[kg]	0	0	0	0	0
L	moment of inertia (I_{yy})	186	286	[kg·cm^2]	0	0	0	0	−
initial configuration									
M	C7-T1 rotation[b]	34.8	6.8	[deg]	0	+	0	0	0

a   response with parameter at high level; difference with average response is
    0   less than 5%,
    −/+   a decrease/increase larger than 5%.
b   the rotations of bodies C0 through C6 are decreased (−) or increased (+) with
    2 deg each such that the orientation of the head does not change.

average effect of a parameter on response R is the average change in response R when the parameter goes from its low to its high level: it is the difference between the average response of the 16 runs for which the parameter was high and the average response of the 16 runs for which the parameter was low. The exact effect of a parameter on the model response depends on the level of the other parameters, since parameters are likely to interact. Because several parameters were changed in each run, the effect of a single parameter on the response is estimated at several combinations of levels for the other parameters. In this way, the results are valid over a wider range of experimental conditions than can be obtained using more traditional designs in which only one parameter is changed in each run. Furthermore, a factorial design also enables the estimation of interaction effects (see Appendix B).

Because two levels were chosen for each parameter, it was implicitly assumed that the model response is (almost) linear over the range of levels chosen [59]. A centre point was added to check for a deviation from linearity; a centre point is a run in which all parameters are at an intermediate value, halfway the high and low level. Here, the response of the centre point equals the response of the calibrated model. A difference
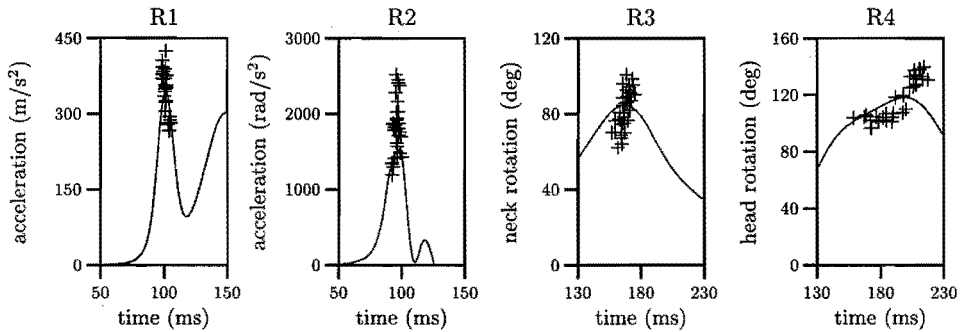
Figure 3.11: Discrete responses R1–R4 of the 32 runs (+, Appendix B) and the continuous response of the calibrated model (solid line).
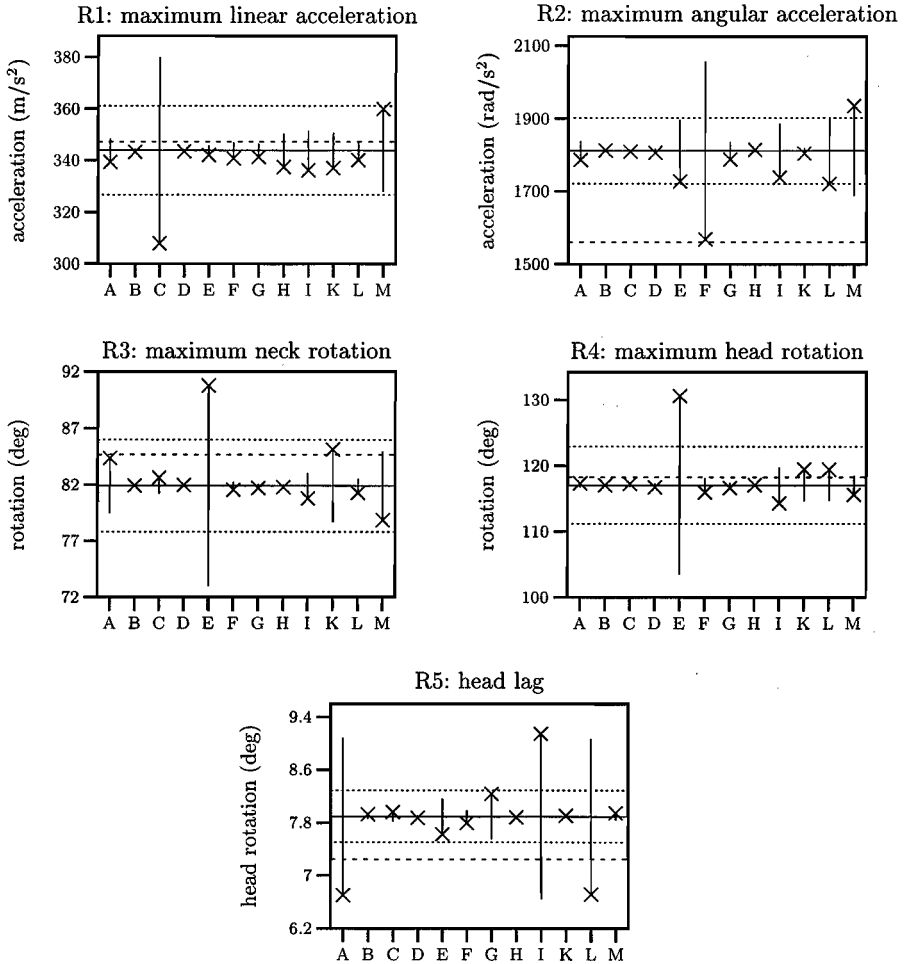
between the centre response and the average response of the 32 runs indicates that the effect of (some of) the parameters on the response is nonlinear.

Results   The parameter levels in each of the 32 runs and the responses are tabulated in Appendix B. Figure 3.11 shows the discrete responses and the continuous response of the calibrated model[3]. Clearly, the magnitudes of the responses differ strongly, but the time at which the maxima occur shows little variation except for head rotation. The responses are more or less evenly distributed around the maxima of the calibrated response for the linear acceleration, head rotation and neck rotation. For the angular acceleration, most responses lie above the maximum head angular acceleration of the calibrated model. The ranges for the maximum linear and angular accelerations were 266–424 m/s^2 and 1193–2522 rad/s^2, the ranges for maximum neck and head rotation were 62–100 deg, and 96–139 deg and the head lag ranged from 4.3 to 12.6 deg.

Figure 3.12 gives the effect of each parameter on the average responses. The average response lies close to the centre response for the maximum linear acceleration and head rotation, expressing that the influence of parameter changes is fairly linear over the chosen parameter range. In contrast, the average response differs largely from the centre response for the angular acceleration and the head lag, indicating that (some of) the parameters affect these responses nonlinearly. It appears that the calibrated model (centre response) has an optimal (small) response for the angular acceleration. Table 3.5 qualifies the influence of variations of the parameters on the model response. The influence of parameters B,D,H is minimal, whereas parameters A,C,E,F,I,L,M affected one or two responses strongly (more than 5% change). The other parameters have a moderate effect on some of the model responses. For the two-parameter interactions, only the interaction between parameters F and I (and their aliases, see Appendix B) influenced a response, the maximum angular acceleration, with more than 5%.

---

3. Responses were computed at each 0.1 ms to ensure that the true maximum responses were captured in the output.

R1: maximum linear acceleration

R2: maximum angular acceleration

R3: maximum neck rotation

R4: maximum head rotation

R5: head lag

Figure 3.12: Average effect of parameters A–M on the responses R1–R5. Solid horizontal line: average response of all 32 runs. Dashed line: response of calibrated model (centre point). Dotted lines: response boundaries at ±5% of average response. Solid vertical line: average effect of parameter on response. Cross (×): average response of all 16 runs in which the parameter was at its high level.

The flexion factor (E) is the most important scale factor: when increased, it strongly increases the head and neck rotations, and it reduces the angular acceleration and increases the head lag moderately. Of the damping coefficients, the flexion/extension coefficient (I) has the strongest influence: it decreases the head lag strongly and the maximum angular accelerations moderately. Increased head mass

(K) enlarges the neck rotation moderately, whereas a larger moment of inertia (L) reduces the angular acceleration and increases the head lag strongly. An increased cervical lordosis (M) leads to larger linear and angular accelerations and to a smaller neck rotation.

3.4 Discussion

The adopted modelling strategy is to proceed from a relatively simple model to a more detailed one. First, the model of Deng and Goldsmith was modified and validated against frontal and lateral impacts as described in detail in De Jager [35]. Second, a new model was developed to remove several shortcomings of the Deng-model. This global model was described in this chapter. It includes head and vertebrae as rigid bodies and intervertebral joints as nonlinear viscoelastic elements. Joint stiffnesses were derived from recent experimental data and modified to calibrate the model response to frontal impacts. Muscles are not included as separate elements, since their effect is incorporated into the intervertebral joint characteristics. Thus, all mechanical behaviour is lumped into the intervertebral joints.

Intervertebral Joint Behaviour   Each intervertebral joint is modelled as a parallel connection of a nonlinear spring and a linear damper, for each of the six degrees of freedom of the joint. Nonlinear elastic behaviour is described by load-displacement curves derived from experimental data for cervical segments reported in the literature. All lower cervical joints have identical force-translation curves, but the moment-rotation curves reflect the regional differences found for *in vivo* experiments characterizing the ranges of motion of each cervical joint. Both upper cervical joints have different moment-rotation curves describing their unique mechanical characteristics. The relatively large translational stiffnesses assigned to these joints lead to small translations under moderate loading and cause the upper joints to behave more or less as ball-and-socket joints.

Linear viscous behaviour is described by constant damping coefficients for the dampers placed parallel to the nonlinear springs. The main reason for choosing this model is its simplicity as only one parameter — the damping coefficient — is needed to describe viscous behaviour. A slightly more complex model is the 'three-parameter solid' or 'standard viscoelastic model' in which the damper is replaced by a series connection of a spring and damper. This model was tried, but simulations revealed that the head-neck model showed strong oscillating behaviour, indicating that the damper did not function optimally. For the three-parameter model, it is well known that the energy dissipation (hysteresis) depends strongly on the deformation rate: it is maximal only for a specific deformation rate, determined by the stiffness and damping coefficients, while it is much smaller for other rates [24]. Deformation rates vary considerably in impacts, causing the damper to dissipate little energy.

Scale factors were introduced to modify the joint stiffnesses such that the model response could be calibrated to match human volunteer responses. These factors can

be considered to represent increased neck stiffness due to muscle tensioning and non-quantified differences between *in vitro* and *in vivo* behaviour. The factors are the same at each vertebral level.

A limitation of the current joint model is that the joint displacements do not interact. It is assumed that a complex displacement can be represented as the linear superposition of displacements in each degree of freedom. That is, load-displacement behaviour for a displacement in one degree of freedom does not depend on displacements in other degrees of freedom. This is probably unrealistic, as was found for the upper cervical spine by Panjabi *et al.* [77]. To include this interaction, joint stiffness for a single degree of freedom should depend not only on that degree of freedom, but also on the other degrees of freedom. Sufficient experimental data, however, is currently lacking and it will be a formidable task to generate such data. Related to this is the limitation that coupling behaviour is not included. That is, a (main) displacement in one degree of freedom does not result in (coupled) displacements in the other degrees of freedom. This usually does not hold for motion segment behaviour, although most coupled displacements were found to be small relative to the main displacement. To include coupling, would require that each joint load depends on all six displacements, which can be represented through a stiffness matrix as used in the Deng-model.

Calibration   The model response was compared with the most severe frontal impacts performed with human volunteers. Joint stiffness (scale factor) and damping were modified to calibrate the model response. A fairly accurate response could be obtained. Reasonable agreement was found for the linear and angular acceleration of the head, the trajectory of the occipital condyles of the head, the neck length, and the neck rotation. Head rotation was too large, which was also reflected by the trajectory of the centre of gravity of the head, showing that the model was too flexible. The head lag was well reflected, but locking of head and neck rotation did not occur; instead, head rotation exceeded neck rotation (overtipping), which was ascribed to the absence of active muscle behaviour, since human cadavers also showed overtipping in frontal impacts. Intervertebral joint rotations were compared with their ranges of motion: they appeared accurate for the upper four joints, but were unrealistically large for the lower four joints.

Head rotation, thus, appears to be too large due to overtipping and the large rotations of the lower joints. Possibly, the joint rotations can be improved when the scale factors can be modified for each joint independently. Then, the stiffnesses of the lower joints can be increased by decreasing their scale factors, while the factors for the other joints remain unchanged in an attempt to obtain joint rotations that are closer to the ranges of motion. A possible explanation for this would be that the neck muscles can more effectively increase the apparent stiffness of the lower joints than of the upper joints. For scale factors varied for each joint level identically, however, it was found that head rotation could hardly be improved without deteriorating the other responses. Moreover, even modified scale factors cannot prevent overtipping of the head, as the joints are passive elements (springs) which cannot generate force independently

of elongation unlike active elements like muscles. Because the upper joints are initially forced into extension, they will eventually rebound into flexion, which is likely to result in overtipping, unless head rotation is counteracted by other loads, such as muscle forces. Apparently, the volunteers prevent excessive head rotation by tensioning their extensor muscles; an effect that cannot adequately be represented by the current intervertebral joint model. These muscle forces may also lead to a larger head lag for the volunteers in comparison with the model. Thus, active muscle behaviour appears essential to adequately describe head-neck dynamics with a mathematical model. Active muscle behaviour will be included in the detailed head-neck model (Chapter 5).

Parametric Study   A fractional factorial design with 32 runs was chosen to quantify the effect of twelve parameters on five model responses. This parametric study can be considered as an initial, screening study to find the most relevant or critical model parameters affecting the model response. In a subsequent study, the effects of these parameters can be studied in more detail, taking the effects of parameter interactions and the nonlinear model responses into account. Further, future model validation should be aimed at checking especially the critical parameters. Similarly, experiments should be conceived to find realistic values for those parameters. Finally, the results of the parametric study can be used to further calibrate the model response as presently rather rough estimates for the scale factors and damping coefficients were used.

In conclusion, a relatively simple head-neck model has been developed, The model comprises rigid head and vertebrae connected through nonlinear viscoelastic intervertebral joints. Joint characteristics were modified, such that the model response to frontal impacts compared reasonably with human volunteer responses. It appeared that active muscle behaviour is essential to accurately describe head rotation.

<div align="right">

4

</div>

Detailed Segment Models
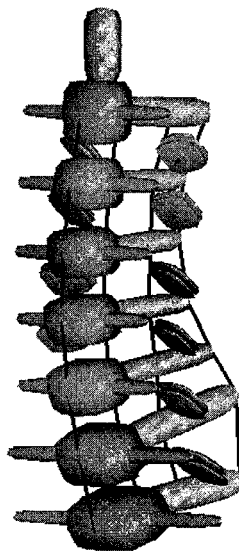
This chapter describes the detailed models of the upper and lower cervical spine which were developed according to the adopted research strategy. These models form an intermediate step between the global head-neck model of the previous chapter and the detailed head-neck model of the next chapter.

The global model was taken as starting point and enhanced to include separate representations of the intervertebral discs, ligaments and facet joints. Section 4.1 describes the detailed model of the lower cervical spine. Section 4.2 presents the validation of motion segments C3-C4 and C5-C6, and Section 4.3 the parametric study with C3-C4. The detailed model of the upper cervical spine is outlined in Section 4.4. Sections 4.5 and 4.6 treat the validation of and parametric study with this model. Section 4.7 concludes this chapter with a discussion.

4.1 Lower Cervical Spine

The detailed model of the lower cervical spine comprises rigid vertebrae, connected by linear viscoelastic intervertebral discs and nonlinear viscoelastic ligaments, and supported through frictionless, nonlinear viscoelastic facet joints. The model is outlined below.

4.1.1 Rigid Vertebrae

Rigid bodies represent vertebrae C2 through T1. These bodies have the same relative position, orientation and inertial characteristics as the bodies in the global model (Table 3.1, Fig. 3.2). Figure 4.1 shows the model of motion segment C3-C4: simple geometric shapes are used to visualize the body, arch and transverse processes of the vertebrae.

frontal oblique view   top view

frontal view   left lateral view
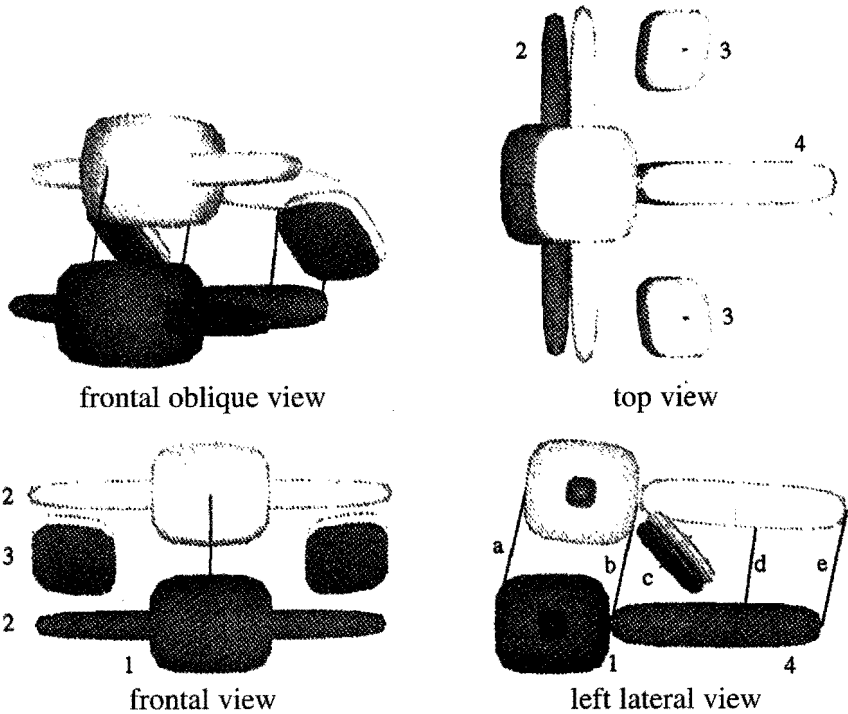
Figure 4.1: Model of motion segment C3-C4. Shown are the vertebrae with 'arch', transverse processes and articular facet surfaces (yellow for C3, orange for C4) and the ligaments (blue). The articular facets are rigidly attached to their respective vertebrae. The intervertebral disc is not shown. Legend: 1. vertebral body, 2. transverse process, 3. articular facets, 4. 'arch and spinous process'; a. anterior longitudinal ligament, b. posterior longitudinal ligament, c. capsular ligament, d. flaval ligament, e. interspinous ligament.

4.1.2 Linear Viscoelastic Intervertebral Discs

The intervertebral disc is modelled as a parallel connection of a linear elastic spring and a linear viscous damper for each of its six degrees of freedom. The loads exerted by the disc on the vertebrae are given by

$$\begin{aligned} F_i &= k_{ti} \cdot t_i + b_{ti} \cdot v_i, \\ M_i &= k_{\phi i} \cdot \phi_i + b_{\phi i} \cdot \omega_i \quad (i = x, y, z), \end{aligned}$$

in which F_i and M_i are the components of the forces and moments relative to the i-axis of the lower body, t_i and ϕ_i the relative translations and rotations of the geometric centre of the disc and v_i and ω_i the relative translational and rotational velocities of the disc centre. The coordinate systems are defined in Section 3.1, Figure 3.2. The disc centre lies approximately in the middle of the intervertebral disc space between the end plates of the disc and has a fixed distance relative to the centre of the upper vertebral body (Appendix A). The translations of the disc centre are measured relative to the lower body coordinate system and the rotations are measured as Bryant angles (in the order x, y, z) describing the orientation of the upper body relative to the lower one. Because the orientation of the T1-coordinate system does not resemble the orientation of vertebra T1 (Fig. 3.2), translations of the C7-T1 disc centre are measured relative to a (disc) coordinate system with the same origin as the local coordinate system of T1 and with a fixed orientation equal to the initial orientation of the local coordinate system of C7; disc loads are also expressed in this disc coordinate system. Disc loads are applied to the vertebrae at the disc centre. Thus, almost the same representation as used for the intervertebral joints of the global model (Section 3.1.2) is used to model the intervertebral discs. The stiffnesses k and damping coefficients b, however, were adapted to represent intervertebral disc behaviour only; in the global model, k and b represented the compound behaviour of disc, ligaments, facet joints and muscles.

Few data were available to quantify cervical disc behaviour as was pointed out in Chapter 2. Here, the stiffness coefficients for *disc* segments presented by Moroney *et al.* [61] were used (Table 2.3) and completed with the average disc stiffness in tension from Pintar *et al.* [83] (Section 2.4.3). Since the disc segments used by Moroney comprised also the anterior and posterior longitudinal ligaments and uncovertebral joints, a possible contribution of these ligaments and joints to disc segment behaviour is now represented in the disc model. The contribution of the ligaments is assumed to be negligibly small, since the deformations are small in Moroney's experiments, causing only small strains and forces in the ligaments (see Section 4.1.4). The contribution of the uncovertebral joints is not known. Also important is the axial preload that Moroney applied to represent the weight of the head, and which may have led to stiffening of the disc segments (Section 2.4.1). Thus, the effect of uncovertebral joints and axial preload are implicitly incorporated in the disc stiffnesses.

No data were available to determine the damping coefficients. The coefficients were set at $b_{ti} = 1000$ Ns/m and $b_{\phi i}=1.5$ Nms/rad, which are similar to those used for the intervertebral joints of the global model. It is, thus, assumed that most of the damping in motion segments originates from the disc. In this chapter, damping

coefficients are of little significance since only (quasi)static loading situations will be considered, but they become relevant in the next chapter, in which impacts with the complete detailed head-neck model will be considered.

4.1.3 Frictionless, Nonlinear Viscoelastic Facet Joints

The articular facet surfaces of the facet joints are modelled as hyperellipsoids. A hyperellipsoid of degree n is specified with

$$\left(\frac{|x|}{a}\right)^n + \left(\frac{|y|}{b}\right)^n + \left(\frac{|z|}{c}\right)^n = 1, \ n \geq 2$$

in which a, b, c are the lengths of the semi-axes of the ellipsoid along the x, y, z-axes of the ellipsoid coordinate system, which originates at the centre of the ellipsoid (Fig. 4.2). The coordinates of the ellipsoid centre are specified in the local coordinate system of the body to which the ellipsoid is rigidly attached. The orientation of the ellipsoid coordinate system is specified relative to the body local coordinate system with Bryant angles. The degree n determines the shape of the hyperellipsoid: the shape is elliptic for $n = 2$ and becomes more rectangular for increasing n. For $n = 4$, a sufficiently accurate representation is obtained for the almost flat cartilage layer covering the articular facets. Table 4.1 gives the geometric data of the ellipsoids, which were derived from Panjabi *et al.* [78] (Appendix A). Position and orientation were slightly adjusted, such that neighbouring facets are initially parallel to and in contact with each other. Facet thickness was set to 2 mm.

Facet joint mechanics is modelled as an almost rigid, frictionless contact interaction between the facet ellipsoids to approximate synovial joint behaviour. Thus, the ellipsoids can slide relative to one another without friction. The contact force F_c is given by the nonlinear viscoelastic characteristic

$$F_c = b_f \cdot \dot{u} + \begin{cases} 2 \cdot 10^9 \cdot u^2 & \text{for } 0 \leq u \leq 3 \cdot 10^{-4} \ [m] \\ 180 + 1.2 \cdot 10^6 \cdot (u - 3 \cdot 10^{-4}) & \text{for } u > 3 \cdot 10^{-4} \ [m], \end{cases}$$

with u the penetration of one ellipsoid into the other, $\dot{u}$ the penetration speed and $b_f = 300$ Ns/m the damping coefficient. The precise definitions of penetration and
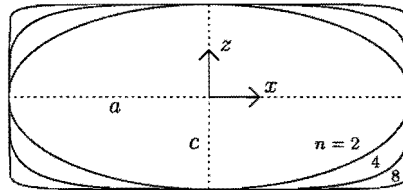
Figure 4.2: Coordinate system, semi-axes and shape of hyperellipsoid for $n = 2, 4, 8$.

Table 4.1: Position, dimensions and orientation of the ellipsoids representing the left articular facet surfaces of the lower cervical spine. For the right surfaces, the y-coordinate and angle ϕ_x change sign. Orientations are specified as Bryant angles in the order y, x, z with $\phi_z = 0$. All ellipsoids have degree $n = 4$.

position of facet on left side	coordinates of centre point			lengths of semi-axes			relative orientation	
	x	y	z	a	b	c	ϕ_y	ϕ_x
	mm			mm			deg	
T1 superior	−14.4	16.6	12.0	6.3	6.8	1.0	−28.1	−8.8
C7 inferior	−17.5	16.8	−8.7	6.3	6.6	1.0	−48.9	−8.8
C7 superior	−14.3	19.3	8.7	5.7	6.3	1.0	−57.6	−7.4
C6 inferior	−14.4	19.4	−6.9	6.1	6.5	1.0	−52.0	−7.4
C6 superior	−14.4	20.0	8.5	5.5	6.2	1.0	−50.8	−13.8
C5 inferior	−13.7	20.3	−6.5	5.6	5.9	1.0	−45.6	−13.8
C5 superior	−15.1	19.2	6.9	5.8	6.0	1.0	−46.9	−10.9
C4 inferior	−14.0	19.0	−7.9	6.1	6.6	1.0	−42.3	−10.9
C4 superior	−16.0	18.8	8.9	6.1	5.8	1.0	−47.2	9.1
C3 inferior	−14.0	18.9	−6.3	6.2	5.7	1.0	−41.9	9.1
C3 superior	−16.1	18.0	7.0	5.8	5.7	1.0	−39.8	16.6
C2 inferior	−13.9	18.0	−10.1	6.2	5.5	1.0	−39.8	16.6

penetration speed are given in [107]. The contact characteristic has no physical origin, but merely represents an almost rigid contact allowing some deformation of the thin cartilage layer covering the articular facets. The quadratic part provides a smooth transition of the contact stiffness from zero for no contact to $1.2 \cdot 10^6$ N/m at 0.3 mm penetration. An upper limit for the contact stiffness was chosen, because a large stiffness leads to small time steps in the numerical integration process and, hence, to long run-times.

4.1.4 Nonlinear Viscoelastic Ligaments

Six ligaments of the lower cervical spine are incorporated in the model: the anterior longitudinal ligament (ALL), the posterior longitudinal ligament (PLL), the flaval ligament (FL), the interspinous ligament (ISL) and the left and right capsular ligament (CL). For simplicity, these broad ligaments are modelled as straight line elements. The origins and insertions of the ligaments were qualified through anatomical landmarks and quantified by the adopted vertebral geometry (Appendix A, Table 4.2). In the model, the capsular ligaments run perpendicular to the facet joints and pass through the centres of the facet surfaces.

Ligament behaviour is modelled with elements producing force only in tension. Ligament force F_l is given by

$$F_l = \begin{cases} F_{el}(\epsilon) + b_l \cdot d\epsilon/dt & \text{for } \epsilon \geq 0 \\ 0 & \text{for } \epsilon < 0. \end{cases}$$

Elastic behaviour is prescribed by the nonlinear force-strain curve $F_{el}(\epsilon)$ with strain ϵ the relative elongation of the ligament with respect to its rest length. The rest length is defined as the length of the ligament in the initial body configuration, assuming that the ligaments are slack nor taut initially. Viscous behaviour is represented by the

Table 4.2: Origins, insertions and untensioned rest lengths of the ligaments of the lower cervical spine. The coordinates are relative to the body local coordinate systems; the body numbers refer to the numbers used in Table 3.1.

spinal level	name	body no.	origin coordinates x	y	z	body no.	insertion coordinates x	y	z	rest length l_0
			mm				mm			mm
C7-T1	ALL	1	8.9	0.0	−3.4	2	8.2	0.0	0.0	18
	PLL	1	−8.9	0.0	3.4	2	−8.2	0.0	0.0	18
	FL	1	−24.0	0.0	5.5	2	−23.3	0.0	−1.5	20
	ISL	1	−46.4	0.0	8.7	2	−53.6	0.0	−4.6	23
	CL	1	−13.5	±16.6	10.2	2	−19.0	±16.8	−7.4	6
C6-C7	ALL	2	8.2	0.0	0.0	3	8.0	0.0	0.0	19
	PLL	2	−8.2	0.0	0.0	3	−8.3	0.0	0.0	18
	FL	2	−23.3	0.0	−1.5	3	−26.3	0.0	−1.9	16
	ISL	2	−53.6	0.0	−4.6	3	−47.3	0.0	−4.1	15
	CL	2	−12.6	±19.3	7.6	3	−16.0	±19.4	−5.7	6
C5-C6	ALL	3	8.0	0.0	0.0	4	7.7	0.0	0.0	18
	PLL	3	−8.3	0.0	0.0	4	−8.1	0.0	0.0	17
	FL	3	−26.3	0.0	−1.9	4	−25.4	0.0	−1.7	15
	ISL	3	−47.3	0.0	−4.1	4	−39.9	0.0	−3.2	16
	CL	3	−12.9	±20.0	7.2	4	−15.1	±20.3	−5.1	6
C4-C5	ALL	4	7.7	0.0	0.0	5	7.7	0.0	0.0	18
	PLL	4	−8.1	0.0	0.0	5	−7.9	0.0	0.0	17
	FL	4	−25.4	0.0	−1.7	5	−25.6	0.0	−0.3	17
	ISL	4	−39.9	0.0	−3.2	5	−36.3	0.0	−0.5	17
	CL	4	−13.6	±19.2	5.5	5	−15.3	±19.0	−6.4	6
C3-C4	ALL	5	7.7	0.0	0.0	6	7.4	0.0	0.0	19
	PLL	5	−7.9	0.0	0.0	6	−7.8	0.0	0.0	18
	FL	5	−25.6	0.0	−0.3	6	−24.0	0.0	0.3	16
	ISL	5	−36.3	0.0	−0.5	6	−35.9	0.0	0.5	16
	CL	5	−14.5	±19.2	7.5	6	−15.3	±18.9	−4.8	6
C2-C3	ALL	6	7.4	0.0	0.0	7	6.3	0.0	0.0	19
	PLL	6	−7.8	0.0	0.0	7	−7.7	0.0	0.0	19
	FL	6	−24.0	0.0	0.3	7	−28.6	0.0	−0.7	19
	ISL	6	−35.9	0.0	0.5	7	−42.0	0.0	−1.2	19
	CL	6	−14.8	±18.0	5.5	7	−15.2	±18.0	−8.6	6

ALL = anterior longitudinal ligament, PLL = posterior longitudinal ligament
FL = flaval ligament, ISL = interspinous ligament, CL = capsular ligament
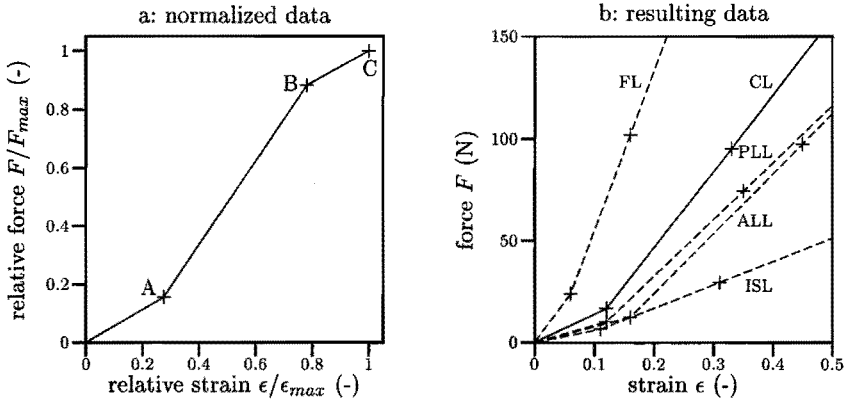
Figure 4.3: (a) Average dimensionless force-strain curve for ligaments. Data are normalized relative to the failure force F_{max} and failure strain ϵ_{max}. (b) Curves used for the ligaments of the lower cervical spine: ALL, PLL, FL, ISL and CL. Data are given in Table 4.3.

constant damping coefficient b_l, which was, arbitrarily, set at 300 Ns/m, a relatively small value compared with the damping coefficients of the discs.

The elastic characteristics of the ligaments are based on the data of Chazal *et al.* [11] and Myklebust *et al.* [64]. Chazal characterized the nonlinear force-strain behaviour of thoracolumbar ligaments at three points as shown in Figure 4.3a for the average data in dimensionless form: the strain relative to the strain ϵ_{max} at failure is given along the horizontal axis, and the force relative to the force F_{max} at failure is given along the vertical axis. Chazal's data, given in Table 4.3, reflect that the ligaments show almost identical behaviour in dimensionless form. Although only 3 of the 43 ligaments tested by Chazal were cervical ligaments, the strain data are used since no other studies were available to provide such detailed characteristics. The failure forces, however, were adapted, since cervical ligaments are significantly weaker than

Table 4.3: Data used for the ligaments of the lower cervical spine derived from Chazal *et al.* [11]; data for the capsular ligaments (CL) are the average data for all ligaments. F_{max} and ϵ_{max} are the failure force and failure strain of the ligaments. F_{max} was derived from Myklebust *et al.* [64].

ligament	A		B		C	
	ϵ/ϵ_{max}	F/F_{max}	ϵ/ϵ_{max}	F/F_{max}	ϵ_{max}	F_{max}
						N
ALL	0.24	0.11	0.80	0.88	0.58	111
PLL	0.22	0.12	0.78	0.90	0.45	83
FL	0.33	0.21	0.77	0.89	0.21	115
ISL	0.33	0.19	0.78	0.87	0.40	34
CL (average)	0.28	0.16	0.78	0.88	0.42	108

comparable thoracolumbar ligaments according to Myklebust, who reported (only) the failure forces and failure elongations of almost all spinal ligaments. Since they did not report untensioned rest lengths of the ligaments, their data cannot be used to compute strains. Therefore, the failure forces of Myklebust are combined with the strain data of Chazal to model ligament behaviour. The average strain data of all ligaments tested by Chazal are used for the capsular ligaments. The failure forces were averaged from the cervical data of Myklebust. Failure behaviour (point C) is not included since the strain calculation may be unrealistic, noting the large differences in elongation-to-failure reported by Chazal and Myklebust; instead, the curve is linearly extrapolated beyond point B, see Figure 4.3b.

4.2 Validation of Motion Segment Models

The lower cervical spine model was validated by comparing the responses of its motion segments with experimental data. Instead of testing all segments, only two representative segments were validated. Segments C3-C4 and C5-C6 were chosen as the facet surface orientations of these segments differ essentially: the upper facets of C4 face backwards and towards the midsagittal plane, whereas those of C6 face backwards and outwards. The other geometric differences are small.

First, the models were validated by simulating experiments done with cervical motion segments and comparing the displacements of the models with the reported displacements. Second, the load-displacement curves for large loads were compared with the curves of the intervertebral joints of the global model (Chapter 3). Third, the centre of rotation for flexion/extension was compared with experimental data.

Table 4.4: Response of models C3-C4 and C5-C6 compared with experimental results presented in Figure 4.4.

load	main displacement[a]	coupled displacements[b]
AS	C3-C4 reasonable; C5-C6 good	more upward translation
PS	good	
LS	poor: more flexible	C5-C6 lateral bending to other side
CMP	good	
LB	good/reasonable	
FLX	poor: less flexible	less anterior shear
EXT	good	
AR	C3-C4 reasonable, C5-C6 poor: more flexible	
a	good: close to average of experimental response	
	reasonable: within SD of experimental response	
	poor: outside SD	
b	differences are noted only for poor agreement with experiments	
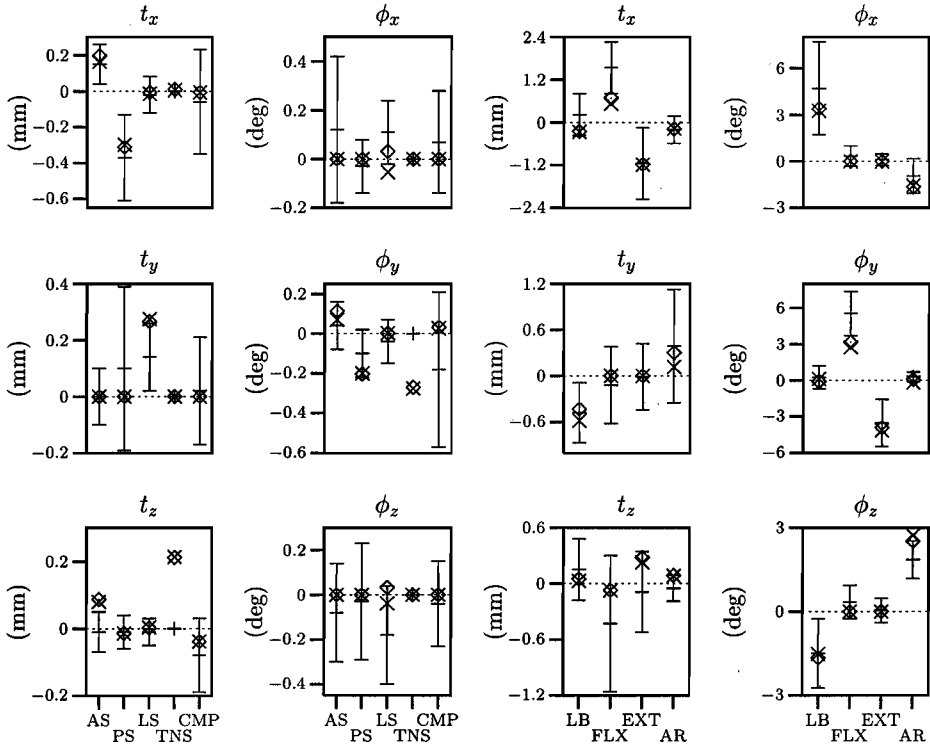
Figure 4.4: Main and coupled displacements of models C3-C4 (◇) and C5-C6 (×) with experimental results (average ± SD) of Moroney *et al.* [61]; for tension, no experimental data are given. The applied loads are given along the horizontal axis and the resulting displacements along the vertical axis: anterior shear (AS, $+t_x$), posterior shear (PS, $-t_x$), lateral shear (LS, t_y), tension (TNS, $+t_z$), compression (CMP, $-t_z$), lateral bending (LB, ϕ_x), flexion (FLX, ϕ_y), extension (EXT, $-\phi_y$), axial rotation (AR, ϕ_z).

4.2.1 Ranges of Motion for Small Static Loads

The models of motion segments C3-C4 and C5-C6 were validated by simulating the motion segment experiments of Moroney *et al.* [61]. Moroney subjected motion segments to static loads (20 N, 1.8 Nm) and measured the resulting three-dimensional displacements at the geometric centre of the upper vertebra (Section 2.4.1). Loads were applied to the upper vertebra in effect at the centre of the disc, such that the direction of the load did not change relative to the lower vertebra. Moroney applied an axial preload of 49 N to the segments, but this preload is not applied in the simulations because its effect was already incorporated in the disc characteristics. The effect of larger preloads on the response of C3-C4 is presented in the next section.

The main and coupled displacements of models C3-C4 and C5-C6 are shown in Figure 4.4 with the experimental results (average ± SD). A qualitative comparison is

presented in Table 4.4. In the models, translations were measured at the geometric centre of the upper vertebral body (C3 or C5), and rotations were measured as Bryant angles in the order x, y, z. Overall, the models are in reasonable to good agreement with the experiments. The models are slightly too flexible in lateral shear and axial rotation, and too stiff in flexion. Almost all coupled displacements agree well with the experiments. The differences in response between C3-C4 and C5-C6 are small for the small loads applied here.

4.2.2 Response to Large Loads

The models were subjected to larger loads as used in the previous section to determine their load-displacement curves. Maximum loads were 500 N and 20 Nm; for extension, a maximum of 13 Nm was used to prevent the vertebral arches from moving through each other (bone-to-bone contact is not defined for the arches). Loads were applied slowly to minimize viscous effects, such that the load-displacement curves represent the elastic response. The curves for segment models C3-C4 and C5-C6 are similar: they differ only slightly for anterior shear, flexion and extension (Fig. 4.5).

The responses of the segment models were compared with the load-displacement curves of the intervertebral joints of the global model, since the latter characteristics are based on experimental data. The segments do not reflect a neutral zone: their initial
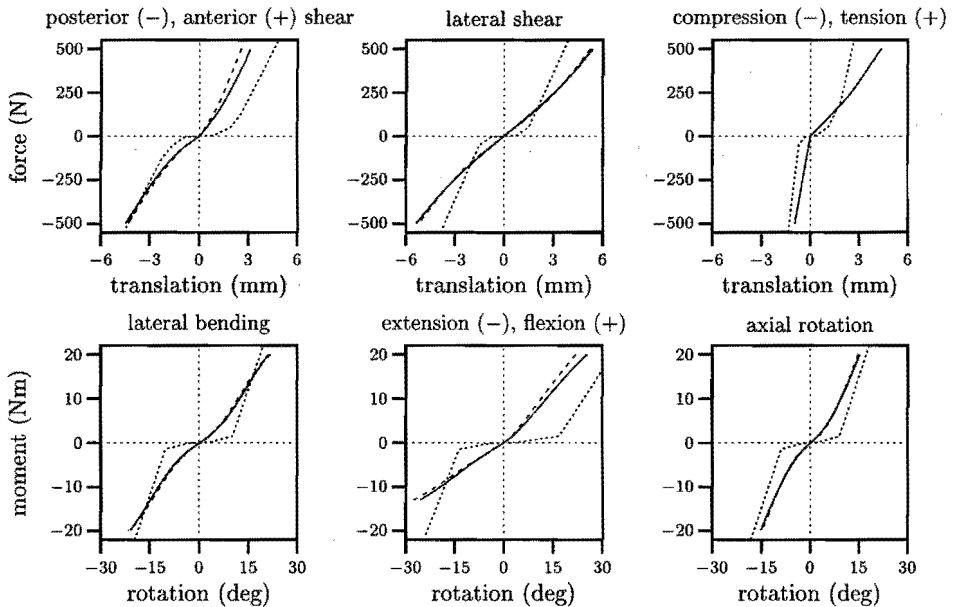
Figure 4.5: Elastic response of models C3-C4 (solid line) and C5-C6 (dashed line) to large loads. The dotted lines are the load-displacement curves from Figure 3.3 for the intervertebral joints of the global model.

stiffness is much larger than found for the global joints, because of the linear stiffness of the disc. For larger displacements, stiffness tends to increase due to additional resistive forces exerted by the ligaments (with nonlinear characteristics) which become more and more strained. This increase in stiffness is not strong enough in lateral shear, tension, lateral bending and extension, such that the segments become more flexible than the global joints. This may indicate that the ligaments cannot effectively oppose the motion for larger displacements in the segment models, as is suggested by the curves for which the stiffness hardly changes along the curve; or it may indicate that the disc stiffness should be nonlinear, such that they can more effectively constrain large displacements.

For C3-C4, Table 4.5 shows the loads in the intervertebral disc, ligaments and facet joints to counterbalance the maximum applied load. Clearly, all elements contribute to resisting the load, although the contribution of the strong PLL and weak ISL is small in most situations, while the contribution of the capsular ligaments is large. In flexion, the facets make contact during most of the motion, but no facet contact is present in maximum flexion, when the forces in the disc are large, while the moment is small compared with the applied moment of 20 Nm. In compression, the applied load is almost entirely supported through the disc.

To determine the effect of axial preloads on motion segment behaviour, C3-C4 was loaded with a compressive force of 500 N applied at the geometric centre of C3 and

Table 4.5: Loads in the intervertebral disc, ligaments and facet joints when C3-C4 is loaded with 500 N or 20 Nm (13 Nm in extension).

	loading situation								
	AS	PS	LS	TNS	CMP	LB	FLX	EXT	AR
disc forces [N]									
F_x	-185	214	-18	-134	64	75	-277	127	3
F_y	0	0	-398	0	0	39	0	0	-132
F_z	-123	81	17	-262	470	10	745	-211	-109
disc moments [Nm]									
M_x	0	0	-0.1	0	0	-7.0	0	0	3.6
M_y	-0.4	1.1	0.1	2.4	-0.2	0.4	-5.3	8.2	1.5
M_z	0	0	-1.1	0	0	4.6	0	0	-6.4
ligament force [N]									
ALL	6	7	4	46	0	1	0	73	10
PLL	10	4	3	28	0	2	4	2	6
FL	106	0	10	32	0	26	374	0	23
ISL	14	0	1	0	0	9	89	0	6
CL left	28	157	97	61	0	330	168	116	261
CL right	28	157	52	61	0	239	168	116	149
facet force [N]									
left	235	0	83	0	20	0	0	258	0
right	235	0	41	0	20	467	0	258	434

posterior (−), anterior (+) shear   compression (−), tension (+)   extension (−), flexion (+)
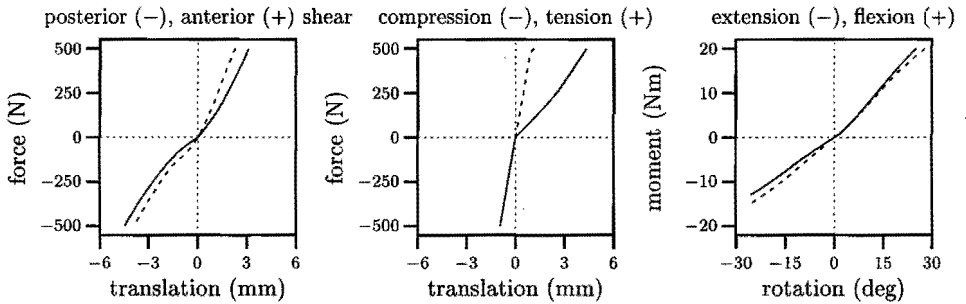

Figure 4.6: The influence of axial preload of 500 N on the response of C3-C4. Shown are the responses without preload (solid line) and with preload (dashed line).

constantly aligned along the z-axis of the coordinate system of C3. Differences were found only for the response to anterior/posterior shear, tension and flexion/extension (Fig. 4.6). The tension curve is now the opposite of the compression curve because the motion segment is unloaded. The compressive preload decreases the stiffness in flexion and extension, due to the bending moment generated by the preload. In anterior and posterior shear, stiffness is increased by the preload.

4.2.3 Centre of Rotation for Flexion/Extension

For C3-C4 and C5-C6, the centre of rotation (COR, Chapter 2) of the upper verte- bra relative to the lower one was determined for flexion/extension loading (up to 10 Nm) applied to the upper vertebra. First, the momentaneous CORs were determined for intermediate positions of C3 relative to C4 with the method of Spiegelman and Woo [99]. The momentaneous CORs showed little variation with a standard deviation less than 1 mm. Second, the average COR was determined as the average position of all momentaneous CORs (Fig. 4.7). This position agrees excellently with the experimental
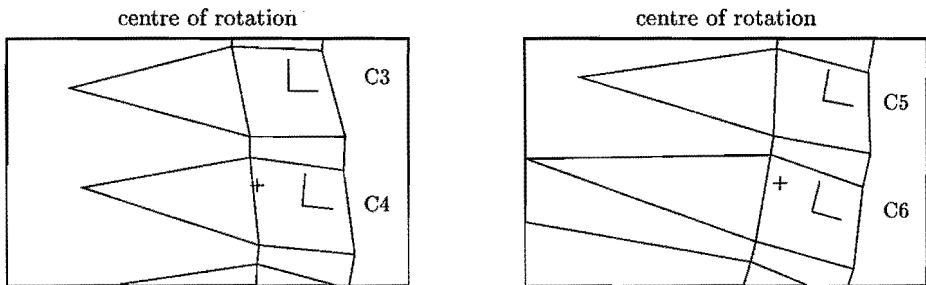
Figure 4.7: The average centre of rotation (+) of C3 relative to C4, and of C5 relative to C6. Solid lines depict the contours of the vertebrae and discs, and the body local coordinate systems.

data of Dvorak *et al.* [19] (Fig. 2.7) and the other studies presented in Section 2.3. The effect of an axial preload of 500 N on the position of the COR was found to be small.

4.3 Parametric Study with Motion Segment Models

A parametric study was conducted to quantify the influence of a parameter on the response of a motion segment to applied moments, for which segment C3-C4 was arbitrarily chosen. To that end, a fractional factorial design was chosen, similar as in Section 3.3. As parameters were selected the stiffnesses of the ligaments and the intervertebral disc, and the orientation of the facet surfaces. The main and the most important coupled displacement were chosen as responses.

To limit the number of parameter variations, the ligaments were put into two groups; in each group, stiffnesses were changed simultaneously. From Table 4.5, it is clear that the capsular ligaments are the most important ligaments in resisting the applied loads. Therefore, the capsular ligaments were put into one group (parameter B) and the other ligaments, which are all midsagittal ligaments, into the other group (A). Table 4.5 may aid to identify which ligament is relevant for the loading situation considered, such that a significant effect of a change in parameter A or B can be attributed to a single ligament. Similarly, the intervertebral disc stiffnesses were divided into a group with the translational stiffnesses (C) and a group with the rotational stiffnesses (D). Parameters E and F are the lateral (ϕ_x) and midsagittal (ϕ_y) rotations of the facet ellipsoids. Parameters G and H, finally, are the (initial) strain of the ligaments when the model is in its initial position. Table 4.7 lists the parameters and the amount of variation relative to the normal situation. Stiffnesses were changed $\pm$ 25% by multiplying the calculated ligament or disc forces with 0.75 or 1.25[1].

To limit the number of loading situations, only applied moments were considered: lateral bending, flexion, extension and axial rotation. Maximum load was 10 Nm. As responses were considered the main displacement and the coupled displacement which is, likely, most strongly affected by the parameter variations (Section 2.3, Table 4.6). Responses were measured when the applied load was maximal.

A fractional factorial design with 16 runs was chosen to study the effect of the parameters on the responses. The design is tabulated in Appendix B. With this design, the effect of a single parameter on the response can be estimated independently of any other parameter and of any interaction of two parameters.

Figure 4.8 illustrates the effect of each parameter on the average response of all runs and Table 4.7 qualifies these effects. The centre response, for the normal situation, is also shown in Figure 4.8: it lies within $\pm$5% of the average response for all main motions, indicating that the effect of the parameters is fairly linear over the chosen variation range.

Increased stiffness of the midsagittal ligaments (parameter A) strongly reduces the response to flexion loading, which can be ascribed to the flaval ligament according

---

1. This was done with the AMPLIFICATION-option in MADYMO.

Table 4.6: Selected loads and model responses R for parametric study with C3-C4 and C0-C2.

load	response main displacement	response coupled displacement
lateral bending	R1a: lateral bending (ϕ_x)	R1b: axial rotation (ϕ_z)
flexion	R2a: flexion (ϕ_y)	R2b: anterior shear (t_x)
extension	R3a: extension (ϕ_y)	R3b: posterior shear (t_x)
axial rotation	R4a: axial rotation (ϕ_z)	R4b: lateral bending (ϕ_x)

to Table 4.5. Enlarged capsular ligament stiffness (B) strongly decreases the response to lateral bending and axial rotation, but only for the main displacements. Increased translational disc stiffnesses (C) moderately reduce the response to extension and flexion. The rotational disc stiffnesses (D) are important in all loading conditions and for all responses; this was already reflected by the data in Table 4.5, indicating that the disc carries a large part of the applied loads. Increased lateral orientation of the facet surfaces (E) increases the main lateral rotation and reduces the main axial rotation, but has no influence on the coupled displacements. In contrast, a larger midsagittal orientation of the facets (F) influences both main and coupled displacements: main lateral bending and main extension are strongly reduced and main axial rotation is strongly enlarged. Initial strain (G,H) and stiffness (A,B) of the ligaments have a comparable influence on the model response: a change of 5% in initial strain has almost the same effect as a change of 25% in stiffness.

Table 4.7: Selected parameters, their range of variation and their effect on model responses R. The responses are explained in Table 4.6.

parameter	level −	level +	R1a	R1b	R2a	R2b	R3a	R3b	R4a	R4b
ligament stiffness										
A ALL, PLL, ISL, FL	−25%	+25%	0	0	−	−	0	0	0	0
B CL, left and right	−25%	+25%	−	0	0	0	0	0	−	0
intervertebral disc stiffness										
C translational stiffnesses	−25%	+25%	0	0	0	0	0	0	0	0
D rotational stiffnesses	−25%	+25%	−	−	−	−	−	−	−	−
facet orientation										
E ϕ_x (left facet)	−15°	+15°	+	0	0	0	0	0	−	0
F ϕ_y (left facet)	−10°	+10°	−	0	0	0	−	−	+	0
initial strain of ligaments										
G ALL, PLL, ISL, FL	−5%	+5%	0	0	−	−	0	0	0	0
H CL, left and right	−5%	+5%	0	0	0	0	0	0	−	0

a   response with parameter at high level; difference with average response is
    0   less than 5%,
   −/+   a decrease/increase in absolute value with more than 5%.
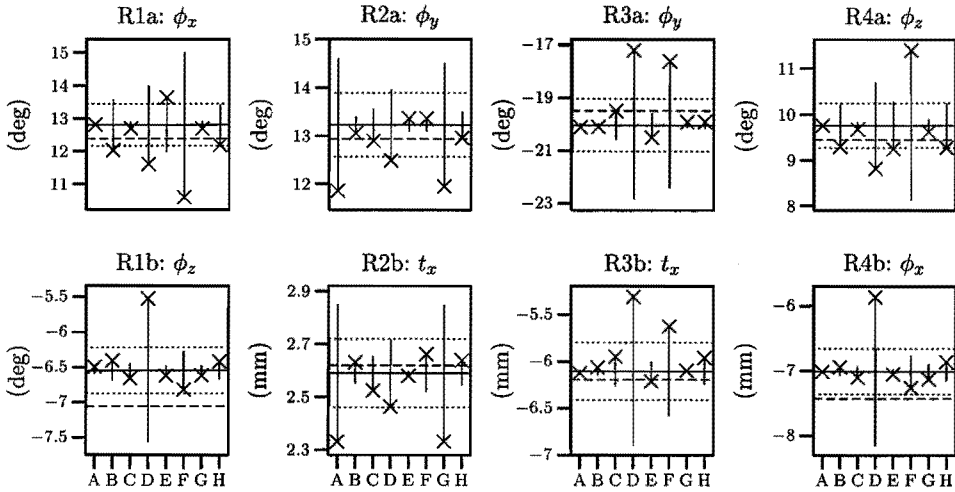
Figure 4.8: Effects of the parameters A–F on the model responses R. Solid horizontal line: average response of all 16 runs. Dashed line: centre response. Dotted lines: response boundaries at ±5% of average response. Solid vertical line: average effect of parameter on response. Cross (×): average response for all 8 runs in which the parameter was at its high level.

4.4 Upper Cervical Spine

The detailed model of the upper cervical spine comprises rigid vertebrae and occiput, connected by nonlinear viscoelastic ligaments and supported through frictionless, nonlinear viscoelastic facet joints. This model is outlined in this section; a preliminary version of the model was developed by Meertens [52] as part of this research. Validation is treated in Section 4.5, and a parametric study is presented in Section 4.6.

4.4.1 Rigid Vertebrae and Occiput

Figure 4.9 shows the model of the upper cervical spine. Rigid bodies represent the axis (C2), its dens, the atlas (C1) and the occiput (C0). The geometric and inertial data of the bodies are the same as for the global model, but mass and moments of inertia of the occiput, the base of the skull, were set equal to those of C2.

4.4.2 Frictionless, Nonlinear Viscoelastic Facet Joints

The facet joints are modelled as frictionless, nonlinear viscoelastic contact interactions between hyperellipsoids, similar as in the lower cervical spine model. Between atlas and dens, two ellipsoids are used to model the synovial joint between the anterior ring of the atlas and the anterior side of the dens. Additionally, a contact interaction is specified between the dens and the lower facets of the atlas to incorporate possible contact of the atlas ring with the dens. All contacts have the same characteristics as used for the lower cervical spine.

<div align="center">frontal oblique view   top view</div>

<div align="center">frontal view   left lateral view</div>
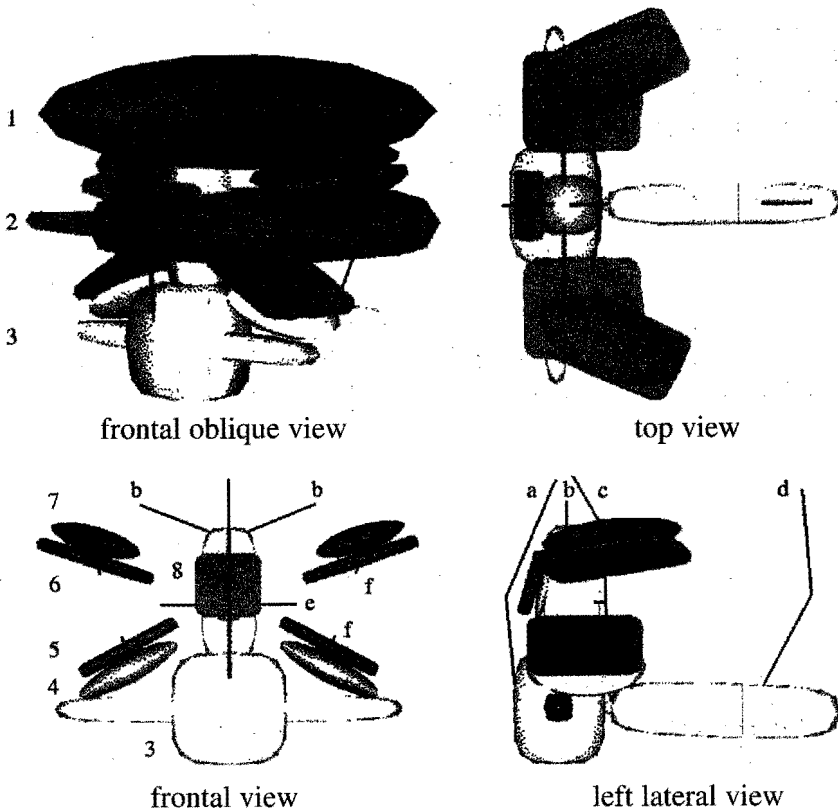
Figure 4.9: Model of segment C0-C2. Shown are the ligaments (blue) and the ellipsoids representing axis with dens, atlas, occiput and articular facet surfaces. The articular facets are rigidly attached to their respective vertebrae. For clarity, the ellipsoids for atlas and occiput are only shown in the upper left picture. Legend: 1. occiput (C0), 2. atlas (C1), 3. axis with dens (C2), 4. upper facets of C2, 5. lower facets of C1, 6. upper facets of C1, 7. occipital condyles, 8. facets for atlas-dens contact; a. anterior membrane, b. alar ligaments, c. tectorial membrane, d. posterior membrane, e. transverse ligament, f. capsular ligaments.

The size and orientation of the ellipsoids (Table 4.8) were derived from anatomical pictures [38, 51] and detailed studies [18, 78, 108, 124], see Meertens [52]. It was assumed that the articular facets are parallel to and in contact with each other in the initial model configuration, and that the facets of the occiput (the occipital condyles) have the same dimensions as the superior facets of the atlas. A limitation of ellipsoids is that they cannot adequately describe the convex-concave articulations between atlas and occiput. To approximate these articulations, the concave facets of the atlas are modelled as almost flat surfaces and the convex facets of the occiput as elliptic surfaces.

Table 4.8: Position, dimensions, orientation and degree of the ellipsoids representing the articular facet surfaces of the upper cervical spine. Orientations are specified with Bryant angles in the order i, j, k as indicated, with $i \neq j \neq k$ and $\phi_k = 0$. For the right surfaces, the y-coordinate and angles ϕ_x and ϕ_z change sign.

position	coordinates of centre point			lengths of semi-axes			relative orientation				degree
of facet	x	y	z	a	b	c	i	ϕ_i	j	ϕ_j	n
	mm			mm				deg		deg	
C2 superior left	−4.1	15.2	5.9	9.0	8.4	2.0	x	−27.7			2
C1 inferior left	−3.9	15.2	−7.2	8.8	8.2	1.0	x	−27.7			8
C1 superior left	−8.0	20.0	5.7	11.3	5.8	1.0	x	18.0	z	−25.2	8
C0 inferior left	−4.0	20.0	−11.2	11.3	5.8	2.0	x	18.0	z	−25.2	2
facet dens	1.5	0.0	18.4	1.0	4.4	5.4	y	−13.2			2
facet atlas	3.7	0.0	2.0	1.0	5.1	4.8	y	−16.0			8
dens ellipsoid	−2.0	0.0	17.2	4.3	4.3	10.0					4

4.4.3 Nonlinear Viscoelastic Ligaments

Most ligaments of the upper cervical spine are modelled with straight line elements, similar as in the model of the lower cervical spine, but the transverse ligament and tectorial membrane are modelled with MADYMO's belt elements as these ligaments can slip over the dens. This dens-ligament contact is represented through a belt system consisting of two belt segments connected to each other at the dens; frictionless slip is

Table 4.9: Origins, insertions, rest lengths and failure forces of the ligaments of the upper cervical spine. The coordinates are relative to the body local coordinate systems, with the body numbers from Table 3.1.

	origin				insertion				rest length	failure force
	body	coordinates			body	coordinates				
ligament	no.	x	y	z	no.	x	y	z	l_0	F_{max}
		mm				mm			mm	N
C1-C2 AM	7	6.3	0.0	0.0	8	7.8	0.0	0.0	17	281
PM	7	−28.6	0.0	−0.7	8	−37.8	0.0	0.0	20	113
CL	7	−4.1	±14.3	4.1	8	−3.9	±16.1	−5.5	7	158
C0-C1 AM	8	7.8	0.0	0.0	9	4.3	0.0	−2.6	19	233
PM	8	−37.8	0.0	0.0	9	−32.6	0.0	−4.3	16	83
CL	8	−8.0	±19.4	3.8	9	−4.0	±20.6	−9.3	7	158
C0-C2 ALAR	7	−1.2	±3.0	26.5	9	2.8	±13.3	−5.8	11	357
TL-left part	7	−6.7	0.0	15.6	8	−5.5	10.3	−0.9	20	354
TL-right part	8	−5.5	−10.3	−0.9	7	−6.7	0.0	15.6		
TM-lower part	7	−7.7	0.0	0.0	7	−6.7	0.0	26.6	36	76
TM-upper part	7	−6.7	0.0	26.6	9	1.7	0.0	−2.1		

AM = anterior membrane	CL = capsular ligament	TL = transverse ligament
PM = posterior membrane	ALAR = alar ligament	TM = tectorial membrane

possible at this connection, such that ligament force and strain are identical in each belt segment. This connection enables the ligaments to curve around the dens. The positions of the ligaments (Table 4.9) were derived from anatomical landmarks [52]. The force-strain behaviour of the ligaments are modelled using the average data of Chazal *et al.* [11] (Fig. 4.3, Table 4.3) combined with the failure forces from Myklebust *et al.* [64] and, for the transverse ligament, from Dvorak *et al.* [20] (Table 4.9).

## 4.5   Validation of Upper Cervical Spine Model

The upper cervical spine model was validated by comparing its ranges of motion with experimental data, its load-displacement curves to those of the upper cervical joints of the global model, and its centres of rotation for flexion/extension to experimental data.

4.5.1   Ranges of Motion for Small Static Moments

The upper cervical spine model was validated by simulating the experiments of Panjabi and co-workers [68, 72, 73, 75], who subjected upper cervical spine specimens to static moments of 1.5 Nm and measured the main and coupled rotations (see Chapter 2). Oda *et al.* [69] presented the coupled translations measured for specific points at the occiput and the atlas. One point was located at the anterior edge of the foramen magnum of the occiput and another one at the anterior ring of the atlas. In the model, these points were positioned at coordinates (9,0,-10) and (5,0,-4) mm in the local coordinate system of C0 and C1, respectively. Rotations were measured using Bryant angles in the order

Table 4.10: Response of C0-C1 and C1-C2 compared with experimental results presented in Figure 4.10.

load	main displacement[a]	coupled displacements[b]
C0-C1		
LB	poor: less flexible	axial rotation to other side
FLX	reasonable	too much posterior shear
EXT	poor: less flexible	
AR	poor: more flexible	lateral bending to other side
C1-C2		
LB	reasonable	lateral shear to other side, axial rotation almost absent
FLX	poor: less flexible	anterior shear (experiment: posterior)
EXT	good	
AR	poor: less flexible	lateral shear and bending too small
a	good: close to average of experimental response	
	reasonable: within SD of experimental response	
	poor: outside SD	
b	differences are noted only for poor agreement with experiments	
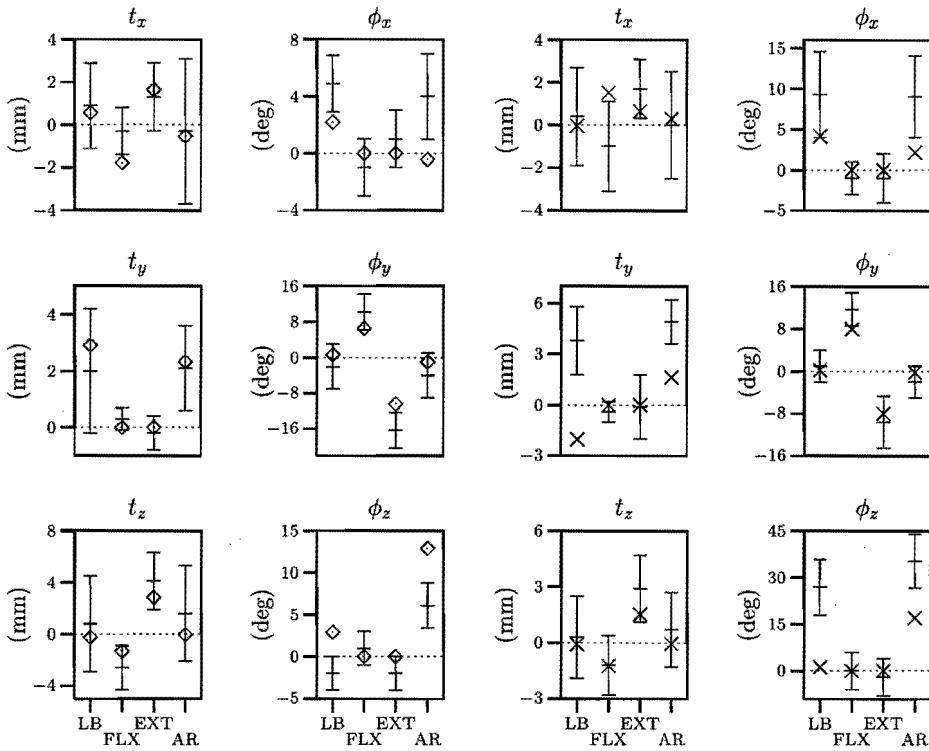
Figure 4.10: Computed main and coupled motions for C0-C1 (◇) and C1-C2 (×) in response to moments of 1.5 Nm compared with experimental data (average ± SD) of Panjabi and co-workers [69, 68, 72, 73, 75]. The applied loads are given along the horizontal axis and the resulting displacements along the vertical axis: lateral bending (LB, ϕ_x), flexion (FLX, ϕ_y), extension (EXT, $-\phi_y$), axial rotation (AR, ϕ_z).

x, y, z. Moments were applied at the occiput such that the direction of the applied moment did not change relative to C0 [73].

Figure 4.10 shows the computed main and coupled displacements with the average experimental displacements, and Table 4.10 gives a qualitative comparison of these displacements. Most main motions of the model are too small, indicating that the model is too stiff. In axial rotation, C0-C1 is too flexible and C1-C2 as well as C0-C2 are too stiff compared with the data. A definite reason for this could not be found, but it may stem from the assumptions introduced to represent the articular facet geometry and the ligament characteristics. A more realistic representation of the convex-concave facet articulations of C0-C1 may lead to a stronger coupling between occiput and atlas, which results in less axial rotation of C0-C1 and improves the response. Most coupled motions of the model are in reasonable to good agreement with the experimental results.

4.5.2 Response to Large Loads

The upper cervical spine model was subjected to large quasi-static loads (500 N, 15 Nm) to determine the load-displacement curves of the C0-C1 and C1-C2 joints. To that end, first, C0 was loaded at the origin of its body local coordinate system to determine C0-C1 behaviour, and, second, C1 was loaded at the origin and along the axes of its body local coordinate system to determine C1-C2 behaviour. Translations were measured at the origin of the body local coordinate systems of C0 and C1.

The load-displacement curves are shown in Figure 4.11 with the curves of the
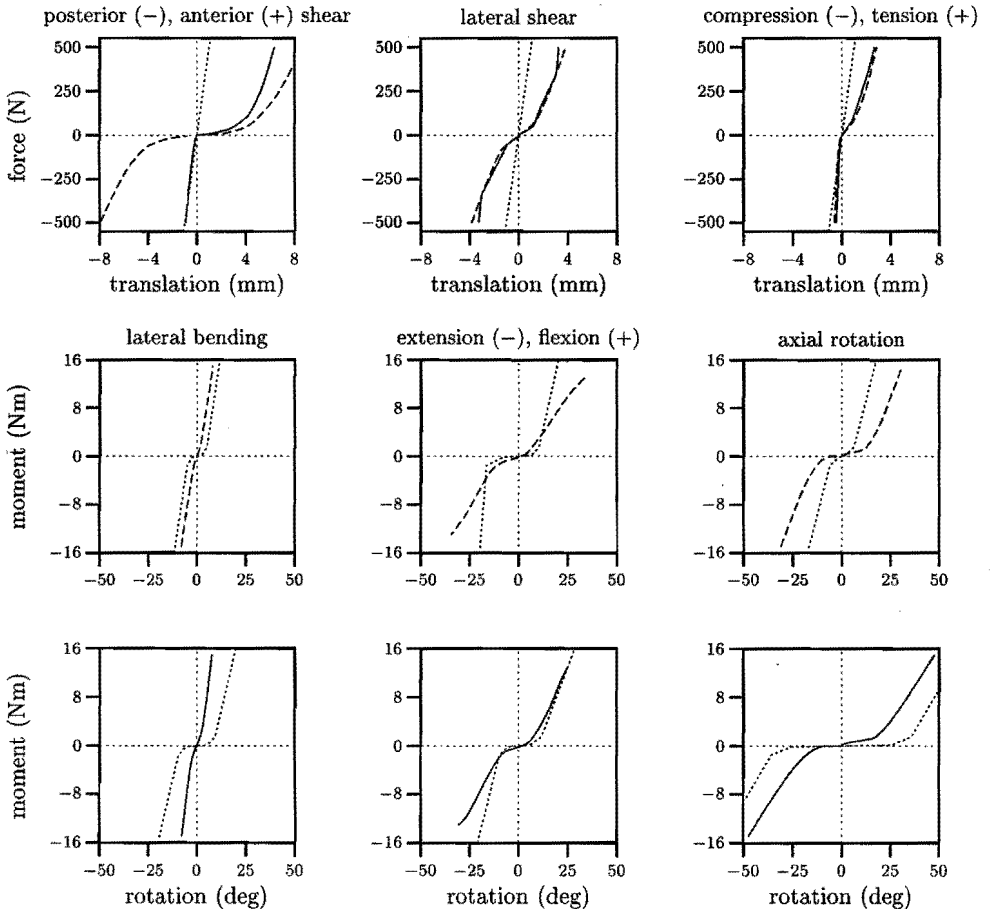
Figure 4.11: Elastic response of C0-C1 (dashed line, top and middle row) and C1-C2 (solid line, top and bottom row) to large loads. The dotted lines are the load-displacement curves for the intervertebral joint of the global model; the moment-rotation curves are the same as in Figure 3.5

upper joints of the global model. All curves clearly reflect the progressive increase in load with increasing displacement, typically for biomechanical structures. The small translation for C1-C2 in posterior shear was caused by contact between the anterior ring of the atlas and the dens. The sudden stiffening of C1-C2 translation in lateral shear was caused by the dens contacting one of the interior facets of the atlas. Most curves show a substantial neutral zone in which little load is needed to deform the structure, reflecting that the ligaments offer little resistance initially. In lateral bending and compression, the neutral zone is absent as the facets, which allow little deformation, are loaded immediately. The responses of C0-C1 are similar to the responses of C1-C2 in lateral shear, tension, compression, lateral bending and extension. The responses of C0-C1 and C1-C2 differ strongly from the (assumed) linear force-translation curves of the global model, but may be realistic, except for the translations in anterior shear of C1-C2 and anterior/posterior shear of C0-C1 which appear unrealistically large (Section 2.3). For C0-C1, this may reflect that the flat upper facets of C1 cannot limit C0 motion as effectively as a more realistic convex-concave interaction would have done. Presently, these translations are limited by ligament forces, which increase progressively with displacement due to the nonlinear characteristics. The same reasoning holds for anterior translation of C1-C2. Although the moment-rotation curves of the detailed

Table 4.11: Loads in the ligaments and facet joints of C0-C2, when C0 is loaded with 500 N, 15 Nm (LB,AR) or 13 Nm (FLX,EXT).

		AS	PS	LS	TNS	CMP	LB	FLX	EXT	AR
ligament force [N]										
C0-C1	AM	0	71	0	49	11	14	0	162	12
	PM	81	0	22	1	11	25	315	0	77
	CL left	20	96	7	116	17	368	230	166	324
	CL right	20	96	51	116	17	0	230	166	421
C1-C2	AM	0	165	0	38	12	37	0	247	28
	PM	92	0	15	24	0	7	249	0	163
	CL left	17	54	22	110	0	267	96	137	355
	CL right	17	54	81	110	0	0	96	137	528
ALAR left		317	293	442	165	16	59	82	385	245
ALAR right		317	293	0	165	16	88	82	385	78
TL		63	2	5	7	2	8	50	18	4
TM		42	0	7	11	0	6	32	9	0
facet force [N]										
C1-C2 left		224	261	274	0	289	0	297	580	289
C1-C2 right		224	261	2	0	289	483	297	580	344
C0-C1 left		200	249	199	0	293	0	440	551	257
C0-C1 right		200	249	0	0	293	460	440	551	258
dens-C1 arch		0	230	0	0	260	0	0	0	0
dens-C1 facet		0	0	171	0	0	190	0	0	0

loading situation

model differ from the curves of the global model, most curves show a similar nonlinear increase in moment with increasing rotation, indicating that the difference in response at large loads originates mainly from the difference in response at small loads, as found in the previous section. Both C0-C1 and C1-C2 appear to be too flexible in extension; a further increase in extension, however, would normally lead to contact between the posterior parts of the ellipsoids representing the vertebrae and, thus, to increased stiffness, but these contacts are not included in the model. In flexion, C0-C1 appears too flexible compared with the global model characteristics. Note, however, that the global characteristics may not be realistic, since several assumptions were introduced to define the curves of the global model.

Table 4.11 shows the loads exerted by the ligaments and facet joints to counterbalance the load applied at C0. Note the large forces in the facet joints and the small forces in the tectorial membrane and transverse ligament. Although no contact is present between the dens and the anterior arch of the atlas for maximum applied moments, dens and arch are in contact during a part of the motion from the neutral to the final position. Thus, this contact is relevant for more loading situations than suggested by the loads in Table 4.11.

4.5.3 Centre of Rotation for Flexion/Extension

The momentaneous and average centres of rotation of C0-C1 and C1-C2 were determined for flexion/extension loading (up to 10 Nm). The momentaneous CORs showed little variation. The average positions (Fig. 4.12) agree well with the experimental data for C1-C2 of Dvorak *et al.* [19] (Fig. 2.7) and for C0-C1 and C1-C2 of Van Mameren *et al.* [43]; the C1-C2 COR lies somewhat lower in the model. Note that the origin of the coordinate system of C0, as shown in Figure 4.12, was positioned at the C0-C1 COR as presented by Van Mameren *et al.* and Kapandji [38] (Appendix A).

centres of rotation
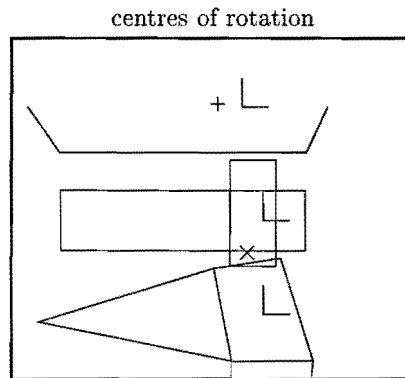
Figure 4.12: Average centre of rotation of C0 relative to C1 (+) and of C1 relative to C2 (×). Solid lines depict the contours of the vertebrae, and the body local coordinate systems.

4.6 Parametric Study with Upper Cervical Spine Model

A parametric study was conducted with C0-C2 to determine the effect of parameter changes on the model response. Selected parameters are the ligament stiffnesses and articular facet orientations. Some stiffnesses were grouped such that eight parameters remained to be varied. The parameters are listed in Table 4.12 with the amount of variation relative to the normal situation. The loading conditions and model responses were chosen identical to the parametric study of C3-C4 (Table 4.6), but the maximum applied load was 8 Nm.

A fractional factorial design in 16 runs was chosen (Appendix B). The effect of each parameter on the average response is shown in Figure 4.13 for both the main and coupled motions of C0-C1 and C1-C2. Since the coupled motions are small, the effects of the parameters appear large, but the absolute change in coupled motions is small. Table 4.12 lists the effects for the main motions. Increased stiffness of the alar ligaments (parameter A) limits extension of C0-C1 and C1-C2, and affects anterior/posterior shear coupled with flexion/extension loading. The anterior and posterior membranes (B,C), being midsagittal ligaments, mainly affect the main and coupled response to flexion/extension. The capsular ligaments (D,E) influence axial rotation and lateral bending most strongly, although they are also relevant for the response to flexion/extension. The lateral facet orientation of C1-C2 (F) affects the main lateral rotation and the lateral rotation coupled with axial loading. The response of C0-C1 is most strongly influenced by its capsular ligaments and facet orientations (parameters D,G,H). The lateral facet orientation (G) also has a large effect on the coupled rotation in lateral bending and axial rotation.

Table 4.12: Selected parameters, their range of variation and their effect on model responses R. The responses are explained in Table 4.6.
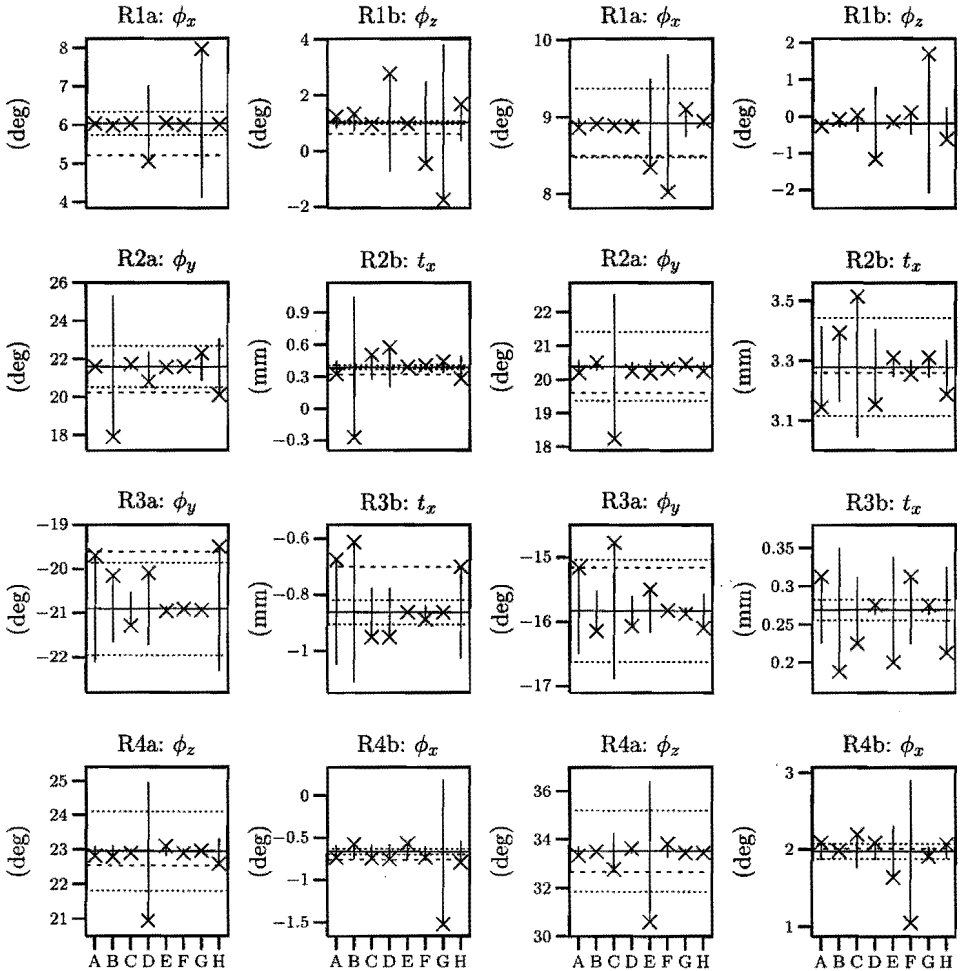
| | | | effect on response[a] | | | | | | | |
| | level | | C0-C1 | | | | C1-C2 | | | |
parameter	−	+	R1a	R2a	R3a	R4a	R1a	R2a	R3a	R4a
ligament stiffness										
A ALAR	−25%	+25%	0	0	−	0	0	0	0	0
B AM, PM C0-C1	−25%	+25%	0	−	0	0	0	0	0	0
C AM, PM C1-C2	−25%	+25%	0	0	0	0	0	−	−	0
D CL C0-C1	−25%	+25%	−	0	0	−	0	0	0	0
E CL C1-C2	−25%	+25%	0	0	0	0	−	0	0	−
facet orientation										
F C1-C2 ϕ_x (left)	−10°	+10°	0	0	0	0	−	0	0	0
G C0-C1 ϕ_x (left)	−10°	+10°	+	0	0	0	0	0	0	0
H C0-C1 ϕ_z (left)	−10°	+10°	0	−	−	0	0	0	0	0

a   response with parameter at high level; difference with average response is
    0   less than 5%,
 −/+ a decrease/increase in absolute value with more than 5%.

Combining the results of Table 4.12 and Figure 4.13 with those of Table 4.11, it appears that the ligament and facet forces are good predictors for the effect parameter changes of ligaments and facets have on the model response. From Table 4.11, however, it was expected that the alar ligaments would also have a large effect on the response to axial loading, but this was not found in the parametric study. Further, it was expected

Figure 4.13: Effect of parameters A–H (Table 4.12) on responses R (Table 4.6). The left two columns are for C0-C1, the right two columns for C1-C2. Solid horizontal line: average response of all 16 runs. Dashed line: centre response. Dotted lines: response boundaries at ±5% of average response. Solid vertical line: average effect of parameter on response. Cross (×): average response for all 8 runs in which the parameter was at its high level.

from the large C1-C2 facet forces, that C1-C2 facet orientation would be relevant for all considered loading situations and not only for lateral bending, as was revealed by the parametric study.

4.7 Discussion

The detailed models of the upper and lower cervical spine comprise rigid vertebrae and occiput, linear viscoelastic intervertebral discs, nonlinear viscoelastic ligaments and frictionless, nonlinear viscoelastic facet joints.

Intervertebral Discs The intervertebral discs are modelled as three-dimensional linear viscoelastic elements. The stiffness data were obtained from the data of Moroney *et al.* [61] for disc segments including also the anterior and posterior longitudinal ligaments and the uncovertebral joints. The effect of these ligaments was assumed negligible, but the (unknown) effect of the uncovertebral joints on disc segment behaviour is implicitly incorporated in the (disc) model. Therefore, the uncovertebral joints are not modelled separately. Moroney used linear regression to derive the disc stiffnesses from the data. It is questionable whether linearity still holds when the applied loads are larger than the relatively small loads used by Moroney. Experiments are needed to verify this.

Ligaments The ligaments are modelled as one-dimensional nonlinear viscoelastic elements resisting loads only in tension. The insertions were derived from the adopted vertebral geometry and can be considered as fairly accurate. Because no single study was available which presented detailed mechanical characteristics of the cervical ligaments, the nonlinear force-strain data of thoracolumbar ligaments (Chazal *et al.* [11]) were scaled with the failure forces of cervical ligaments (Myklebust *et al.* [64]) to obtain nonlinear force-strain curves. Although the experimental set-ups in the studies of Chazal and Myklebust are alike, the reported failure displacements differ strongly for comparable ligaments, but an explanation could not be found. Consequently, the reliability of the used force-strain curves is questionable and should be checked when reliable, detailed data becomes available.

Further, two assumptions need to be checked experimentally. The first one is the assumption that the ligaments are taut nor slack initially. The parametric study with segment C3-C4 revealed that an initial strain of 5% of the ligament's reference length has almost the same effect on the model response as a change in stiffness with 25%, indicating that initial strain may strongly affect the model response. The second assumption is the representation of the membrane-like ligaments as line elements. Recently, Mommersteeg *et al.* [58] found that knee ligaments need to be considered as multi-bundle structures to quantify their mechanical behaviour accurately, since their fibre bundles are nonuniformly loaded. Mathematically, this requires the ligaments to be modelled by several line elements representing the differently positioned and orientated fibre bundles within the same ligament. More advanced experimental

set-ups combined with numerical optimisation are needed to obtain the mechanical characteristics of the individual elements. Presently, only data from (traditional) uniaxial tensioning experiments are available for (cervical) spinal ligaments, for which the representation of ligaments as single line elements is sufficient.

Facet Joints The facet joints are modelled as almost rigid contact-interactions between hyperellipsoids representing the articular facets. The ellipsoids can slide frictionless relative to one another. The dimensions, position and orientation of the ellipsoids were derived fairly accurately from reported experimental data, especially for the facets of the lower cervical spine. The shape of a hyperellipsoid can be varied from elliptic to (almost) flat, which suffices for most facet surfaces, except for the concave facets of the atlas, which had to be approximated as flat surfaces. In the next MADYMO version (5.2, spring 1996), rigid bodies may be given arbitrary surfaces, enabling a more realistic representation of the facet geometry than is currently possible with hyperellipsoids.

Validation Motion segments C3-C4 and C5-C6 were validated to check the accuracy of the lower cervical spine model. The main and coupled motions agreed well with the experimental results of Moroney *et al.* [61] for small loads (20 N, 1.8 Nm) applied to the upper vertebra. The response to large loads (500 N, 20 Nm) was in reasonable to good agreement with the behaviour of the intervertebral joints of the global model, the characteristics of which are based on experimental data (Chapter 3). A major difference is the absence of a neutral zone for the segment models, due to the linear stiffness of the intervertebral discs. The centre of rotation of the upper vertebra relative to the lower one was in excellent agreement with experimental data for flexion/extension.

The upper cervical spine model was also validated with experimental data. For small moments (1.5 Nm), the main motions of C0-C1 and C1-C2 were generally smaller than the experimental motions, indicating that the model is too stiff. Most coupled translations and rotations agreed reasonably with the data. The same differences in response were also found for large loads (500 N, 15 Nm) when the responses were compared to the intervertebral joint characteristics of the global model. A comparable nonlinear stiffening behaviour was found, but the displacements were smaller. These differences may be caused by the assumptions introduced to represent the ligament characteristics and the facet surfaces. The centres of rotation of C0-C1 and C1-C2 for flexion/extension agreed well with experimental data, indicating that the coupling between flexion/extension and anterior/posterior translation is well described by the model.

In conclusion, detailed models of the lower and upper cervical spine were developed according to the adopted research strategy. The mechanical behaviour of lower cervical motion segments agrees well with experimental data for various different loading conditions. The mechanical behaviour of the upper cervical spine model shows some discrepancies with experimental results, but can be considered as satisfactory. In the next chapter, these models are joined to form a detailed model of the cervical spine.
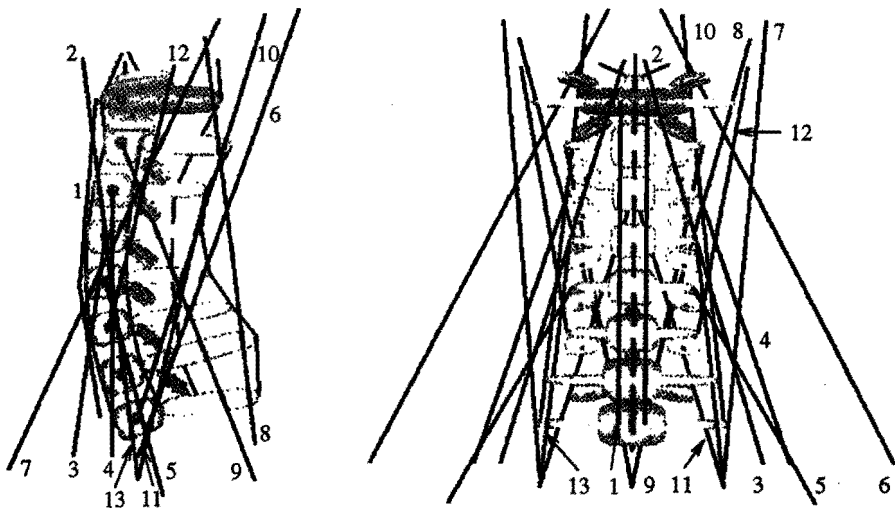
Detailed Head-Neck Model
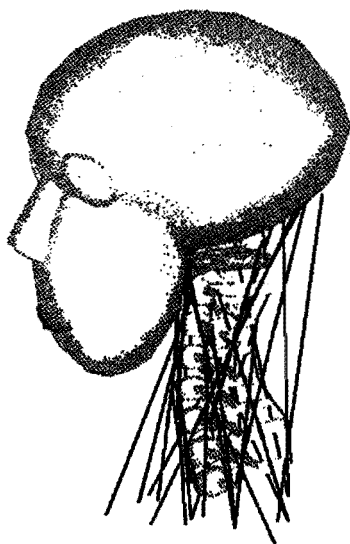
This chapter presents the detailed head-neck model that was developed to study the dynamic behaviour of the human head and neck in acceleration impacts. The detailed model provides the deformations and loads of the soft tissues of the cervical spine, and is, therefore, suited to study injury mechanisms. It forms the last step in the adopted research strategy, which is to proceed from a simple to a detailed model. Section 5.1 describes the model with emphasis on the new aspects. Validation of the model is treated in Sections 5.2 and 5.3 presenting the response of the model to frontal and lateral acceleration impacts. Tissue loads are compared with reported failure loads in Section 5.4. Section 5.5 gives the results of the parametric study that was performed with the model for frontal impacts. Model and results are discussed in Section 5.6.

5.1 Model Description

The detailed head-neck model was constructed by joining the detailed models of the
upper and lower cervical spine (presented in Chapter 4) and adding Hill-type muscle el-
ements (Fig. 5.1). The detailed model consists of rigid vertebrae and a rigid head, linear
viscoelastic intervertebral discs, nonlinear viscoelastic ligaments, contractile muscles,
and frictionless, nonlinear viscoelastic facet joints. The initial body configuration and
the inertial data of the detailed model are the same as of the global model (Table 3.1).
Hereafter, only the new aspects of the model are treated: first, the geometric and me-
chanical characteristics of the muscle elements are presented; second, the deformation-
rate sensitivity, which is explicitly incorporated into the model, is described.

5.1.1 Hill-type Muscle Elements

The major neck muscles are included in the model to study the effect of passive and
active muscle behaviour on the head-neck response to impacts. Only the stronger and
more superficially located muscles were selected. Thus, the deep cervical muscles are
not included in the model. These muscles, which run from one vertebra to another, do
not directly influence the motion of the head, but have an indirect influence as they
act to stiffen the spine. It is not known whether this effect is significant (in impacts)
and it will be difficult to quantify experimentally; therefore, no attempt was made to

Figure 5.1: Lateral and frontal view of the detailed head-neck model. Yellow ellipsoids repre-
sent the skull and the vertebrae with 'arch', transverse processes and articular facet surfaces.
Blue and red line elements depict the ligaments and the muscles, respectively. Muscle numbers
refer to Table 5.1.

include this effect or to compensate for it.

The muscles are represented through fourteen mid-sagittal symmetrical pairs of Hill-type muscle elements provided by MADYMO. A simplified geometric representation was chosen in which each muscle force is directed along the straight line connecting origin and insertion (line of action). Such representations are widely used in studies of the upper and lower limbs [117] and in studies on the function of muscles in head-neck stabilization [98, 115]. This representation seemed justifiable to gain a first impression of the relevance of muscles in impacts. An important limitation is that the muscles cannot curve around the vertebrae, which may lead to inaccurate lines of action for large intervertebral rotations, but this cannot be prevented with the current muscle elements of MADYMO. The coordinates of the origins and insertions of the muscles (Table 5.1) represent an average position, since most cervical muscles have several origins and insertions. These positions are based on detailed anatomy textbooks [38, 86, 87], data on bony geometry [74, 80] and choices made by other researchers in this field [15, 96, 115].

The MADYMO Hill-type muscle elements can describe passive and active behaviour [107]. The muscle elements comprise a contractile element (CE) describing the active force F_{CE} generated by the muscle through contraction and a parallel elastic element (PE) describing the passive elastic force F_{PE} due to elongation of the muscle tissues. Muscle force F_{mus} is the sum of both forces, thus

$$F_{mus} = F_{CE} + F_{PE}.$$

Table 5.1: Geometric parameters for the left muscles in the detailed head-neck model; for the right muscles the y-coordinates change sign. Body numbers refer to the numbers used in Table 3.1. Rest length l_0 is the muscle length in the initial upright configuration of the model.

muscle name	origin body no.	x	y	z	insertion body no.	x	y	z	area A_{pcsa}	rest length l_0
		mm				mm			cm^2	mm
1 longus colli (C1-C5)	4	10	5	0	8	10	5	0	0.4	73
1 longus colli (C5-T1)	1	15	5	0	4	10	5	0	0.4	51
2 longus capitis	5	0	24	0	9	19	4	−4	0.4	73
3 scalenus anterior	1	25	50	−15	5	0	24	0	0.9	90
4 scalenus medius	1	10	60	−15	6	0	25	0	1.0	109
5 scalenus posterior	1	−10	70	−30	4	0	23	0	0.9	97
6 trapezius	1	0	100	−15	9	−64	10	15	1.8	204
7 sternocleidomastoid	1	50	35	−20	9	−33	50	11	3.7	192
8 splenius capitis	1	−45	0	−10	9	−28	44	4	1.5	164
9 splenius cervicis	1	−45	0	−24	7	0	26	0	0.4	143
10 semispinalis capitis	1	0	35	0	9	−51	18	13	3.1	164
11 semispinalis cervicis	1	0	35	−24	6	−36	0	0	2.3	120
12 longissimus capitis	3	0	25	0	9	−16	43	−7	0.3	106
13 longissimus cervicis	1	0	35	−24	5	0	24	0	0.3	95

Passive muscle behaviour is modelled similar as in the model of Deng and Goldsmith [15] by the nonlinear force-strain relation

$$F_{PE} = A_{pcsa} \frac{k \cdot \epsilon}{1 - \epsilon/a}$$

with ϵ the strain of the muscle, k the passive muscle stiffness, a the strain asymptote, and A_{pcsa} the physiologic cross-sectional area of the muscle (Fig. 5.2a). The strain is defined as $\epsilon = l_r - 1$ in which the dimensionless muscle length $l_r = l/l_{ref}$ with l the momentaneous muscle length and l_{ref} the optimum or reference length at which active force is generated most efficiently. The cross-sectional areas A_{pcsa} were derived from Moroney *et al.* [60].

Active muscle behaviour is modelled using the standard functions provided by MADYMO, which resemble the functions widely used in studies on muscle coordination [113, 116, 129]. These *generic* functions are scaled by the rest length l_0 and cross-sectional area A_{pcsa} to represent a specific muscle. The active force is given by

$$F_{CE} = A \cdot F_{max} \cdot f_H(v_r) \cdot f_L(l_r).$$

Factor A, the active state, is the normalized activation level of the muscle and varies between 0 (rest state) and 1 (maximum activation). Parameter F_{max} is the muscle force at maximum activation in isometric conditions and at the reference length. It follows from $F_{max} = \sigma_{max} \cdot A_{pcsa}$ with σ_{max} the maximum isometric muscle stress. The dimensionless lengthening velocity is defined as $v_r = v/V_{max}$ with v the momentaneous lengthening velocity and V_{max} the maximum shortening velocity of the muscle. It is assumed that V_{max} is independent of the active state. Function f_H is the normalized active force-velocity relation (Hill-curve). The standard curve has separate functions
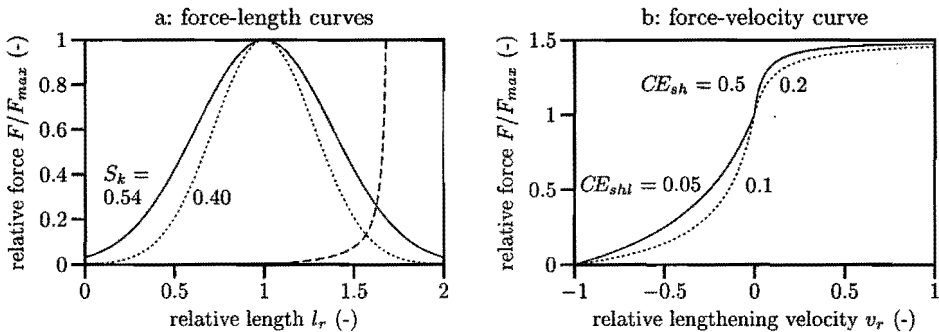
Figure 5.2: Muscle functions. (a) Normalized passive force-length curve F_{PE} (dashed) and standard active force-length curve f_L for $S_k = 0.54$ (solid) and $S_k = 0.40$ (dotted). (b) Standard force-velocity curve f_H (Hill-curve) for $CE_{sh} = 0.5, CE_{shl} = 0.05$ (solid) and $CE_{sh} = 0.2, CE_{shl} = 0.1$ (dotted). The other parameter values are listed in Table 5.2. The curve for F_{PE} and the solid curves for f_L and f_H are used in the head-neck model.

for lengthening and shortening of the CE-element:

$$f_H(v_r) = \begin{cases} 0 & v_r \leq -1 \\ \dfrac{1 + v_r}{1 - v_r/CE_{sh}} & -1 < v_r \leq 0 \\ \dfrac{1 + v_r CE_{ml}/CE_{shl}}{1 + v_r/CE_{shl}} & v_r > 0. \end{cases}$$

The shape is determined by the parameters CE_{sh} and CE_{shl}, whereas CE_{ml} defines the maximum force the muscle can generate during lengthening relative to the maximum isometric force F_{max} (Fig. 5.2b). Function f_L is the normalized active force-length relation with standard function

$$f_L(l_r) = e^{-\left(\frac{l_r - 1}{S_k}\right)^2},$$

in which parameter S_k determines the shape (width) of the curve (Fig. 5.2a).

Muscle activation is described by two dynamical processes: neural excitation and active state dynamics. The normalized neural excitation E ($0 \leq E \leq 1$) is described by the first-order system

$$\frac{dE}{dt} = \frac{u - E}{T_e}$$

with dE/dt the derivative of E towards time t, T_e the time-constant and u the normalized neural input ($0 \leq u \leq 1$) [113]. Here, it is assumed that the activation of a muscle is determined by a single neural input: the muscle is not activated for $u = 0$ and maximally activated for $u = 1$. The normalized active state A ($0 \leq A \leq 1$) is described by the first-order system

$$\frac{dA}{dt} = \frac{E - A}{T_a} \quad \text{with time-constant } T_a = \begin{cases} T_{ac} & \text{if } E > A \quad \text{activation} \\ T_{da} & \text{else} \qquad \text{deactivation.} \end{cases}$$

Deactivation is not considered here.

Muscle dynamics is fully described by time-constants T_e and T_{ac}, and the neural input u. The time-constants lie in the range $25 \leq T_e \leq 50$ ms and $5 \leq T_{ac} \leq 15$ ms

Table 5.2: Mechanical parameters for passive and active muscle behaviour used in the model.

muscle parameter	symbol	value	unit	Reference
maximal isometric stress	σ_{max}	75	N/cm^2	[116]
optimum length	l_{ref}	$1.05 \cdot l_0$	m	[114]
maximum shortening velocity	V_{max}	$5.0 \cdot l_0$	1/s	[114, 116]
shape force-velocity curve (shortening)	CE_{sh}	0.5	–	[114, 116]
shape force-velocity curve (lengthening)	CE_{shl}	0.05	--	[107]
maximum relative force (lengthening)	CE_{ml}	1.5	--	[116, 129]
shape active force-length curve	S_k	0.54	–	[107]
passive force-length stiffness	k	3.34	N/cm^2	[14]
passive force-length asymptote	a	0.7	–	[14]
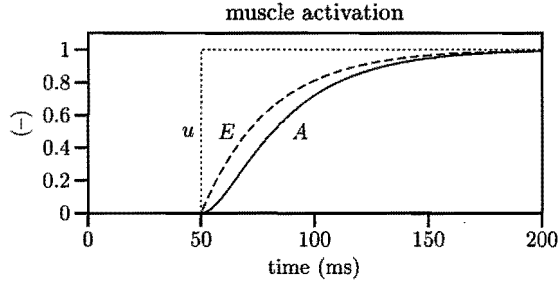
Figure 5.3: Time signals of neural input u, neural excitation E and active state A for $t_r = 50$ ms, $T_e = 30$ ms and $T_{ac} = 10$ ms. Signal A is used in the model to describe muscle contraction.

according to Winters and Stark [113]. A step response is assumed for input u: it changes instantaneously from 0 to 1 at a certain reflex time t_r. Reflex time is defined as the time it takes to start activating a neck muscle in reaction to an external disturbance such as an impact. Muscle contraction time is the time lapse between the onset of muscle activation and the moment of maximum muscle activation ($A \geq 0.95$). Figure 5.3 shows the change of u, E and A with time for $t_r = 50$ ms, $T_e = 30$ ms and $T_{ac} = 10$ ms. Note the fast rise and slow decay of A. The muscle contraction time is about 100 ms.

Reported reflex times for neck muscles range from 25 to 90 ms for the unexpected impact and contraction times vary from 25 to 100 ms [23, 88, 93, 103]. For an anticipated impact as may occur in a frontal impact (visual reflex), reflex times will be smaller and can even be negative if the reflex starts before the moment of impact. For the model, the muscle activation signal of Figure 5.3 is chosen for simulations of sled acceleration impacts performed with human volunteers (Sections 5.2 and 5.3). This means that the muscles start to react at the time the sled starts to accelerate, as it takes about 50 ms for the sled to start moving after the volunteer initiated the impact (at time zero).

5.1.2 Deformation-Rate Sensitivity

Soft tissues, such as intervertebral discs and ligaments, exhibit stiffening behaviour: the stiffness of the tissue increases with increasing deformation rate. The viscoelastic models used to represent the discs and ligaments (Chapter 4) cannot account for the stiffening of tissues [24]. Stiffening, therefore, is explicitly included in the model. In MADYMO, this can be done through an amplification factor M that transforms the static elastic force F_{stat} to the dynamic elastic force $F_{dyn} = M \cdot F_{stat}$.

Experiments have revealed that the increase in stiffness is moderate for soft tissues: stiffness increases two to five times when the deformation rate increases a factor 100 to 1000 relative to quasi-static loading rates of about 10 mm/s or 10 deg/s [10, 24, 49, 127]. Because the deformation rates vary considerably in impacts, it is assumed that the dynamic stiffness averages twice the static stiffness Thus, $M = 2$ is used to account for the deformation-rate sensitivity of the discs and ligaments.

The amplification factor is included in the parametric study (Section 5.5).

5.2 Response to Frontal Impact

As a first step in the validation of the model, a frontal impact performed with human volunteers was simulated using both active and passive muscle behaviour. First, the model responses are compared with the human volunteer response corridors presented in Section 3.2. Second, the positions of the centres of rotation are compared with published data.

A simulation of a frontal impact of 200 ms takes 1020 CPU-seconds using MADYMO with a fifth order Runge-Kutta-Merson integration with variable time step on an SG Indigo 2 R4400 workstation. Virtually the same results are obtained using a fourth order Runge-Kutta-Merson integration with a fixed time step of $5 \cdot 10^{-5}$ s, costing 390 CPU-seconds, which still is ten times the CPU-time required to run the global model.

5.2.1 Validation with Response Corridors

The detailed model was subjected to the same frontal impact as the global model and the same response corridors are used for validation (see Section 3.2). Both passive and active muscle behaviour were simulated to study the effect of muscle contraction on the head-neck response. The active and passive response are the response for the model with and without muscle activation, respectively. Figure 5.4 depicts the model configurations and shows that the muscle lines of action appear to become unrealistic after about 140 ms for both responses. The active response is compared with the response corridors first, and then with the passive response.

| 80 ms | 100 ms | 120 ms | 140 ms | 160 ms | 180 ms |
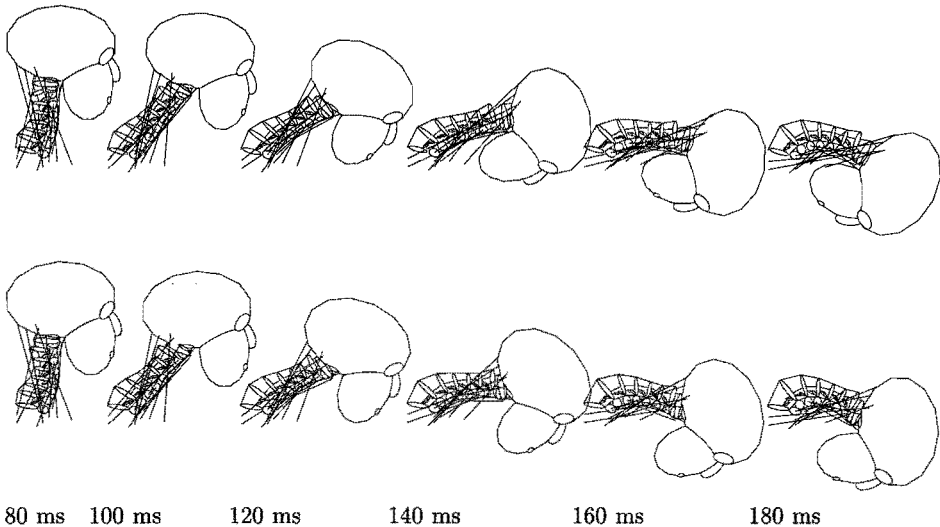
Figure 5.4: Configurations of model with passive (top) and active (bottom) muscle behaviour between 80 and 180 ms for the frontal impact.
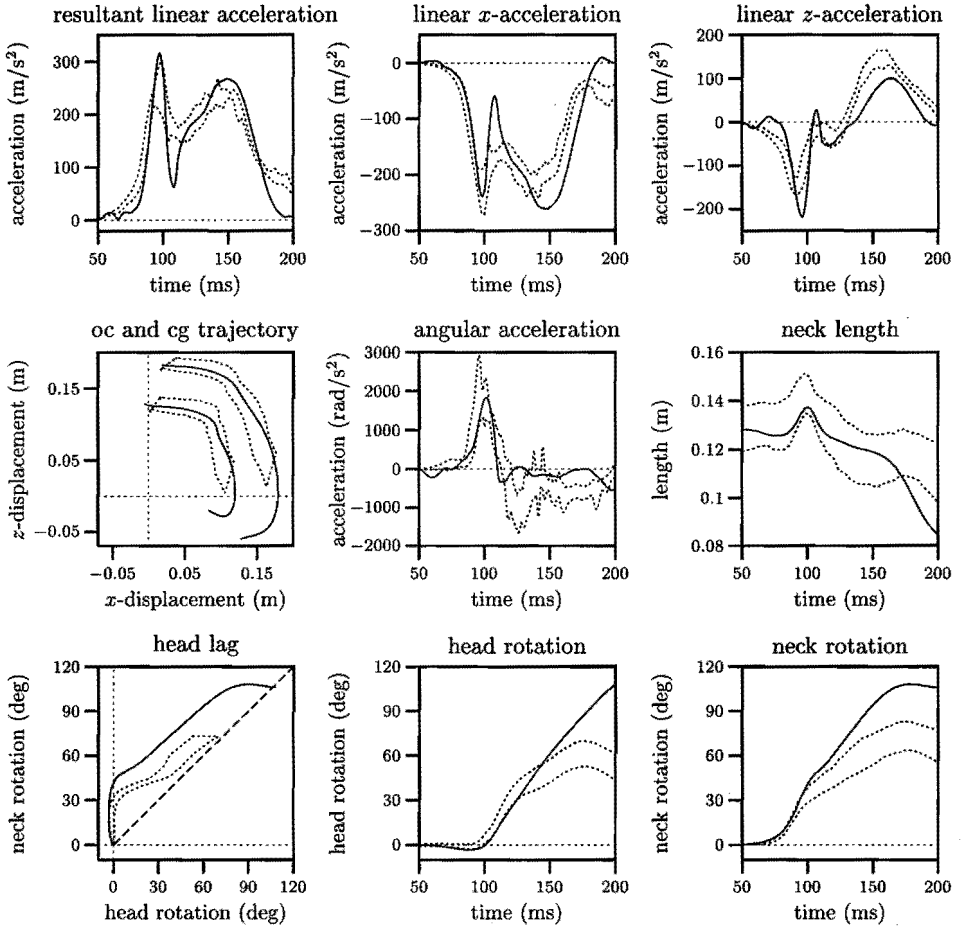
Figure 5.5: Response of the model with active muscle behaviour (solid line) and human volunteer response corridors described in Section 3.2 (dotted lines) for the frontal impact.

Figure 5.5 compares the active model response with the response corridors. The linear accelerations of the head centre of gravity compare well with the corridors, although the minimum about 110 ms for the resultant acceleration is too strongly reflected by the model. Initially, the angular acceleration of the head agrees favourably but, after 120 ms, it is minimal for the model while it is still significant for the volunteers. The neck length response is accurate up to 170 ms. The trajectories of the occipital condyles and centre of gravity of the head nicely follow the response corridors but, eventually, the downward displacements (z) become too large, showing that the model is more flexible than the human volunteers. This is also reflected by the head and neck rotation, which fall within the corridors up to 150 ms and 100 ms, respec-
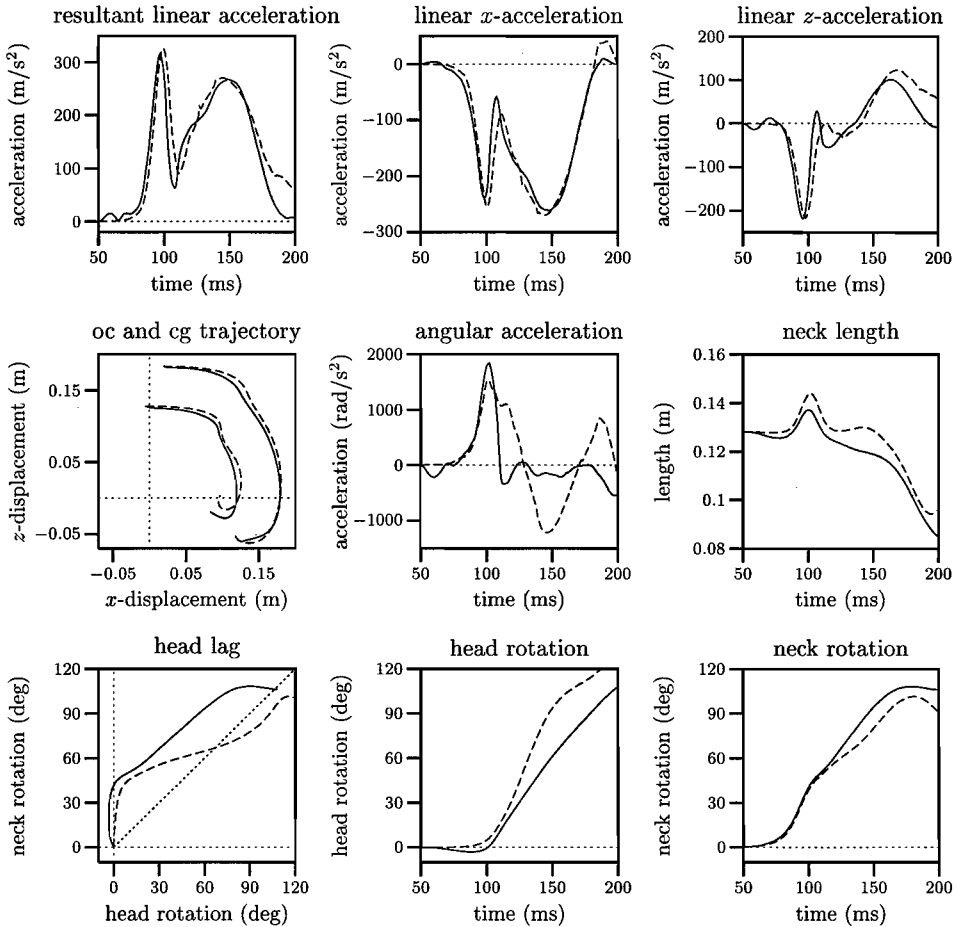
Figure 5.6: Response to frontal impact of the model with active (solid line) and passive (dashed line) muscle behaviour.

tively, before they become much too large. The maximum head rotation would have been limited if chin-torso contact was included in the model (Fig. 5.4); chin-torso contact did not occur for the volunteers. The head lag is too strongly reflected by the model, because the head flexion starts somewhat late while neck rotation begins early in comparison with the volunteer responses. The head lag response also shows that, head and neck move more or less as one unit, after the head lag and up to 80 deg head rotation; that is, rotation of the head relative to the neck is almost absent. This 'locking' phenomenon was also seen for the volunteers and causes the neck rotation to be larger than the head rotation during the entire impact. Locking is, thus, adequately reflected by the model.
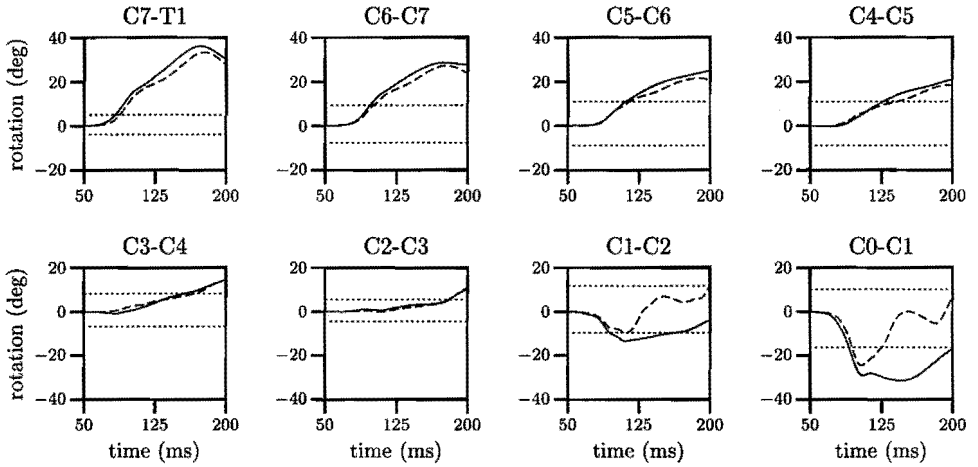
Figure 5.7: Flexion/extension of the intervertebral joints for the active (solid line) and passive (dashed line) model with static *in vivo* ranges of motion (dotted lines, Table 3.3 and 3.4).

Figure 5.7 depicts the intervertebral joint rotations for the active and passive response in comparison with the *in vivo* ranges of motion for static flexion/extension. Both upper cervical joints go into extension, while the other joints go into flexion, illustrating that the head rotation lags behind the neck rotation. The maximum extension of C0-C1 is about twice the range of motion. The C0-C1 rotation shows that the rotation of the head relative to the neck changes little between 100 and 160 ms which confirms the observation regarding locking. The rotation of C1-C2, C2-C3 and C3-C4 are moderate and exceed the ranges of motion only slightly, whereas the rotation of the lowest three joints are much larger than the ranges of motion (which was also the case for the global model). Apparently, these joints are not stiff enough to resist the large bending moments generated by the inertial loading of the head and vertebrae. This may be due to inappropriate stiffnesses of the intervertebral discs and ligaments, which are the same for each vertebral level, or due to the unrealistic lines of action, through which the muscles cannot adequately constrain the head-neck motion. The extreme joint rotations cause the unrealistically large neck and head rotation.

Figure 5.6 compares the active response with the passive response. Muscle contraction, clearly, influences the response. Head angular acceleration is strongly affected: the acceleration is minimal after 120 ms for the active response, while it strongly oscillates for the passive response. The linear accelerations as well as the trajectories of the occipital condyles and centre of gravity of the head change little due to muscle contraction; this is also reflected by the model configurations (Fig. 5.4). The head rotation and, consequently, the head lag show a stronger change in response. For the passive response: the head lag decreases somewhat, the head rotation increases, the rotation of head and neck are no longer locked, and the head rotation eventually exceeds the

neck rotation. This indicates that the muscles are responsible for both the head lag and locking of head and neck rotation, which confirms the observations made by Wismans *et al.* [119], who found similar differences between the experimental head-neck responses of human volunteers and human cadavers subjected to sled acceleration impacts. The neck length response shows that the muscles compress the neck to some extent. Neck rotation is larger for the active model because the lines of action of the muscles become unrealistic for large rotations such that the head is pulled towards the torso rather than pulled back and upwards. This is also reflected by the intervertebral joint rotations (Fig. 5.7): the rotations of the lower joints are increased due to muscle contraction, which is in contradiction with the expectation that muscle tensioning stiffens the neck and, consequently, leads to less rotation. The muscles compress the neck and increase the lower joint rotations as soon as the joints go into flexion. Since the muscles do not follow the curvature of the neck, the muscles increase the neck rotation instead of decreasing it.

Muscle contraction strongly affects the rotation of both upper cervical joints. First, C0-C1 and C1-C2 go into extension due to inertia effects for both the passive and active response. Then, the muscles increase the extension further for the active response, while the head rebounds into flexion for the passive response. Consequently, head lag is larger for the active response. The extension is such that the skull almost contacts the arch of the atlas (this contact is not included in the model). This large extension may be due to inappropriate balancing of muscle forces: in the model, all muscles are activated identically, while the human volunteers tend to stabilize their head and neck. It may also be due to inadequate modelling of the upper cervical spine. In the model, only a few structures are present to limit extension of the upper joints. In Chapter 4, it was already found that the upper joints were too flexible in extension for large static loads.

5.2.2 Centres of Rotation

The segmental centres of rotation (CORs) were determined for the active model to further validate the model response, since the response corridors give no indication whether the vertebral motions are adequate. The joint rotations were verified quantitatively by comparing them with the ranges of motion. The CORs are a qualitative measure for the vertebral kinematics as they depend on both the rotations and translations of a vertebra relative to its adjacent lower vertebra. Therefore, CORs can be used to verify the vertebral kinematics.

The dynamic CORs of the model are compared with the quasi-static CORs found for volunteers performing slow flexion/extension movements (Section 2.3), as data on the CORs were not available for dynamic loading. The CORs depend on the cervical anatomy and the applied load. For the quasi-static CORs, bending moments are the dominant loads producing the vertebral motions. It is expected that the dynamic CORs deviate little from the quasi-static CORs as long as bending is the dominant load. In impacts, however, also large shear and compression/tension forces may be present which can cause a shift of the CORs in any direction, as explained by Bogduk *et al.* [7].
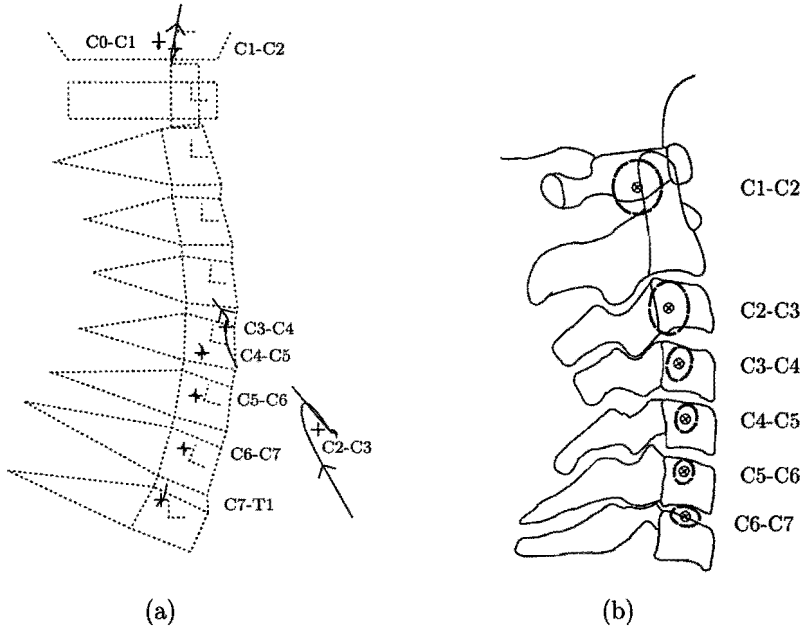
Figure 5.8: (a) Path of the momentaneous centres of rotation (CORs) of a vertebra relative to its lower adjacent vertebra (solid line), and the average COR (+). The dotted lines outline the vertebral geometry; also shown are the x, z-axes of the body local coordinate systems. (b) CORs as presented by Dvorak *et al.* [19], see Section 2.3.

Centres of rotation were determined between 50 and 160 ms using the method of Spiegelman and Woo [99]. Momentaneous CORs were computed for each two vertebral positions that were 70 ms apart, and with the vertebral positions at a 2 ms interval; that is, 21 momentaneous CORs were computed from the paired vertebral positions at (50,120), (52,122), $\cdots$, (90,160) ms (Fig. 5.8). For 70 ms, relative rotations were large enough to give accurate results. The momentaneous CORs show little variation, except for C3-C4 and C2-C3: the large anterior translations of these joints cause their CORs to lie remote from the vertebrae. Apparently, bending is not the dominant load (or deformation, see Fig. 5.7) for these joints, which results in a shift of the CORs. For C1-C2, a sudden sliding motion of the facet joints at about 154 ms causes the momentaneous CORs to change erratically and move outside the picture.

Average CORs were computed as the average position of the momentaneous CORs. The average CORs of the model lie close to the average positions found for human volunteers, except for C2-C3 and C3-C4 (compare Fig. 5.8a and b). The COR for C1-C2 lies above the dens for the model, whereas it is found at the posterior side and halfway the height of the dens for the volunteers Thus, the dynamic CORs of the model compare well with the quasi-static CORs of the volunteers, indicating that the (relative)

kinematic behaviour of the vertebrae are accurately described by the model, at least for loading conditions in which bending is dominant over shear and axial forces.

For the model, the CORs move upwards (and backwards) for the motion after 160 ms because of a decrease of the relative orientations combined with a strong compression and posterior shear of the discs occurring at the end of the simulation. This loading situation differs from the loading situation (bending) used to determine the CORs for the volunteers. Therefore, the momentaneous CORs after 160 ms were not considered here.

5.3 Response to Lateral Impacts

Additional to the frontal impact, the model is validated for lateral impacts corresponding to sled acceleration tests performed with human volunteers. First, the response corridors are presented. Then, the responses of the models with active and passive muscle behaviour are compared with the volunteer responses.

5.3.1 Response Corridors

The model is validated for a lateral impact by comparing its response with the response corridors derived from human volunteer sled acceleration tests performed at the NBDL. These tests were previously analyzed by Wismans et al. [118] and recently by Thunnissen [104] using a two-pivot model similar as described in Section 3.2 for the frontal impacts. The lateral impacts were less severe than the frontal impacts; the peak sled acceleration was about $7g$ instead of $14g$. The volunteer responses were pooled and response corridors were defined at plus and minus one standard deviation of the average volunteer response. The average lateral (y) acceleration of vertebra T1 is used as input to the model to simulate the impact (Fig. 5.9); this acceleration is expressed in the laboratory coordinate system. The following corridors are used:

- The x, y, z-components of the linear acceleration of the head centre of gravity relative to the laboratory coordinate system.
- The lateral and axial angular acceleration of the head in the laboratory coordinate system (about the x- and z-axis).
- The trajectory of the centre of gravity and the occipital condyles of the head in the frontal plane (y, z) relative to the T1-anatomical coordinate system.
- The neck length: the linear distance between the occipital condyles and the origin of the T1-anatomical coordinate system.
- The lateral (ϕ_x) and axial (ϕ_z) rotation of the head in the T1-anatomical coordinate system.

The lateral rotation is defined as the rotation of the head-link of the two-pivot model (Fig. 3.6) in the frontal plane; for the detailed head-neck model, this is equal to the lateral rotation of the z-axis of the head local coordinate system when projected onto the frontal plane. Axial rotation is defined as the second rotation of a MADYMO flexion-torsion joint (between head and T1), in which the first rotation (bending) is
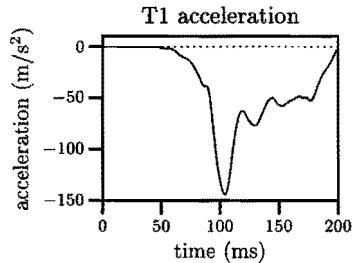
Figure 5.9: Lateral acceleration of vertebra T1 used to simulate the lateral impact.

the angle between the initial and momentaneous head z-axis and the second rotation (torsion) is the rotation about the head z-axis [119]. Bending transforms the z-axis directly from its initial to its momentaneous position and torsion moves the x-and y-axis into their momentaneous positions.

5.3.2 Validation

The lateral impact was simulated with the model using active and passive muscle behaviour. For the model with muscle contraction, only the muscles on the left side were activated to oppose the motion of the head and neck to the right. The model configurations are depicted in Figure 5.10, which shows that the lines of action of the muscle appear realistic for the active model, due to the moderate lateral bending of the neck, while they tend to become unrealistic for the passive model. The active response is compared with the response corridors first and then with the passive response.

Figure 5.11 shows the active response and the response corridors. All responses compare well with the corridors. The trajectories of the occipital condyles and centre of gravity follow the corridors adequately and exceed the corridors only slightly. The neck length, which differs somewhat initially, increases slightly for the model during the impact, while it decreases for the volunteers. The linear acceleration of the head centre of gravity agree well with the corridors, although the x- and y-acceleration increase a little too early, and the z-acceleration is smaller compared with the volunteers. The angular accelerations compare favourably with the volunteer responses, but, after 130 ms, the angular acceleration of the model hardly changes in contrast to the accelerations of the volunteers. The z-angular acceleration increases too soon, which is also reflected by the axial rotation of the head, causing it to lie outside the corridor. Even though the trends compare well, axial rotation becomes too large for the model eventually.

The lateral head rotation closely resembles the corridor. The lateral rotations of the intervertebral joints are shown in Figure 5.13. Most rotations are close to the *in vivo* ranges of motion as determined for static lateral bending, except for the lowest two joints, the rotations of which are much larger than the ranges of motion. Both upper cervical joints bend slightly to the left (less than 5 deg) compensating, in part, the large rotations of the lower joints to the right, which causes the cg-trajectory to resemble the corridors more closely than the oc-trajectory does.

Figure 5.12 compares the active and passive responses. Muscle contraction affects the head-neck motion strongly, which is also reflected by Figure 5.10, indicating that muscles are strong enough to significantly alter the head-neck response to impacts. Especially, the trajectories and the lateral head rotation are strongly improved due to muscle tensioning, but axial rotation becomes too large. When Figures 5.12 and 5.11 are compared, it follows that muscle tensioning causes most model responses to change sooner than the volunteer responses. Also, it appears that the model would have followed most corridors even better if the muscles would have been tensed less than maximally, noting that most passive responses appear to lie at the other side of the corridors in comparison with the active responses. If the upper torso had been included, the head would have contacted the right shoulder for the passive response limiting the lateral head rotation. Muscle tensioning leads to smaller lateral rotations for all joints, but the extension of the upper cervical joints were found to increase. The joints of which the (lateral) rotations are most strongly altered due to muscle tensioning are C7-T1, C1-C2 and C0-C1 (Fig. 5.13). The muscle forces even cause the latter two joints to bend slightly to the other (left) side.

80 ms   100 ms   120 ms   140 ms   160 ms   180 ms
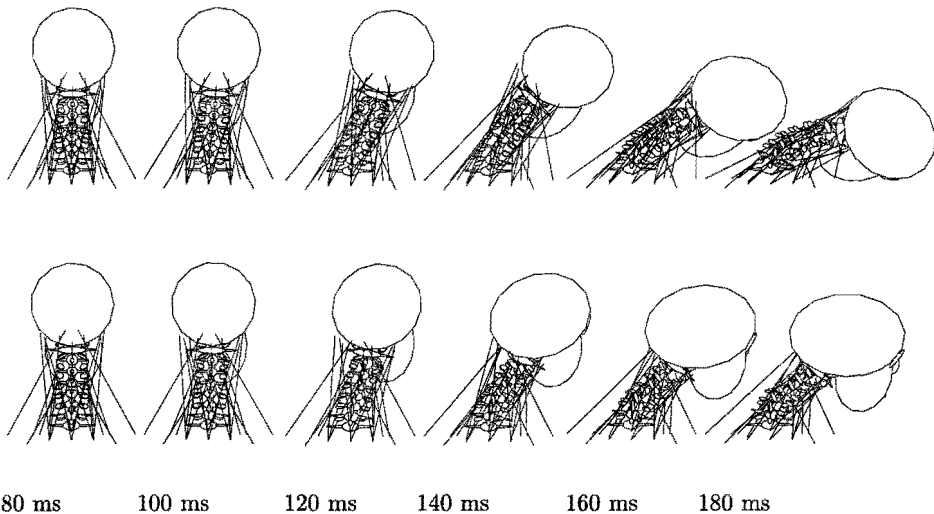
Figure 5.10: Configurations of model with passive (top) and active (bottom) muscle behaviour between 80 and 180 ms for the lateral impact.
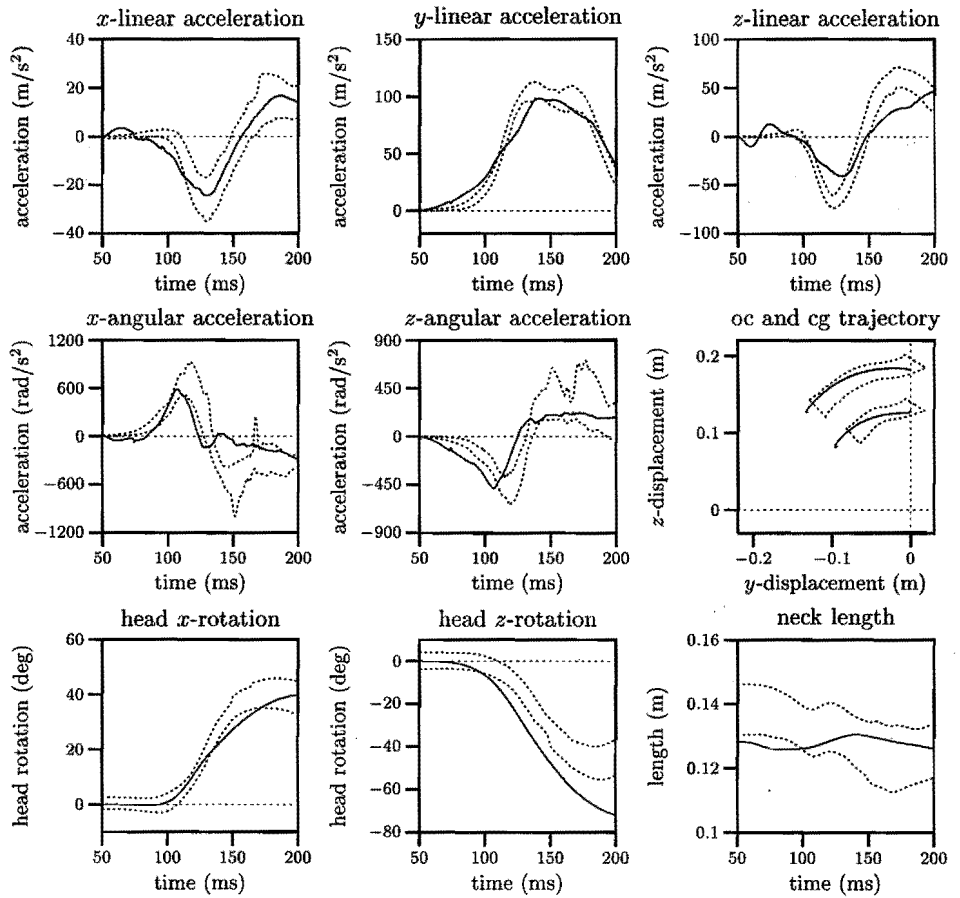
Figure 5.11: Response of the model with active muscle behaviour (solid line) and human volunteer response corridors (dotted lines) for the lateral impact.
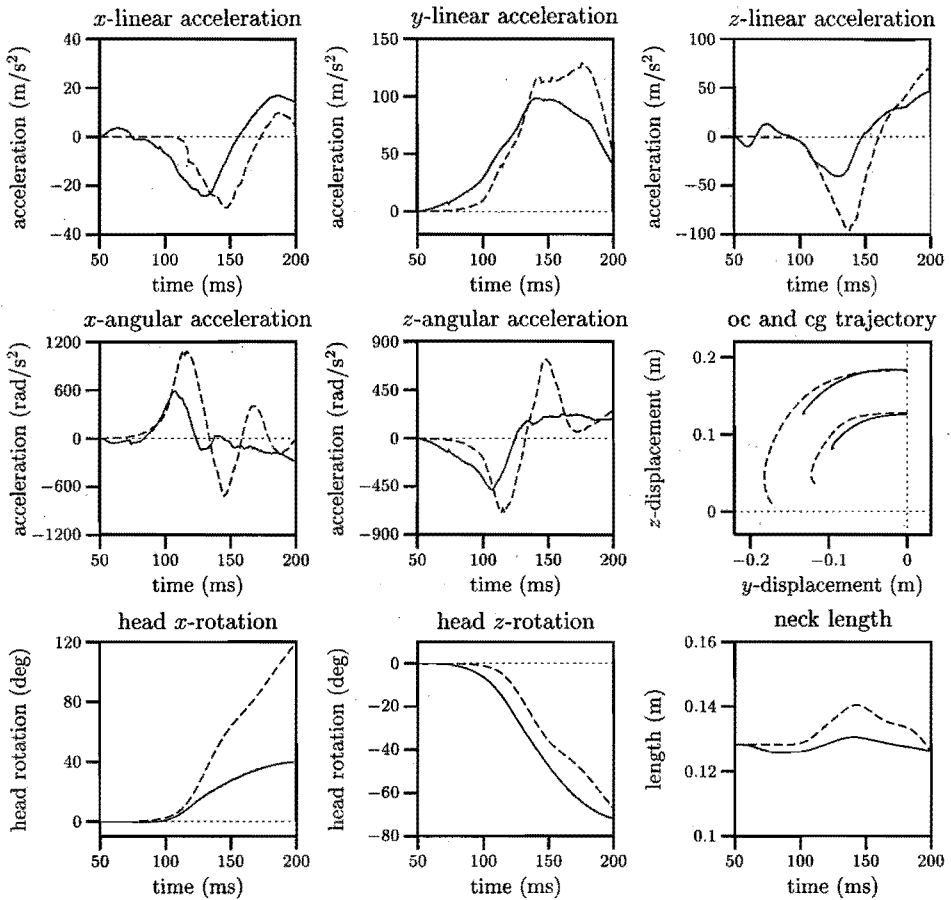
Figure 5.12: Response to lateral impact of the model with passive (dashed line) and active (solid line) muscle behaviour.
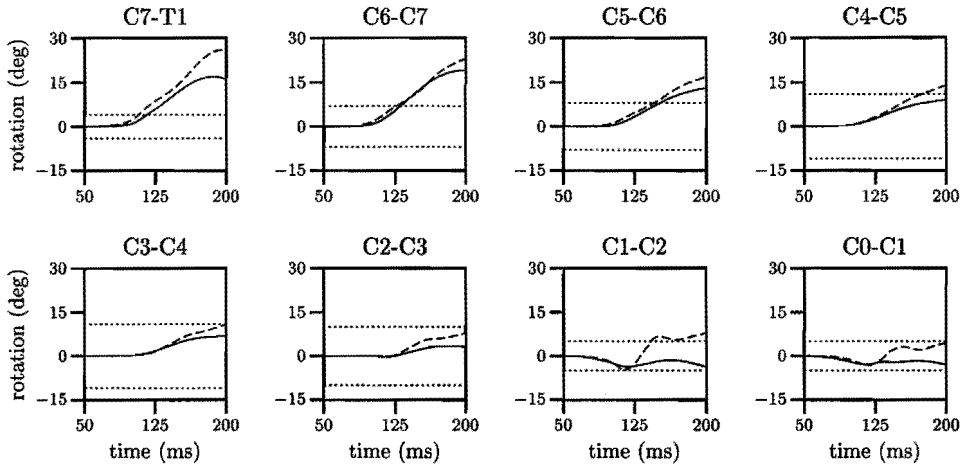
Figure 5.13: Lateral bending (ϕ_x) of the intervertebral joints for the active (solid line) and passive (dashed line) model with static *in vivo* ranges of motion (dotted lines, Table 2.1). Joint rotations were calculated as Bryant angles in the order x, y, z.

5.4 Soft Tissue Loads

The detailed model can provide the loads and deformations the individual tissues are subjected to in impacts. This section presents the tissue loads as they give insight into the contribution and function of each tissue in resisting the inertial loading. First, tissue loads are given for the frontal and lateral impact with active and passive muscle behaviour. Then, the tissue loads are compared with reported failure loads.

Frontal Impact   Figure 5.14 shows the maximum resulting tissue loads for the frontal impact. Only the first 150 ms were used, as after 150 ms the deformations of especially the lower joints become so large that the results may be unrealistic. Anteriorly, the discs carry most of the load, while the anterior and posterior longitudinal ligaments (ALL,PLL) are subjected to small loads. Posteriorly, the flaval ligaments (FL) are subjected to larger forces than the interspinous ligaments (ISL). For C7-T1, the forces in the disc and capsular ligaments (CL) are extremely large and unrealistic because of the large translation and rotation of C7 relative to T1; the capsular ligaments are stretched more than 100% due to the large separation of the facet joints of C7-T1. The large forces in the alar ligaments, the anterior membranes and the capsular ligaments of C0-C1 are caused by resisting the extension of the head relative to the neck (head lag).

The muscles compress the neck: muscle tensioning drastically increases the compressive forces carried by the facet joints (especially of the upper cervical spine) and the lower discs. Consequently, the forces in the anterior and posterior longitudinal ligaments and the capsular ligaments decrease. Muscle tensioning slightly increases the moments in the discs due to increased rotation. The loads exerted on the vertebrae by

the flaval and interspinous ligament change slightly through muscle tensioning: they decrease for C4-C5 and above and increase for C5-C6 and below. The forces of the upper cervical ligaments also change little, except for the posterior membranes (PM) which become unloaded due to the large extension of C0-C1-C2 (Fig. 5.7).

Lateral Impact   Figure 5.15 shows the maximum loads the tissues are subjected to during the first 150 ms of the lateral impact. Most of the maximum loads are smaller for the lateral than for the (more severe) frontal impact. Further, the midsagittal ligaments (ALL, PLL, FL, ISL) are subjected to smaller deformations in the lateral impact than in the frontal impact.

The muscles generate large compressive forces in the discs and facet joints and reduce the loads in the anterior and posterior longitudinal ligaments. The facets of the upper cervical spine are loaded at both sides indicating that the muscles effectively prevent right lateral bending of these joints; this is also reflected by the joint rotations (Fig. 5.13). The resultant bending moment in the discs are moderately affected by muscle tensioning as are their respective joint rotations. The forces in the flaval and interspinous ligament illustrate that flexion of C7-T1 is larger for the active response, while flexion of the other joints is smaller. The increased forces in the anterior membranes (AM) of C0-C1 and C1-C2 are due to the extension of both upper cervical joints which were much larger for the active response.

Muscle Forces   Figure 5.16 depicts the maximum forces of the (left) muscles for the active response to the frontal and lateral impact. Muscle forces are negligible (less than 5 N) for the passive response in both impacts, indicating that, for the model, the passive contribution of the muscles is insignificant in impacts. In general, the maximum muscle forces are larger for the lateral impact, most likely because the muscle lines of action are realistic for the lateral impact only. Most significantly, the scalenus muscles (especially the scalenus anterior) and the sternocleidomastoid are more effective in the lateral impact.

Tissue Loads versus Failure Loads   Tissue loads are compared with failure loads as a further check on the validity of the model: tissue loads should be tolerable, that is, below or only slightly above the failure loads, since the human volunteers were not injured in the sled impact tests. Thus, extreme loads indicate inaccuracies of the model. In addition, this comparison illustrates how the detailed model can be used eventually, to determine the possible occurrence of injuries in simulated impacts.

Few data were available for the failure loads of the tissues in dynamic loading conditions. Yoganandan et al. [127] pulled cervical anterior longitudinal and flaval ligaments to failure at various elongation rates. The average failure force increased from 127 N at 9 mm/s, via 173 N at 250 mm/s to 343 N at 2500 mm/sec, indicating that the dynamic failure force is maximally about $343/127 = 2.7$ times as large as the quasi-static failure force. Myklebust et al. [64] presented quasi-static failure forces (elongation rate: 10 mm/s) for the upper and lower cervical ligaments (see Tables 4.3
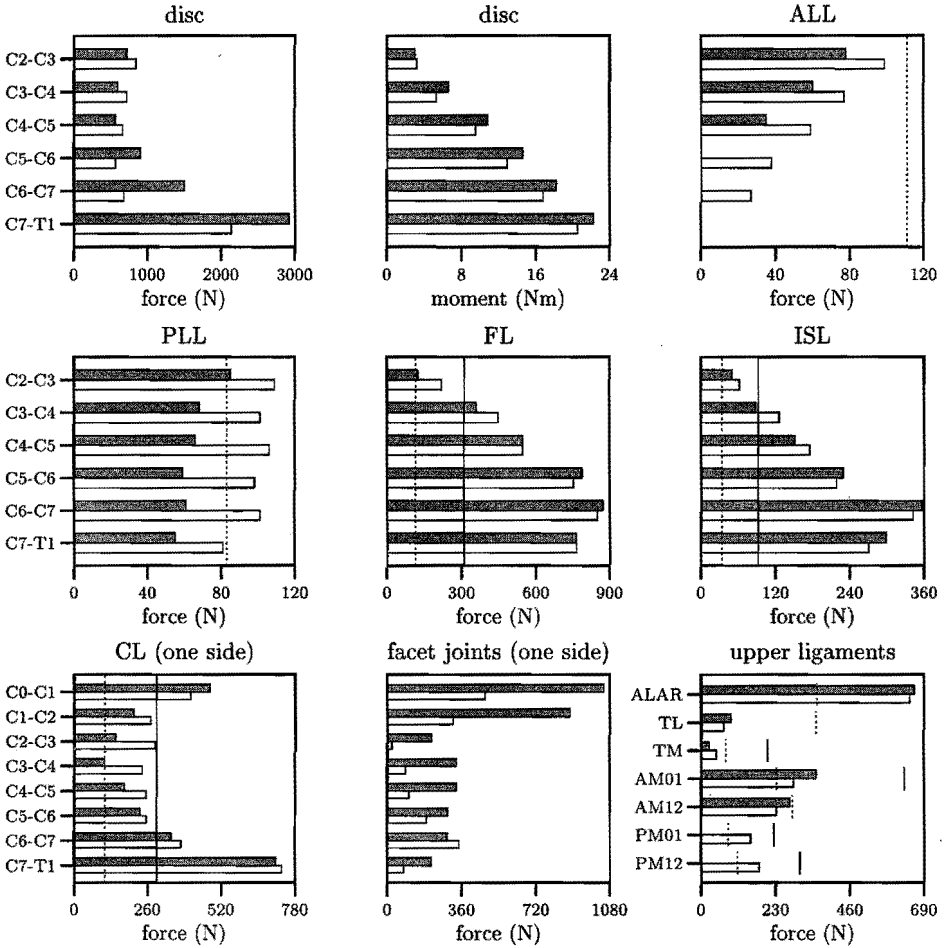
**Figure 5.14:** Maximum resulting loads in the tissues during the first 150 ms of the frontal impact for the model with (grey bars) and without (white bars) muscle activation. The vertical lines depict lower (dashed) and upper bounds (solid) for the failure forces of the ligaments (see text). ALL,PLL: anterior and posterior longitudinal ligament; FL: flaval ligament; ISL: interspinous ligament; CL: capsular ligament; ALAR: alar ligament; TL: transverse ligament; TM: tectorial membrane; AM,PM: anterior and posterior membrane of C0-C1 and C1-C2.

and 4.9). These failure forces and their assumed dynamic equivalents (factor 2.7) are included in Figures 5.14 and 5.15 as vertical lines to provide a lower and an upper bound indicating possible failure of the ligaments.

    For the frontal impact, the forces in most of the anteriorly located ligaments (ALL,PLL,AM,TL,TM) hardly exceed the lower bound, while the forces in the other
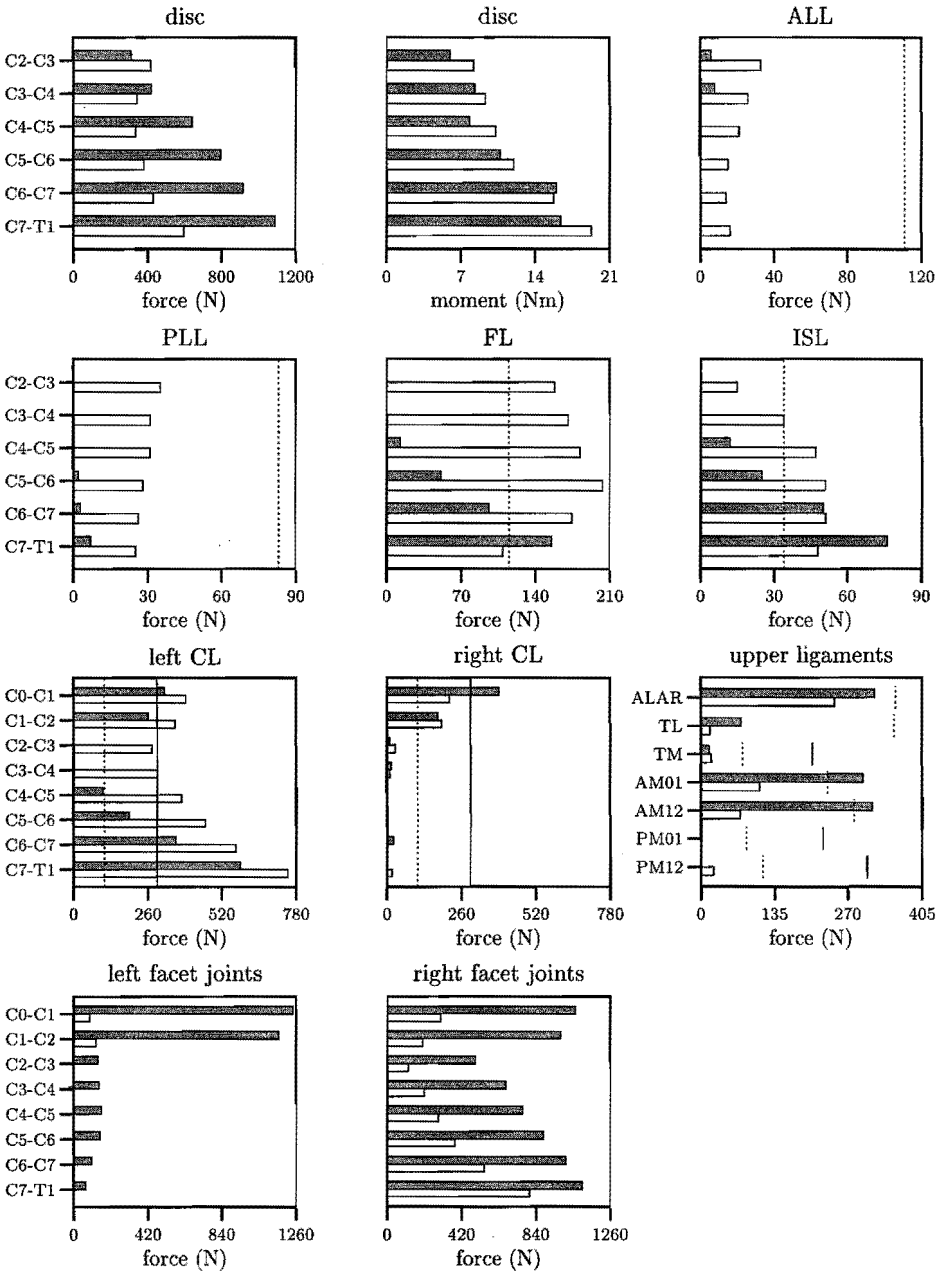
Figure 5.15: Maximum resulting loads in the tissues during the first 150 ms of the lateral impact for the model with (grey bars) and without (white bars) muscle activation. Legend: see Figure 5.14.
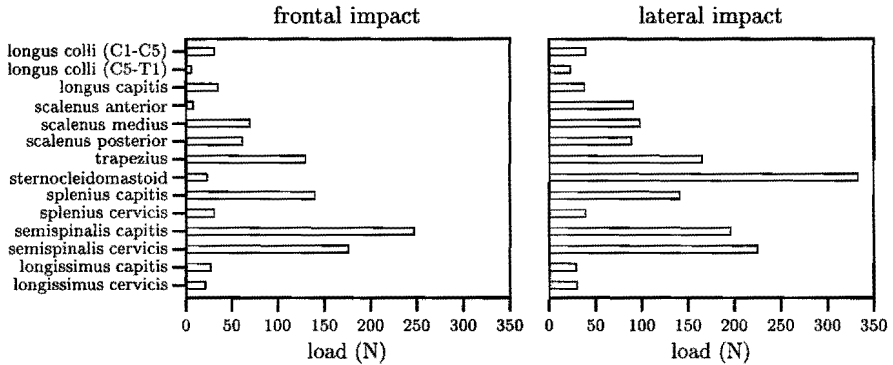
Figure 5.16: Maximum forces in left muscles for active response to frontal and lateral impact.

ligaments even exceed the upper bound, reflecting that the intervertebral rotations are indeed unrealistically large. For the lateral impact, most ligament forces are smaller and close, if not below, the lower bound. The forces in the left capsular ligaments are within reasonable vicinity of the upper bound, except for C7-T1.

Moroney et al. [61] (Section 2.4.1) found that static failure loads for disc segments averaged 3.5 Nm in flexion, 3.2 Nm in extension and 8.2 Nm in lateral bending. Cervical discs failed at 580 N in quasi-static tension, according to Pintar [83], and at 3140 N compression, 860 N tension and 5.0 Nm axial torsion, according to Yamada [125]. For combined or dynamic loading, no data were available.

In the frontal impact, the disc forces originated from compression and, to a lesser extent, anterior shear, while the disc moments were due to flexion alone. The resulting forces are smaller than the compressive failure force of 3140 N of Yamada, but the moments are much larger than the failure moment of 3.5 Nm of Moroney. Even if it is assumed that the dynamic failure moment is about three times the static failure moment, most disc moments are still too large, indicating (again) the unrealistically large joint rotations.

In the lateral impact, the disc forces stem from compression and lateral shear, which are mostly of comparable magnitude, and the disc moments were caused by combined lateral bending and axial torsion. The disc forces are much smaller than the compressive failure force of 3140 N (Yamada). The dynamic disc moments appear reasonable compared with the static failure moments of 8.2 Nm for lateral bending (Moroney) and 5.0 Nm for axial torsion (Yamada).

For the compressive failure loads of the bony articular facets, no data were available. Yamada reported that cervical vertebrae failed at 3100 N compression, so that the calculated facet joint loads appear to be tolerable.

5.5 Parametric Study for Frontal Impacts

A parametric study was performed with the detailed model analogous to the study done with the global model (Section 3.3). Eight parameters were selected to study their effect on the passive model response to frontal impacts, requiring an experimental design with 16 runs. Muscle contraction was not included, since muscle behaviour is not adequately represented in the model for frontal impacts.

Experimental Design Eight parameters were selected and, for each parameter, a high and a low level were arbitrarily chosen, such that their average equals the original value (Table 5.3). Amplification was chosen as it reflects the average deformation-rate sensitivity (stiffening) of the discs and ligaments in the model, and may, thus, have a strong influence on the model response. Damping coefficients of the tissues were included to evaluate their influence on the model response, because their values were not based on experimental data but arbitrarily chosen. The initial strain (or slack) of the ligaments was included, as it was found to be important to the response of motion segment models to static loading (Chapter 4). The mass and moment of inertia of the head were included for comparison with the parametric study of the global model.

Five discrete responses were chosen to characterize the model response comparable to what was done for the global model:

- R1, the maximum resultant linear acceleration of the head centre of gravity (first peak);
- R2, the maximum angular acceleration of the head;
- R3, the maximum neck rotation;
- R4, the head rotation at 175 ms, which was used instead of the maximum head rotation as that did not occur within 200 ms of the impact; and
- R5, the head rotation when the neck rotation equals 25 deg (head lag).

An experimental design with 16 runs (Appendix B) was used, which is sufficient to estimate the effect of a single parameter independently of other parameters and of two-parameter interactions. The centre response (with no parameter changed) was added to the design.

Results The responses R1–R4 for the 16 runs are shown in Figure 5.17 and tabulated in Appendix B. The ranges were 291–383 m/s^2 and 1168–2011 rad/s^2 for the maximum linear and angular acceleration, respectively, and 106–116 deg and 91–115 deg for the head and neck rotation, respectively (Fig 5.17). The timing of the maximum linear and angular accelerations was hardly influenced by the parameters as opposed to the timing of the maximum neck rotation.

Figure 5.18 depicts the average effects of the parameter changes on the model response. It shows that the centre response lies closely to the average response, except for the head lag, indicating that the effect of the parameters on the response is fairly linear for the chosen range of variation. Head rotation at 175 ms is hardly affected by any parameter, but this may reflect that the response measured at a fixed time is not

Table 5.3: Selected parameters, with range of variation and effect on model responses R1–R5.

| parameter		level −	+	unit	effect on response[a] R1	R2	R3	R4	R5
A	Amplification M	1.5	2.5	[−]	+	+	−	0	+
damping coefficients									
B	disc - translation b_t	700	1300	[Ns/m]	0	0	0	0	0
C	disc - rotation b_r	1.0	2.0	[Nms/rad]	0	−	0	0	+
D	ligament b_l	100	500	[Ns/m]	0	−	0	0	+
E	facet contact b_f	100	500	[Ns/m]	0	0	0	0	0
F	initial strain ligaments	−5%	+5%	[−]	0	0	0	0	+
G	head mass m	4.2	5.2	[kg]	0	0	0	0	0
H	head moment of inertia (I_{yy})	186	286	[kg·cm^2]	0	−	0	0	−

a   response with parameter at high level; difference with average response is
   0   less than 5%,
   −/+ a decrease/increase with more than 5%.

a good measure for the sensitivity of the model to parameter changes. The maximum angular acceleration and head lag are strongly influenced by several parameters (Table 5.3). The maximum linear acceleration and neck rotation are changed with more than 5% by the change in the amplification factor.

An increase of the amplification (parameter A) increases the maximum linear and angular acceleration and decreases the neck rotation. Variations in the translational damping of the intervertebral discs (B) have little effect on the response, whereas enlarged rotational damping of the intervertebral discs (C) strongly decreases the angular acceleration and reduces the head lag. Increased ligament damping (D) leads to smaller linear and angular accelerations and a smaller head lag. Damping of the facet contacts (E) has hardly any effect on the model responses. Larger initial strains of the
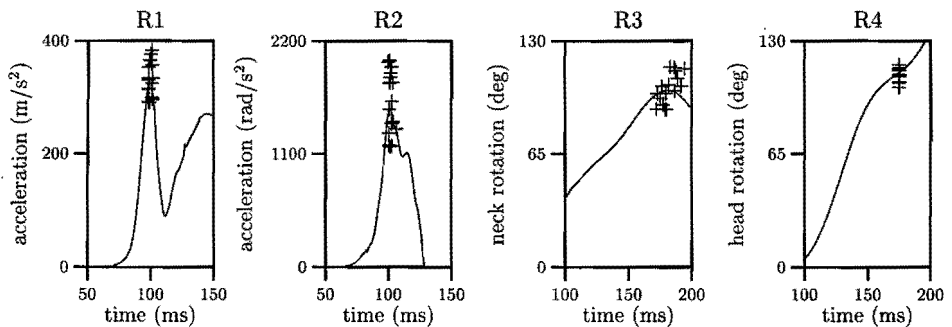
Figure 5.17: Centre response of the passive model (solid line) and discrete responses R1–R4 (+, Appendix B) of the 16 runs.
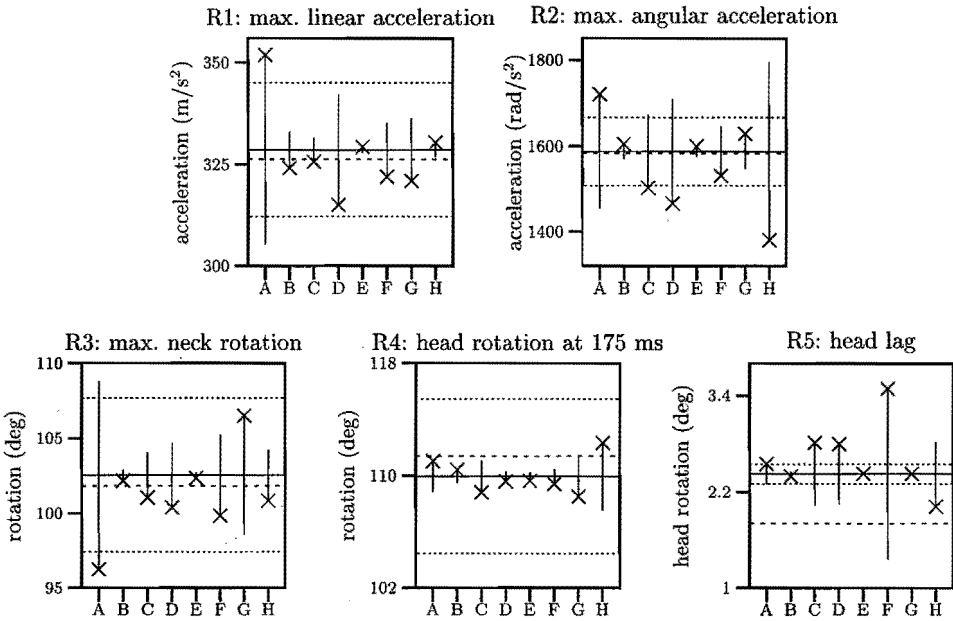
Figure 5.18: Average effect of parameters A–H on responses R1–R5. Solid horizontal line: average response of all 16 runs. Dashed line: centre response. Dotted lines: response boundaries at ±5% of average response. Solid vertical line: average effect of parameter on response. Cross (×): average response for all 8 runs in which the parameter was at its high level.

ligaments (F) moderately reduce the maximum accelerations and the neck rotation and strongly reduce the head lag. An increased head mass (G) slightly decreases the linear acceleration and enlarges the neck rotation. A larger moment of inertia of the head (H) reduces the angular acceleration strongly and the linear accelerations moderately, and increases the head lag. Head mass and moment of inertia have the same effect on the response of the detailed model as on the response of the global model, although the average effects differ in magnitude.

Of all two-parameter interactions, only the interactions AB and AE (and aliased interactions, see Appendix B) have an average effect of more than 5% on the head lag. The effect of two-parameter interactions is small or nil for all other responses.

5.6 Discussion

This chapter presented the detailed head-neck model, which was formed by joining the detailed models of the upper and lower cervical spine (presented in Chapter 4) and adding muscle elements. This final model comprises rigid vertebrae and head, which

are supported through frictionless, nonlinear viscoelastic facet joints and connected by linear viscoelastic intervertebral discs, nonlinear viscoelastic ligaments and contractile Hill-type muscle elements. The model provides the loads and deformations of the individual soft tissues making it suited to study injuries.

Validation   The model was validated for frontal and lateral impacts by simulating sled acceleration tests performed with human volunteers. The impacts were simulated using active and passive muscle behaviour.

For the frontal impact, the active model was too flexible compared with human volunteers. The linear and angular accelerations of the head agreed satisfactorily with the volunteer responses, but the deformation of the model was too large as shown by the trajectories of the occipital condyles and the centre of gravity of the head, and the rotations of the head and neck. Muscle tensioning influenced the model response, but did not significantly improve it. This was attributed to the representation of the muscles as straight lines: these lines of action become unrealistic for large rotations as the muscle elements do not follow the curvature of the neck. Consequently, the muscles cannot effectively oppose the motion of head and neck resulting in too large head and neck rotations. The intervertebral joint rotations showed that the large head and neck rotations were mainly caused by the extreme flexion of the lowest three joints which strongly exceeded the *in vivo* ranges of motion for flexion. Qualitatively, however, the joint deformations appeared accurate as reflected by their centres of rotation resembling the positions found for human volunteers performing slow flexion-extension movements. The centres of rotation for C2-C3 and, to a lesser extent, C3-C4 deviated strongly, due to the small rotations and large shear displacements of these joints.

For the lateral impact, the active model agreed excellently with the volunteers, while the passive model was too flexible. Thus, muscle tensioning strongly improved the response. For the active response, the joint rotations were moderate, such that the lines of action of the muscles remained realistic throughout the entire impact. The lateral joint rotations agreed well with the *in vivo* ranges of motion, except for C7-T1 and C6-C7, the rotations of which were too large.

Maximum tissue loads were determined for the frontal and lateral impact and compared with reported failure loads. For the frontal impact, the forces in especially the flaval, interspinous and capsular ligaments were much larger than the failure forces, illustrating that the joint rotations were too large. For the lateral impact, most tissue loads were well below the failure loads, indicating that the tissues are correctly incorporated into the model.

Muscle Representation   The geometrically simplified representation of the muscles seems to be the major limitation of the model. This representation cannot adequately account for the curving of the muscles around the vertebrae, which results in inaccurate muscle lines of action for large joint rotations, as was found for the frontal impact. The lateral impact illustrated that the muscles do influence (and improve) the model response significantly and that the muscle elements function adequately for moderate

joint rotations. An improved muscle model should allow for intermediate points that can be connected to the vertebrae and through which the muscle can slide to mimic the muscle-vertebra contact.

Another limitation is that the deep cervical muscles are not included. These many, short muscles usually run from one vertebra to an adjacent one and, among other things, act to stiffen the neck such that the head can be maintained in an upright position. To include these muscles, would greatly increase the complexity of the model. A possibility to represent the deep muscle activity needed to stabilize the neck is to increase the ligament forces by increasing the initial strain of the ligaments. Winters and Peles [115] used this approach in their *physical* head-neck model to improve the stability of that model. The parametric study showed that increased initial strains of the ligaments can be used for this approach, as it reduces the linear and angular accelerations and neck rotation of the model.

To activate the muscles, simply the active state of the muscles was prescribed for each muscle identically. This resulted in a strong extension of the head, because the extensors are stronger than the flexors. In the human volunteer, however, the muscles are activated such that head and neck remain upright. To incorporate this into the model, would require neural excitation of the muscles through a complex feedback control mechanism, which was beyond the primary interest of this study.

Tissue Characteristics The discs have linear load-displacement characteristics obtained for small loads, which may, in part, account for the large joint deformations. With nonlinear characteristics, the resistive force would increase more rapidly for larger deformations as tissue stiffness increases with deformation, resulting in smaller deformations needed to resist the applied load compared with the linear characteristics.

The sensitivity of tissue stiffness to deformation rate (stiffening) was explicitly included in the model through a constant amplification factor reflecting the average increase in stiffness for impacts. The parametric study revealed that this factor has a significant influence on the neck rotation and on the accelerations of the head. Unfortunately, it is difficult to determine the average stiffening for an impact. Reasonably, the factor ranges from 1 for (quasi)static loading, in which stiffening does not occur, to about 3 for (severe) dynamic impacts with large deformation rates [10, 24, 49, 127].

Damping coefficients were arbitrarily set in the model as adequate data were lacking. The parametric study showed that the model response is relatively insensitive to variations in the translational damping of the discs and the damping of the facet joints, but sensitive to the rotational damping of the discs and the damping of the ligaments. Future experimental and numerical studies should aim at deriving the latter coefficients.

Joint Rotations In both the frontal and the lateral impact, the rotations of the lowest joints, especially C6-C7 and C7-T1, exceeded the static *in vivo* ranges of motion. In dynamic impacts, it may well be possible that the ranges of motion are 1 to 2 deg larger, as is postulated by Melvin *et al.* [53], but the rotations are about 10 to 15

deg larger than the ranges of motion of 5 to 10 deg for these joints. Thus, these joint rotations are unrealistically large.

One explanation may be that the C6-C7 and C7-T1 joints are significantly stiffer than the other joints, as suggested by their smaller *in vivo* ranges of motion, although most experimental studies on motion segments failed to find significant differences in stiffness with vertebral level (Section 2.4.1). Shea *et al.* [97] even found that motion segments from the C2-C5 region were significantly stiffer in compression and extension than segments from the C5-T1 region. The failure loads and displacements of cervical ligaments reported by Myklebust *et al.* [64] indicate that the lower ligaments (C5-T1) are stiffer. In the model, discs and ligaments have the same stiffness at each vertebral level.

Another explanation may be the absence of the deep cervical muscles in the model, in addition to the inaccurate representation of the muscle lines of action (for the frontal impact only). The muscles may be strong enough to stiffen the segments sufficiently to prevent excessive joint rotations for the volunteers. It may be possible that muscles can more effectively increase the apparent stiffness of the lower joints than of the upper joints. This effect may be more pronounced at the junction of the thoracic and cervical spine due to additional thoracic muscles inserting on the lower cervical vertebrae.

Upper Cervical Spine   The large influence of the muscles on the rotations of the C0-C1-C2 joints and on the loads of the upper cervical tissues suggest that these joints may not be accurately modelled. Especially the large extension of C0-C1 caused by the extensors in the frontal impact, showed that the upper cervical spine is too flexible in extension, as was also shown for large static loads in Chapter 4. The omission of the suboccipital muscles seems important, as these muscles may lead to a significant increase in stiffness of the upper joints, but these muscles cannot limit extension of the upper cervical spine. Extension may be limited through the most anteriorly located neck muscles, which were not included in the model as their primary function is to move the jaw and not to control head-neck motion. Further, the facet joints have a more complex shape than can be modelled with the hyperellipsoids used here, but the effect that this simplified representation may have on the response could not be estimated.

In conclusion, a detailed mathematical model of the human head and neck was developed for acceleration impact studies. For frontal impacts, the model was too flexible because the muscles could not follow the curvature of the neck and, consequently, could not effectively oppose the head-neck motion. For lateral impacts, the model with active muscle behaviour showed excellent correspondence with human volunteers. As the lateral response is promising, it is expected that the response to frontal impacts can be improved with better muscle modelling. It is also expected that the present model is suitable for frontal impacts in which the neck rotation is limited, because a less severe impact is simulated, or because the head contacts an airbag or a head rest.

6

Conclusions and Recommendations
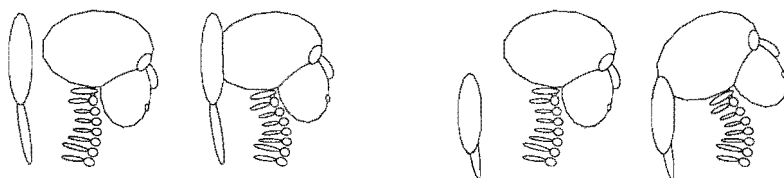
The research described in this thesis originated from the need to understand the mechanism of neck injuries in automotive accidents better. The rationale was that mathematical models are suited for this purpose, which resulted in the research objective to develop and validate a detailed three-dimensional mathematical model describing the dynamic behaviour of the human head and neck in accident situations in which no head contact occurs. The strategy was to proceed from a simple and comprehensible model (the global model), for gaining insight, to a complex model (the detailed model), suitable for assessing injury mechanisms. The global model will be particularly useful for car safety improvement and dummy neck development, whereas the detailed model will especially be useful to study injuries of the cervical spine, even though the validation of both models was only partly satisfactory. This chapter summarizes the major findings of this research. The global and the detailed model are compared with each other. Recommendations are given to improve the models and enhance their validation. Finally, possible applications are presented.

Global Head-Neck Model A relatively simple model with few anatomical details was developed first. This global model consists of rigid bodies for the head and vertebrae, which are connected through nonlinear viscoelastic intervertebral joints, representing the lumped mechanical behaviour of the intervertebral disc, ligaments, facet joints and muscles. The load-displacement characteristics of the joints were derived from reported mechanical behaviour of (motion) segments of the upper and lower cervical spine. The joints have scalable characteristics to account for the stiffening effect that muscle tensioning may have on intervertebral joint behaviour. Scaling allows also for calibration of the model response.

The model was calibrated to match the head-neck response of human volunteers subjected to frontal impacts, and a reasonable agreement between model and volunteers response could be obtained. The linear and angular accelerations of the head and the overall neck response agreed satisfactorily, but head rotation was too large, probably due to the absence of active muscle behaviour and to the large rotations of the lowest intervertebral joints. The model response was not calibrated for other impact directions, but this may be done in the same way as was done for the frontal impact.

Detailed Head-Neck Model The global model was enhanced to include more anatomical details. This detailed model comprises rigid head and vertebrae connected through intervertebral discs, facet joints, ligaments and muscles. The intervertebral discs are three-dimensional linear viscoelastic elements. The ligaments are nonlinear viscoelastic line elements resisting force in tension only, and the muscles are contractile Hill-type line elements describing both passive and active muscle behaviour. The facet joints are frictionless, nonlinear viscoelastic contact interactions between hyperellipsoids representing the articular facets of the vertebrae.

The model was validated for a frontal and a lateral impact by simulating sled acceleration tests performed with human volunteers. In the frontal impact, the linear and angular head accelerations agreed satisfactorily, but the head and neck rotations were too large compared with the volunteer responses. The model was too flexible, because the muscles could not curve around the vertebrae, such that their (straight) lines of action became unrealistic and the muscles failed to effectively constrain the head-neck motion and to stiffen the joints. The intervertebral rotations, especially of the lowest joints, were too large compared with the *in vivo* ranges of motion, indicating that the joints were too flexible. Qualitatively, joint kinematics was described reasonably well as reflected by the centres of rotations of the joints resembling those found for human volunteers performing slow flexion-extension movements. In the lateral impact, the model agreed excellently with the volunteers. The joint rotations were moderate, such that the muscle lines of action remained realistic and the muscles could effectively limit head-neck motion. The lateral rotations of the lowest joints were too large compared with the *in vivo* ranges of motion.

Comparison of Global and Detailed Model The main difference between the global and the detailed model is found for the head-neck rotation in response to the frontal

impact. For the human volunteers, head rotation initially lags behind neck rotation (head lag) and this is accurately reflected by both models. Then, head and neck move more or less as one unit (locking), such that head rotation does not exceed neck rotation. Locking is adequately simulated by the detailed model *with* muscle activation. For the global model, head rotation eventually exceeds neck rotation (overtipping) similarly as was found for the detailed model *without* muscle activation and for human cadavers. Even though neck muscles may not be strong enough to withstand the impact, they apparently cause locking of head and neck rotation. Thus, active muscle behaviour is essential to realistically describe the head-neck response to impacts.

Recommendations   To further improve the global and the detailed model, the following recommendations are given regarding possible enhancements of the models and additional experiments needed for better modelling and validation.

Experiments quantifying the mechanical characteristics of cervical (motion) segments are recommended to improve the joint characteristics of the global model and to enable enhanced validation of the segmental response of the detailed model. These experiments should address the following aspects: a) possible variations in segmental characteristics with vertebral level, b) viscoelastic characteristics due to dynamic loading, c) the influence of axial preload caused by muscle tensioning on segment behaviour, and d) the segmental response to combinations of loads to characterize the dependency of load-displacement behaviour in a single direction to displacements in other directions. Loading conditions used in these experiments should resemble the loads (in magnitude and in rate) as may be experienced in crashes and volunteer acceleration impacts.

Also recommended are experiments quantifying the nonlinear viscoelastic characteristics of cervical intervertebral discs and cervical spinal ligaments to improve the detailed model. Current publications give either linear characteristics or insufficient data to fully reproduce the nonlinear load-displacement curves, for example, by presenting only the stiffness of the most linear part of the curve, or only the load and displacement at failure of the specimens.

Probably the most important limitation of the detailed model is the muscle modelling, especially for impacts in which the intervertebral joint rotations are large. Currently, the muscles cannot follow the curvature of the neck, as they are modelled as straight line elements connecting origin to insertion. An improved muscle model would allow for intermediate sliding points through which the muscles can pass to simulate the curving of the muscle around the vertebrae. The use of these sliding points is presently only possible for passive spring elements (belt systems) in MADYMO. Another solution would be to divide a muscle in several smaller muscle elements, but then the forces in each muscle element are likely to differ due to differing elongations and elongation rates. Further, only the large superficial muscles were represented and the deep cervical muscles neglected.

Another limitation of the detailed model is the modelling of the articular facets through hyperellipsoids, which can only represent convex or almost flat surfaces with an elliptic or rectangular shape. This is sufficient for the facets of the lower cervical

spine, but insufficient for the facets of the upper cervical spine, which are concave and have a complex shape. In the next MADYMO version (5.2, spring 1996), rigid bodies can be given arbitrary surfaces and it is recommended to use these surfaces for the articular facets of, at least, the upper cervical spine.

A common factor in the global and the detailed model are the excessive rotations of the lowest cervical joints in comparison with the *in vivo* ranges of motion. Apparently, the lower joints are too flexible in both models. It is possible that the passive properties of (the tissues of) these joints are stiffer in reality, as is suggested by their *in vivo* ranges of motion, though *in vitro* studies fail to find significant differences with the other joints of the lower cervical spine. It is also possible that the deeper muscles originating form the (upper) torso and inserting on the lower cervical vertebrae generate forces large enough to limit the rotations of these joints. Both possibilities should be verified experimentally.

It is possible that the future availability of improved mechanical characteristics may necessitate the use of more advanced viscoelastic models than the ones currently used, to adequately represent the behaviour of the soft tissues. An example of such an advanced model is quasi-linear viscoelasticity [24], which can accurately describe the viscoelastic response of various biological tissues for cyclic loading, creep and relaxation [63, 62, 91, 123].

The global and detailed model should be validated for other impact directions and other impact severities. Sled acceleration tests have been reported with both human volunteers and human cadavers in frontal, lateral and frontal oblique directions and at various impact severities [6, 21, 118, 119]. Low-velocity rear-end impact tests have been performed with human volunteers using real cars [45, 46, 102] and sleds [70]. To simulate these tests, it may be necessary to include a geometrically realistic head or skull for obtaining a proper contact interaction between head and head-rest, or chin and torso. The cited references give sufficient information for, at least, a qualitative comparison of reported and simulated head-neck responses.

The kinematics of the vertebrae need to be quantified experimentally for dynamic impacts resembling the sled acceleration tests. Such data on vertebral motions would allow a more precise validation of the head-neck models for these impacts. A first, qualitative attempt was recently presented for low-velocity frontal, lateral and rear-end impacts with volunteers of which the cervical spine was monitored through cineradiography at 90 frames/s [44]. The results of that study may be useful to enhance the validation of the head-neck models.

A further validation of the mechanics of the detailed model may be realized through experiments performed with isolated cervical spine specimens (with or without skull), which provide at least sufficient data on the overall (load-displacement) response of the specimens [47, 63, 65, 66, 81, 84, 85, 128]. These experiments may also provide detailed information about the motion of the vertebrae as well as the occurrence of injuries and, thus, allow for a more detailed validation of the model than is possible with volunteer sled acceleration tests. The loading conditions, however, differ from those in acceleration impacts and most often resemble an (axial) impact to the head

as may occur in diving or when the head hits the windscreen in automotive accidents. Further, the passive *in vivo* response of the models in flexion, extension and lateral bending can be validated against the data of McGill *et al.* [50] who determined the bending stiffness of the neck of human volunteers with relaxed muscles.

Applications Both models can be used to predict the human head-neck response to various impact situations, which makes them useful for car safety improvement and dummy neck development. Unless more detailed information about the head-neck response is needed, the global model is preferable for these applications, because it is a computationally efficient model which can readily be modified to represent a taller or shorter neck, since few geometrical and inertial parameters characterize the model. The model is particularly useful in car safety design studies: it can be used in a model of a car occupant to study the effect of head rests, airbags and the car interior on the occupant's head-neck response in simulated crashes. Further model validation, however, is needed for contact situations and rear-end impacts.

The global model may be used to improve dummy necks: effects of changes in (a mathematical model of) the dummy neck on its response to impacts can be compared with the response of the global model to see whether the response of the dummy neck improves. This, of course, is especially relevant for impacts for which experimental data are lacking.

The detailed model is, in principle, useful for studying injury mechanisms because deformations and loads of the individual soft tissues can be assessed. The calculated loads and deformations can be used to formulate failure tolerances by reproducing experiments done with either motion segments or complete cervical spines and correlating the experimentally obtained injuries with the predicted tissue loads and deformations. Once appropriate tolerance levels for the tissue are known, injury mechanisms can be incorporated in the model such that the model will, eventually, be able to predict the probability of the occurrence of injuries in reconstructed accidents.

Appendix A

Geometric Construction of the Models

This appendix provides details about the geometric construction of the global model and the detailed models.

Configuration of Vertebrae C2-C7 The initial configuration of the lower cervical vertebrae was derived from Nissan and Gilad [67]. They determined the *in vivo* midsagittal dimensions of vertebrae C2-C7 and the intervertebral discs from lateral X-rays of the cervical spines of more than 130 healthy young males standing erect. They idealised the midsagittal outline of the vertebrae by a quadrangular box for the vertebral body to which a triangular arc with spinous process is attached (Fig. A.1). Intervertebral disc height was measured between the posterior and the anterior corners of adjacent vertebral bodies. Average values with standard deviations were reported for all dimensions $(a - h, k)$.

A few assumptions were introduced to reconstruct the vertebral configurations. First, it was assumed that the posterior height h of the intervertebral disc was measured perpendicular to the lower endplate a of the upper vertebra. Second, the geometric centre of the body was assumed to lie at the middle of diagonal k. Third, the origin $\mathcal{O}$ of the body local coordinate system was positioned at the geometric centre of the body; the coordinate system has its x-axis parallel to the lower endplate. Consequently, the orientation of a body relative to its lower adjacent body equals the relative orientation of adjacent lower endplates. Fourth, point CG for the centre of gravity lies at the posterior side of the vertebral body where the x-axis intersects line d. With these assumptions, the relative position and orientation of the vertebrae C2 through C7 and the position of their centres of gravity were determined using elementary trigonometry. The reconstructed configuration is shown in Figure A.1; the data are presented in Table 3.1.

Configuration of C0-C1-C2 The configuration of the upper cervical vertebrae were based on the data presented by Doherty and Heggeness [17] and Schaffler *et al.* [92]. Figure A.2 shows schematically the relative position of the origins $\mathcal{O}$ of the body local coordinate systems and the centres of gravity of the bodies C0, C1, and C2 as well
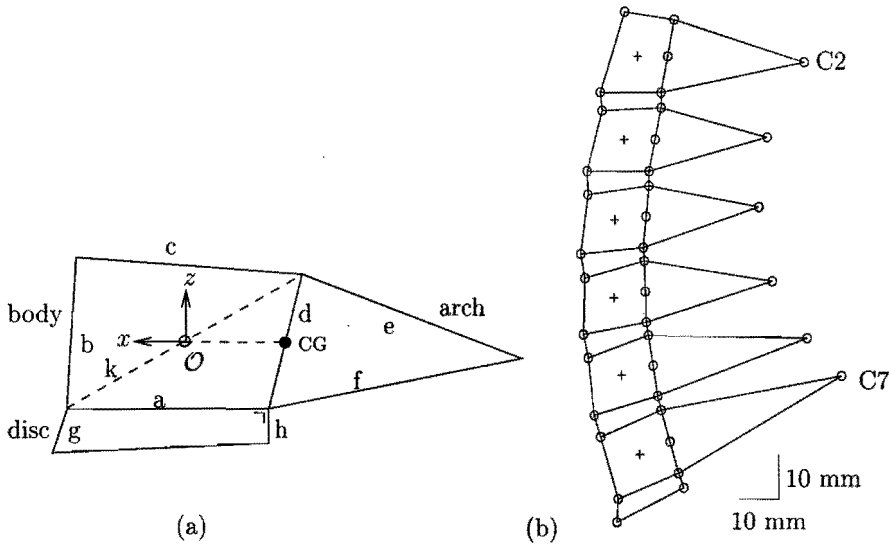
Figure A.1: (a) Reconstruction of vertebral geometry using the dimensions $(a-h, k)$ presented by Nissan and Gilad. (b) Reconstructed configuration of the lower cervical vertebrae C2-C7.

as the position of the occipital condyles. The coordinate system of C1 was positioned at the upper half of the dens as C1 has no body. Its origin lies 16.5 mm above the origin of the C2 coordinate system. The position of the cg of C1 was chosen similar to C2: 7.7 mm posterior to the origin. For C0, the coordinate system was positioned at the apparent centre of rotation of C0 relative to C1, which is located 12 mm above and 4 mm posterior to the occipital condyles, according to drawings by Van Mameren et al. [43] and Kapandji [38]. The bodies of C0, C1, and C2 were given the same orientation as the reference coordinate system. Thus, C0 is oriented such that the head looks forward. The cg of the head was given the position reported for the NBDL-volunteers (Thunnissen et al. [105]): it lies 23 mm anterior and 55 mm superior to the occipital condyles.

Configuration of C7-T1   The position of C7 relative to T1 was determined as follows. An approximate distance of 18 mm between the origins of the body local coordinate systems was estimated using the data of Nissan and Gilad for C7 and the C7-T1 disc, and the data of Panjabi et al. [80] for T1. The coordinates s_x and s_z for C7 followed from $s_x = l \sin \phi$ and $s_z = l \cos \phi$, with $\phi = 20.8$ deg the orientation of C7 relative to the T1-coordinate system. Note that the T1-coordinate system is not aligned with the endplate of T1.

Articular Facet Geometry   The articular facet surfaces are represented through hyperellipsoids which require the specification of the lengths of the semi-axes, the position
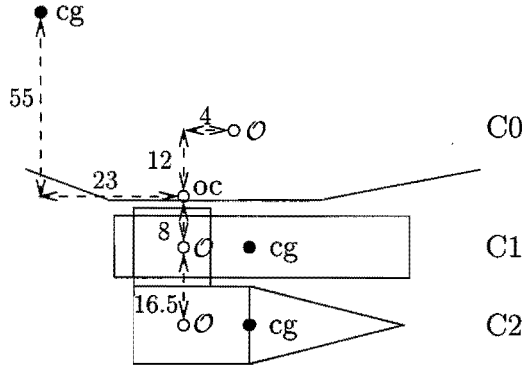
Figure A.2: Used configuration for the upper cervical spine. Origins ($\mathcal{O}$) and centres of gravity (•) for the rigid bodies representing C0, C1 and C2; oc is occipital condyles. Lengths in mm; drawing is not to scale.

of the centre and the orientation of the ellipsoids.

The anterior-posterior and lateral diameters of the ellipsoids were derived from Panjabi et al. [78], who measured the cervical articular facets by approximating their surfaces as ellipses. Facet thickness (the superior-inferior diameter) was set to 2 mm.

Panjabi et al. also presented the superior-inferior and lateral distances between the centres of the cervical facets of the same cervical vertebra for vertebrae C2 through C7, but they did not specify the facet positions with reference to the vertebra itself. To reconstruct the positions, it was assumed that: a) the middle of the superior-inferior distance lies at the same height as the geometric centre of the vertebral body, b) the lateral position of the left and right facets are the same because of midsagittal symmetry, and c) the facet centres lie posterior to the centre of gravity at a horizontal distance of half the anterior-posterior diameter of the facet surface (thus, $a = 0.5 \cdot c$ in Figure A.3).
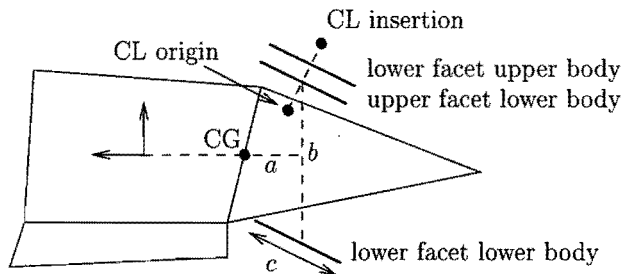

Figure A.3: Position of facet surfaces and capsular ligaments (CL).

The orientation of the facets were also derived from Panjabi *et al.* [78]. The orientations of adjacent vertebrae were averaged, including the relative orientation of the vertebrae, such that the facets are parallel to each other in the initial configuration of the model. The vertical position of the superior facets was adjusted slightly to have the facets in contact with each other in the initial configuration.

Position of Ligaments   The origins and insertions of the lower cervical ligaments were based on anatomical landmarks (Fig. A.4). The anterior and posterior longitudinal ligaments (ALL, PLL) were located where the x-axis intersects the anterior and posterior border of the vertebral body. Thus, the PLL originates at the same position where the centre of gravity is located. The interspinous ligament (ISL) connects adjacent spinous processes. The flaval ligament (FL) originates on the line connecting the centre of gravity to the spinous process, at a distance equal to the anterior-posterior diameter of the spinal canal (scd) as reported by Panjabi *et al.* [74]. The origins and insertions of the capsular ligaments (CL) were positioned at 2 mm from the centre of the facet ellipsoids and, in lateral view, perpendicular to the anterior-posterior axis of the ellipsoids (Fig.A.3). Thus, the CLs have an approximate length of 6 mm.

Position of Intervertebral Disc Centre   The centre of the intervertebral disc is quantified to enable the measurement of its translational deformations and to define the point at which the resulting intervertebral disc forces are applied to the vertebrae. The disc centre was assumed to lie right below the geometric centre of the upper vertebral body at a distance $h/2$ (half the posterior disc height, Fig. A.1) inferior to the lower endplate (Fig. A.4). Thus, the x, y-coordinates are zero for all discs; the z-coordinate equals $-9.8, -8.7, -8.3, -8.3, -8.6$ and -9.2 mm for C2-C3 down to C7-T1, respectively.

disc centre
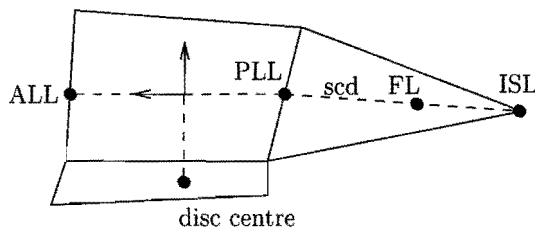
Figure A.4: Position of anterior and posterior longitudinal ligaments (ALL,PLL), flaval ligament (FL), interspinous ligament (ISL), and centre of intervertebral disc. scd is the anterior-posterior of the spinal canal.

Appendix B

Experimental Designs for Parametric Studies

This appendix presents the fractional factorial designs used in the parametric studies with the global head-neck model (Section 3.3), the detailed segment models (Sections 4.3 and 4.6) and the detailed head-neck model (Section 5.5).

32-Run Fractional Factorial for Global Model   For the global model, a fractional factorial design with 32 runs was chosen to study the effect of twelve parameters on five model responses (Table B.2). The columns A–E of the design follow from a full factorial for five parameters and, thus, contain all $2^5 = 32$ combinations of high and low levels of these parameters. The generators for the other columns are F=ABC, G=BDC, H=CDE, J=ACD, K=ADE, L=BDE, M=ABE; that is, column F follows from multiplication of the columns A, B and C, etcetera. This design allows the estimation of the effects of up to sixteen parameters independently of one another and of two-parameter interactions. Here, twelve parameters were used.

The estimated effects of parameters on the model response are average effects, because the exact effect of a change in a single parameter on the model response may depend on the level of the other parameters: the parameters interact. Thus, to obtain a realistic prediction of a single-parameter effect, not only its average effect needs to be known, but also the significant interactions of that parameter with the other parameters. In practice, only two-parameter interactions are relevant [59].

For the 32-run design in 12 parameters, it is not possible to give independent estimates of all 66 two-parameter interactions, since each two-parameter interaction is aliased with three or four other two-parameter interactions (Table B.1). For example, the AB-interaction can not be discriminated from the CF-interaction, because the

Table B.1: Aliases for the two-factor interactions of the 32-run design in Table B.2.

AB=CF=EM=GI=KL	AG=BI=DF=HM	AM=BE=DL=GH
AC=BF=DI=HK	AH=CK=EI=FL=GM	BD=CG=EL=FI=KM
AD=CI=EK=FG=LM	AI=BG=CD=EH	BH=CL=EG=FK=IM
AE=BM=DK=HI	AK=BL=CH=DE	CE=DH=FM=GL=IK
AF=BC=DG=HL	AL=BK=DM=FH	CM=EF=GK=IL

Table B.2: Levels of the parameters A–M and responses R1–R5 for each of the 32 runs.

run	A	B	C	D	E	F	G	H	I	K	L	M	R1 m/s^2	R2 rad/s^2	R3 deg	R4 deg	R5 deg
1	−	−	−	−	−	−	−	−	−	−	−	−	424	2279	70	105	9.2
2	+	−	−	−	−	+	−	−	+	+	−	+	369	1929	76	101	8.2
3	−	+	−	−	−	+	+	−	−	−	+	+	405	1761	62	104	6.5
4	+	+	−	−	−	−	+	−	+	+	+	−	356	1571	80	107	7.0
5	−	−	+	−	−	+	+	+	+	−	−	−	277	1860	68	96	12.6
6	+	−	+	−	−	−	+	+	−	+	−	+	323	2454	78	104	7.6
7	−	+	+	−	−	−	−	+	+	−	+	+	334	1920	64	101	9.5
8	+	+	+	−	−	+	−	+	−	+	+	−	266	1428	82	109	4.4
9	−	−	−	+	−	−	+	+	+	+	+	−	357	1793	74	106	9.5
10	+	−	−	+	−	+	+	+	−	−	+	+	379	1697	67	104	5.1
11	−	+	−	+	−	+	−	+	+	+	−	+	377	1822	70	102	12.2
12	+	+	−	+	−	−	+	−	−	−	−	−	389	2164	77	104	6.1
13	−	−	+	+	−	+	−	−	−	+	+	−	281	1480	76	107	6.3
14	+	−	+	+	−	−	−	−	+	−	+	+	349	1876	69	101	6.4
15	−	+	+	+	−	−	+	−	−	+	−	+	351	2522	74	103	9.7
16	+	+	+	+	−	+	+	−	+	−	−	−	287	1781	75	96	9.5
17	−	−	−	−	+	−	−	+	−	+	+	+	393	2408	88	137	6.0
18	+	−	−	−	+	+	−	+	+	−	+	−	356	1297	91	127	5.7
19	−	+	−	−	+	+	+	+	−	+	−	−	375	1342	96	133	8.2
20	+	+	−	−	+	−	+	+	+	−	−	+	370	2026	84	119	9.3
21	−	−	+	−	+	+	+	−	+	+	+	+	325	1414	87	130	9.0
22	+	−	+	−	+	−	+	−	−	−	+	−	294	1805	95	139	5.1
23	−	+	+	−	+	−	−	−	+	+	−	−	282	1872	94	131	11.6
24	+	+	+	−	+	+	−	−	−	−	−	+	353	1713	89	126	5.9
25	−	−	−	+	+	−	+	−	+	−	−	+	392	2024	80	118	11.7
26	+	−	−	+	+	+	+	−	−	+	−	−	376	1193	100	134	6.8
27	−	+	−	+	+	+	−	−	+	−	+	−	370	1353	86	125	8.5
28	+	+	−	+	+	−	−	−	−	+	+	+	384	2373	92	138	4.3
29	−	−	+	+	+	+	−	+	−	−	−	+	344	1609	85	125	7.9
30	+	−	+	+	+	−	−	+	+	+	−	−	267	1855	98	133	7.9
31	−	+	+	+	+	−	+	+	−	−	+	−	281	1943	91	137	6.3
32	+	+	+	+	+	+	+	+	+	+	+	+	304	1413	90	130	7.1
								average response					344	1812	82	117	7.9
								response at centre point					347	1561	85	118	7.2

columns AB (column A times column B) and CF are identical. A rule-of-thumb, however, is that at least one of the parameters has a single significant effect in a significant two-parameter interaction.

For the global head-neck model, the only significant two-parameter interaction was BD=CG=EL=FI=KM for the maximum head angular acceleration. Of these 5

Table B.3: Fractional factorial for 8 parameters in 16 runs.

run	A	B	C	D	E	F	G	H
			level of parameter					
1	−1	−1	−1	−1	−1	−1	−1	−1
2	1	−1	−1	−1	1	−1	1	1
3	−1	1	−1	−1	1	1	1	−1
4	1	1	−1	−1	−1	1	−1	1
5	−1	−1	1	−1	1	1	−1	1
6	1	−1	1	−1	−1	1	1	−1
7	−1	1	1	−1	−1	−1	1	1
8	1	1	1	−1	1	−1	−1	−1
9	−1	−1	−1	1	−1	1	1	1
10	1	−1	−1	1	1	1	−1	−1
11	−1	1	−1	1	1	−1	−1	1
12	1	1	−1	1	−1	−1	1	−1
13	−1	−1	1	1	1	−1	1	−1
14	1	−1	1	1	−1	−1	−1	1
15	−1	1	1	1	−1	1	−1	−1
16	1	1	1	1	1	1	1	1

interactions, FI and, to a lesser extent, EL are most likely to be significant while the others are probably insignificant as the main effects of these parameters are smaller than 5% of the average response.

16-Run Fractional Factorial for the Detailed Models The same 16-run design was used for the motion segment model, the upper cervical spine model and the detailed head-neck model. This design allows the effect of maximally eight parameters to be estimated independently of one another and of two-parameter interactions.

The design (Table B.3) followed from a full factorial in four parameters (columns A–D) augmented with E=ABC, F=BCD, G=ABD, H=ACD for the remaining four parameters. The two-parameter interactions are given in Table B.4. The responses for the detailed head-neck model are listed in Table B.5. (The responses for the detailed segment models are not given).

Table B.4: Aliases for the two-factor interactions of the 16-run design in Table B.3.

AB=CE=DG=FH	AF=BH=CG=DE	AC=BE=DH=FG	AG=BD=CF=EH
AD=BG=CH=EF	AH=BF=CD=EG	AE=BC=DF=GH	

Table B.5: Responses R1–R5 for each of the 16 runs for the detailed head-neck model.

run	response R1	R2	R3	R4	R5
	m/s^2	rad/s^2	deg	deg	deg
1	334	1948	115	109	0.9
2	383	1792	105	113	0.7
3	300	1890	115	106	2.7
4	366	1610	91	116	2.2
5	325	1179	101	111	2.7
6	357	1847	100	106	4.2
7	296	1395	114	111	1.1
8	377	2011	97	111	1.9
9	291	1168	109	111	3.0
10	331	1795	91	110	4.3
11	314	1183	104	114	0.9
12	334	1996	104	110	1.5
13	291	1531	113	103	2.2
14	353	1300	90	113	1.6
15	291	1342	100	106	4.9
16	315	1413	93	110	4.0
average response	329	1588	103	110	2.4
centre response	326	1583	102	111	1.8

Bibliography

[1] Allen Jr., B.L., R.L. Ferguson, T.R. Lehmann, and R.P. O'Brien. A mechanistic classification of closed, indirect fractures and dislocations of the lower cervical spine. *Spine*, 7:1–27, 1982.

[2] Amevo, B., D. Worth, and N. Bogduk. Instantaneous axes of rotation of the typical cervical motion segments: a study in normal volunteers. *Clinical Biomechanics*, 6:111–117, 1991.

[3] Association for the Advancement of Automotive Medicine. *The Abbreviated Injury Scale - 1990 revision*, Des Plaines, Illinois, USA, 1990.

[4] Backaitis, S.H., editor. *Biomechanics of impact injury and injury tolerances of the head-neck complex*. SAE Progress in Technology, PT 43. 1993.

[5] Barnsley, L., S. Lord, and N. Bogduk. Clinical review: whiplash injury. *Pain*, 58:283–307, 1994.

[6] Bendjellal, F., C. Tarrière, D. Gillet, P. Mack, and F. Guillon. Head and neck responses under high G-level lateral deceleration. In *Proceedings of the 31st Stapp Car Crash Conference*, 1987. SAE Paper No. 872196.

[7] Bogduk, N., B. Amevo, and M. Pearcy. A biological basis for instantaneous centres of rotation of the vertebral column. *Proceedings of the Institution of Mechanical Engineers, Part H: Journal of Engineering in Medicine*, 209:177–183, 1995.

[8] Bosio, A.C. and B.M. Bowman. Simulation of head-neck dynamic response in -Gx and +Gy. In *Proceedings of the 30th Stapp Car Crash Conference*, pp. 345–378, 1986. SAE Paper No. 861895.

[9] Bunketorp, O., B. Romanus, and P.O. Kroon. Head and neck injuries in traffic accidents in Göteborg in 1983. In *International Conference on the Biomechanics of Impacts*, pp. 1–15. IRCOBI, 1985.

[10] Chang, H., L.G. Gilbertson, V.K. Goel, J.M. Winterbottom, C.R. Clark, and A. Patwardhan. Dynamic response of the occipito-atlanto-axial (C0-C1-C2) complex in right axial rotation. *Journal of Orthopaedic Research*, 10:446–453, 1992.

[11] Chazal, J., A. Tanguy, M. Bourges, G. Gaurel, G. Escande, M. Guillot, and G. Vanneuville. Biomechanical properties of spinal ligaments and a histological study of the supraspinal ligament in traction. *Journal of Biomechanics*, 18:167–176, 1985.

[12] Dauvilliers, F., F. Bendjellal, M. Weiss, F. Lavaste, and C. Tarrière. Development of a finite element model of the neck. In *Proceedings of the 38th Stapp Car Crash Conference*, pp. 77–91, 1994. SAE Paper No. 942210.

[13] Deans, G.T., J.N. Magalliard, M. Kerr, and W.H. Rutherford. Neck sprain - a major cause of disability following car accidents. *Injury*, 18:10–12, 1987.

[14] Deng, Y.-C. *Human Head/Neck/Upper-Torso Model Response to Dynamic Loading*. Ph.D. thesis, University of California, 1985.

[15] Deng, Y.-C. and W. Goldsmith. Response of a human head/neck/upper-torso replica to dynamic loading - II. Analytical/numerical model. *Journal of Biomechanics*, 20:487–497, 1987.

[16] Deutscher, C. *Bewegungsablauf von Fahrzeuginsassen beim Heckaufprall. Ermittlung von objektiven Meßwerten zur Beurteilung von Verletzungsart und - schwere*. Ph.D. thesis, Technische Universität München, 1993.

[17] Doherty, B.J. and M.H. Heggeness. The quantitative anatomy of the atlas. *Spine*, 19:2497–2500, 1994.

[18] Doherty, B.J. and M.H. Heggeness. Quantitative anatomy of the second cervical vertebra. *Spine*, 20:513–517, 1995.

[19] Dvorak, J., M.M. Panjabi, J.E. Novotny, and J.A. Antinnes. In vivo flexion/extension of the normal cervical spine. *Journal of Orthopaedic Research*, 9:828–834, 1991.

[20] Dvorak, J., E. Schneider, P. Saldinger, and B. Rahn. Biomechanics of the craniocervical region: the alar and transverse ligaments. *Journal of Orthopaedic Research*, 6:452–461, 1988.

[21] Ewing, C.L. and D.J. Thomas. Human head and neck response to impact acceleration. Monograph 21 USAARL 73-1, Naval Aerospace and Regional Medical Centre, Pensacola, 1972.

[22] Faverjon, G., C. Henry, C. Thomas, C. Tarrière, A. Patel, C. Got, and F. Guillon. Head and neck injuries for belted front occupants involved in real frontal crashes: Patterns and risks. In *International Conference on the Biomechanics of Impacts*, pp. 301–317. IRCOBI, 1988.

[23] Foust, D.R., D.B. Chaffin, R.G. Snyder, and J.K. Baum. Cervical range of motion and dynamic response and strength of cervical muscles. In *Proceedings of the 17th Stapp Car Crash Conference*, pp. 285–308, 1973. SAE Paper No. 730975.

[24] Fung, Y.C. *Biomechanics: Mechanical Properties of Living Tissues*. Springer-Verlag, New York, 2nd edition, 1993.

[25] Goel, V.K., C.R. Clark, K. Gallaes, and Y.K. Liu. Moment-rotation relationships of the ligamentous occipito-atlanto-axial complex. *Journal of Biomechanics*, 21:673–680, 1988.

[26] Goel, V.K., C.R. Clark, K.G. Harris, and K.R. Schulte. Kinematics of the cervical spine: effects of multiple total laminectomy and facet wiring. *Journal of Orthopaedic Research*, 6:611–619, 1988.

[27] Goel, V.K., C.R. Clark, D. McGowan, and S. Goyal. An *in-vitro* study of the kinematics of the normal, injured and stabilized cervical spine. *Journal of Biomechanics*, 17:363–376, 1984.

[28] Gore, D.R., S.B. Sepic, and G.M. Gardner. Roentgenographic findings of the cervical spine in asymptomatic people. *Spine*, 11:521–524, 1986.

[29] Harris, J.H., B. Edeiken-Monroe, and D.R. Kopaniky. A practical classification of acute cervical spine injuries. *Orthopedic Clinics of North America*, 17:15–30, 1986.

[30] Harris, S. The real number of road traffic accident casualties in the Netherlands: a year-long survey. *Accident Analysis and Prevention*, 22:371–378, 1990.

[31] Huelke, D.F. Anatomy of the human cervical spine and associated structures. In *The Human Neck - Anatomy, Injury Mechanisms and Biomechanics*, pp. 1–7, 1979. SAE Special Publication SP-438, Paper No. 790130.

[32] Huelke, D.F. and G.S. Nusholtz. Cervical spine biomechanics: A review of the literature. *Journal of Orthopaedic Research*, 4:232–245, 1986.

[33] Huston, R.L., J.C. Huston, and M.W. Harlow. Comprehensive, three-dimensional head-neck model for impact and high-acceleration studies. *Aviation, Space, and Environmental Medicine*, 49:205–210, 1978.

[34] de Jager, M. Mathematical modelling of the human cervical spine: A survey of the literature. In *International Conference on the Biomechanics of Impacts*, pp. 213–227. IRCOBI, 1993.

[35] de Jager, M., A. Sauren, J. Thunnissen, and J. Wismans. A three-dimensional head-neck model: Validation for frontal and lateral impacts. In *Proceedings of the 38th Stapp Car Crash Conference*, pp. 93–109, 1994. SAE Paper No. 942211.

[36] Janevic, J., J.A. Ashton-Miller, and A.B. Schultz. Large compressive preloads decrease lumbar motion segment flexibility. *Journal of Orthopaedic Research*, 9:228–236, 1991.

[37] Jenkins, D.B. *Hollinhead's Functional Anatomy of the Limbs and Back*. W.B. Saunders Company, Philadelphia, sixth edition, 1991.

[38] Kapandji, I.A. *Bewegingsleer, Deel 3: De Romp en de Wervelkolom*. Stafleu Van Hoghum Houten, Houten/Antwerpen, 1984. (In Dutch) English Edition: The Physiology of the Joints, Volume 3: The Trunk and the Vertebral Column; Churchill Livingstone, Edinburg, 1974.

[39] Kazarian, L. Injuries to the human spinal column: Biomechanics and injury classification. *Exercise and Sport Science Reviews*, 9:297–352, 1982.

[40] Kleinberger, M. Application of finite element techniques to the study of cervical spine mechanics. In *Proceedings of the 37th Stapp Car Crash Conference*, pp. 261–272, 1993. SAE Paper No. 933131.

[41] Lövsund, P., Å. Nygren, B. Salen, and C. Tingvall. Neck injuries in rear end collisions among front and rear seat occupants. In *International Conference on the Biomechanics of Impacts*, pp. 319–325. IRCOBI, 1988.

[42] Maag, U., D. Desjardins, R. Bourbeau, and C. Laberge-Nadeau. Seat belts and neck injuries. In *International Conference on the Biomechanics of Impacts*, pp. 1–13. IRCOBI, 1990.

[43] van Mameren, H., H. Sanches, J. Beursgens, and J. Drukker. Cervical spine motion in the sagittal plane II: Position of segmental averaged instantaneous centers of rotation - a cineradiographic study. *Spine*, 17:467–474, 1992.

[44] Matsushita, T., T.B. Sato, K. Hirabayashi, S. Fujimura, T. Asazuma, and T. Takatori. X-ray study of the human neck motion due to head inertia loading. In *Proceedings of the 38th Stapp Car Crash Conference*, pp. 55–64, 1994. SAE Paper No. 942208.

[45] McConnell, W.E., R.P. Howard, H.M. Guzman, J.B. Bomar, J.H. Raddin, J.V. Benedict, H.L. Smith, and C.P. Hatsell. Analysis of human test subject kinematic responses to low velocity rear end impacts. In *Vehicle and Occupant Kinematics: Simulation and Modelling*, pp. 21–30, 1993. SAE Special Publication SP-975, Paper No. 930889.

[46] McConnell, W.E., R.P. Howard, J. Van Poppel, R. Krause, H.M. Guzman, J.B. Bomar, J.H. Raddin, J.V. Benedict, and C.P. Hatsell. Human head and neck kinematics after low velocity rear-end impacts – Understanding "whiplash". In *Proceedings of the 39th Stapp Car Crash Conference*, pp. 215–238, 1995. SAE Paper No. 952724.

[47] McElhaney, J.H., B.J. Doherty, J.G. Paver, B.S. Myers, and L. Gray. Combined bending and axial loading responses of the human cervical spine. In *Proceedings of the 32nd Stapp Car Crash Conference*, pp. 21–28, 1988. SAE Paper No. 881709.

[48] McElhaney, J.H. and B.S. Myers. Biomechanical aspects of cervical trauma. In *Accidental Injury: Biomechanics and Prevention*, edited by A.M. Nahum and J.W. Melvin, pp. 311–361. Springer-Verlag, 1993.

[49] McElhaney, J.H., J.G. Paver, H.J. McCrackin, and G.M. Maxwell. Cervical spine compression responses. In *Proceedings of the 27th Stapp Car Crash Conference*, pp. 163–177, 1983. SAE Paper No. 831615.

[50] McGill, S.M., K. Jones, G. Bennet, and P.J. Bishop. Passive stiffness of the human neck in flexion, extension, and lateral bending. *Clinical Biomechanics*, 9:193–198, 1994.

[51] McMinn, R.M.H., R.T. Hutchings, and B.M. Logan. *A Color Atlas of Head and Neck Anatomy*. Mosby-Wolfe Publishing, 2nd edition, 1994.

[52] Meertens, W. *Mathematical Modelling of the Upper Cervical Spine with MADYMO*. Master's thesis, Eindhoven University of Technology, Eindhoven, The Netherlands, 1995. Report WFW-95.108.

[53] Melvin, J.W., J.H. McElhaney, and V.L. Roberts. Improved neck simulation for anthropometric dummies. In *Proceedings of the 16th Stapp Car Crash Conference*, pp. 45–60, 1972. SAE Paper No. 720958.

[54] Merrill, T., W. Goldsmith, and Y.C. Deng. Three-dimensional response of a lumped parameter head-neck model due to impact and impulsive loading. *Journal of Biomechanics*, 17:81–95, 1984.

[55] Mertz, H.J. Anthropomorphic test devices. In *Accidental Injury: Biomechanics and Prevention*, edited by A.M. Nahum and J.W. Melvin, pp. 66–84. Springer-Verlag, 1993.

[56] Milne, N. The role of zygapophysial joint orientation and uncinate processes in controlling motion in the cervical spine. *Journal of Anatomy*, 178:189–201, 1991.

[57] Milne, N. Composite motion in cervical disc segments. *Clinical Biomechanics*, 8:193–202, 1993.

[58] Mommersteeg, T.J.A., L. Blankevoort, R. Huiskes, J.G.M. Kooloos, and J.M.G. Kauer. Characterization of the mechanical behavior of human knee ligaments: a numerical-experimental approach. *Journal of Biomechanics*, 29:151–160, 1996.

[59] Montgomery, D.C. *Design and Analysis of Experiments*. John Wiley & Sons, 2nd edition, 1984.

[60] Moroney, S.P., A.B. Schultz, and J.A.A. Miller. Analysis and measurement of neck loads. *Journal of Orthopaedic Research*, 6:713–720, 1988.

[61] Moroney, S.P., A.B. Schultz, J.A.A. Miller, and G.B.J. Andersson. Load-displacement properties of lower cervical spine motion segments. *Journal of Biomechanics*, 21:769–779, 1988.

[62] Myers, B.S., C.A. Van Ee, D.L.A. Camacho, C.T. Woolley, and T.M. Best. On the structural and material properties of mammalian skeletal muscle and its relevance to human cervical impact dynamics. In *Proceedings of the 39th Stapp Car Crash Conference*, pp. 203–214, 1995. SAE Paper No. 952723.

[63] Myers, B.S., J.H. McElhaney, and B.J. Doherty. The viscoelastic responses of the human cervical spine in torsion: Experimental limitations of quasi-linear theory, and a method for reducing these effects. *Journal of Biomechanics*, 24:811–818, 1991.

[64] Myklebust, J.B., F. Pintar, N. Yoganandan, J.F. Cusick, D. Maiman, T.J. Myers, and A. Sances Jr. Tensile strength of spinal ligaments. *Spine*, 13:526–531, 1988.

[65] Nightingale, R.W., B.J. Doherty, B.S. Myers, J.H. McElhaney, and W.J. Richardson. The influence of end condition on human cervical spine injury mechanisms. In *Proceedings of the 35th Stapp Car Crash Conference*, pp. 391–399, 1991. SAE Paper No. 912915.

[66] Nightingale, R.W., J.H. McElhaney, W.J. Richardson, and B.S. Myers. Dynamic responses of the head and cervical spine to axial impact loading. *Journal of Biomechanics*, pp. 307–318, 1996.

[67] Nissan, M. and I. Gilad. The cervical and lumbar vertebrae – anthropometric model. *Engineering in Medicine*, 13:111–114, 1984.

[68] Oda, T., M.M. Panjabi, J.J. Crisco III, H.U. Bueff, D. Grob, and J. Dvorak. Role of tectorial membrane in the stability of the upper cervical spine. *Clinical Biomechanics*, 7:201–207, 1992.

[69] Oda, T., M.M. Panjabi, and J.J. Crisco III. Three-dimensional translational movements of the upper cervical spine. *Journal of Spinal Disorders*, 4:411–419, 1991.

[70] Ono, K. and M. Kanno. Influences of the physical parameters on the risk to neck injuries in low impact speed rear-end collisions. In *International Conference on the Biomechanics of Impacts*, pp. 201–212. IRCOBI, 1993.

[71] Otte, D. and J.R. Rether. Risk and mechanisms of injuries to the cervical spine in traffic accidents. In *International Conference on the Biomechanics of Impacts*, pp. 17–31. IRCOBI, 1985.

[72] Panjabi, M., J. Dvorak, J. Duranceau, I. Yamamoto, M. Gerber, W. Rauschning, and H.U. Bueff. Three-dimensional movements of the upper cervical spine. *Spine*, 13:726–730, 1988.

[73] Panjabi, M., J. Dvorak, J.J. Crisco III, T. Oda, P. Wang, and D. Grob. Effects of alar ligament transection on upper cervical spine rotation. *Journal of Orthopaedic Research*, 9:584–593, 1991.

[74] Panjabi, M.M., J. Duranceau, V. Goel, T. Oxland, and K. Takata. Cervical human vertebrae: Quantitative three-dimensional anatomy of the middle and lower regions. *Spine*, 16:861–869, 1991.

[75] Panjabi, M.M., J. Dvorak, J.J. Crisco III, T. Oda, A. Hilibrand, and D. Grob. Flexion, extension, and lateral bending of the upper cervical spine in response to alar ligament transections. *Journal of Spinal Disorders*, 4:157–167, 1991.

[76] Panjabi, M.M., C. Lydon, A. Vasavada, D. Grob, J.J. Crisco III, and J. Dvorak. On the understanding of clinical instability. *Spine*, 19:2642–2650, 1994.

[77] Panjabi, M.M., T. Oda, J.J. Crisco III, J. Dvorak, and D. Grob. Posture affects motion coupling patterns of the upper cervical spine. *Journal of Orthopaedic Research*, 11:525–536, 1993.

[78] Panjabi, M.M., T. Oxland, K. Takata, V. Goel, J. Duranceau, and M. Krag. Articular facets of the human spine: quantitative three-dimensional anatomy. *Spine*, 18:1298–1310, 1993.

[79] Panjabi, M.M., D.J. Summers, R.R. Pelker, T. Videman, G.E. Friedlaender, and W.O. Southwick. Three-dimensional load-displacement curves due to forces on the cervical spine. *Journal of Orthopaedic Research*, 4:152–161, 1986.

[80] Panjabi, M.M., K. Takata, V. Goel, D. Frederico, T.Oxland, J. Duranceau, and M. Krag. Thoracic human vertebrae: quantitative three-dimensional anatomy. *Spine*, 16:888–901, 1991.

[81] Panjabi, M.M., A.A. White III, D. Keller, W.O. Southwick, and G. Friedlaender. Stability of the cervical spine under tension. *Journal of Biomechanics*, 11:189–197, 1978.

[82] Penning, L. Functional anatomy of joints and discs. In *The Cervical Spine*, edited by H.H. Sherk, E.J. Dunn, F.J. Eismont, J.W. Fielding, D.M. Long, K. Ono, L. Penning, and R. Raynor, pp. 33–56. J.B. Lippincott Company, Philadelphia, PA, 2nd edition, 1989.

[83] Pintar, F.A., J.B. Myklebust, A. Sances Jr., and N. Yoganandan. Biomechanical properties of the human intervertebral disk in tension. In *1986 Advances in Bioengineering*, pp. 38–39. American Society of Mechanical Engineers, 1986.

[84] Pintar, F.A., N. Yoganandan, A. Sances Jr., J. Reinartz, G. Harris, and S.J. Larson. Kinematic and anatomical analysis of the human cervical spinal column under axial loading. In *Proceedings of the 33rd Stapp Car Crash Conference*, pp. 191–214, 1989. SAE Paper No. 892436.

[85] Pintar, F.A., N. Yoganandan, L. Voo, J.F. Cusick, D.J. Maiman, and A. Sances, Jr. Dynamic characteristics of the human cervical spine. In *Proceedings of the 39th Stapp Car Crash Conference*, pp. 195–202, 1995. SAE Paper No. 952722.

[86] Platzer, W., editor. *Pernkopf Anatomy. Atlas of Topographic and Applied Human Anatomy*, volume 1: Head and Neck. Urban & Schwarzenberg Baltimore–Munich, 3rd edition, 1989.

[87] Quiring, D.P. *The Head, Neck, and Trunk. Muslces and Motor Points*. Lea & Febiger, Philadelphia, 1947.

[88] Reid, S.E., G. Raviv, and S.E. Reid, Jr. Neck muscle resistance to head impact. *Aviation, Space, and Environmental Medicine*, pp. 78–84, 1981.

[89] Roberson, R.E. and R. Schwertassek. *Dynamics of Multibody Systems*. Springer-Verlag, 1988.

[90] Sances Jr., A., J.B. Myklebust, D.J. Maiman, S.J. Larson, J.F. Cusick, and R.W. Jodat. The biomechanics of spinal injuries. *CRC Critical Reviews in Biomedical Engineering*, 11:1–76, 1984.

[91] Sauren, A.A.H.J., M.C. van Hout, A.A. van Steenhoven, F.E. Veldpaus, and J.D. Janssen. The mechanical properties of porcine aortic valve tissues. *Journal of Biomechanics*, 16:327–337, 1983.

[92] Schaffler, M.B., M.D. Alson, J.G. Heller, and S.R. Garfin. Morphology of the dens: A quantitative study. *Spine*, 17:738–743, 1992.

[93] Schneider, L.W., D.R. Foust, B.M. Bowman, R.G. Snyder, D.B. Chaffin, T.A. Abdelnour, and J.K. Baum. Biomechanical properties of the human neck in lateral flexion. In *Proceedings of the 19th Stapp Car Crash Conference*, pp. 455–485, 1975. SAE Paper No. 751156.

[94] Scott, M.W., W.E. McConnell, H.M. Guzman, R.P. Howard, J.B. Bomar, H.L. Smith, J.V. Benedict, J.H. Raddin, and C.P. Hatsell. Comparison of human and ATD head kinematics during low-speed rearend impacts. In *Human Surrogates: Design, Development & Side Impact Protection*, pp. 1–8, 1993. SAE Special Publication SP-945, Paper No. 930094.

[95] Seemann, M.R., W.H. Muzzy, and L.S. Lustick. Comparison of human and Hybrid III head and neck dynamic response. In *Proceedings of the 30th Stapp Car Crash Conference*, 1986. SAE Paper No. 861892.

[96] Seireg, A. and R.J. Arvikar. *Biomechanical Analysis of the Muscoloskeletal Structure for Medicine and Sports*. Hemisphere Publishing Corporation, New York, NY, 1989.

[97] Shea, M., W.T. Edwards, A.A. White, and W.C. Hayes. Variations of stiffness and strength along the human cervical spine. *Journal of Biomechanics*, 24:95–107; 689–690, 1991.

[98] Snijders, C.J., G.A. Hoek van Dijke, and E.R. Roosch. A biomechanical model for the analysis of the cervical spine in static postures. *Journal of Biomechanics*, 24:783–792, 1991.

[99] Spiegelman, J.J. and S. L.-Y. Woo. A rigid-body method for finding centers of rotation and angular displacements of planar joint motion. *Journal of Biomechanics*, 20:715–721, 1987.

[100] Spitzer, W.O., M.L. Skovron, L.R. Salmi, J.D. Cassidy, J. Duranceau, S. Suissa, and E. Zeiss. Scientific monograph of the Quebec task force on whiplash-associated disorders: redefining 'whiplash' and its management. *Spine*, 20(8S):S2–S73, 1995.

[101] Stearn, S. Sampling and weighting techniques for a large complex sample of accident data. In *International Conference on the Biomechanics of Impacts*, pp. 75–87. IRCOBI, 1988.

[102] Szabo, T.J., J.B. Welcher, R.D. Anderson, M.M. Rice, J.A. Ward, L.R. Paulo, and N.J. Carpenter. Human occupant kinematic response to low speed rear-end impacts. In *Occupant Containment and Methods of Assessing Occupant Protection in the Crash Environment*, 1994. SAE Special Publication SP-1045, Paper No. 940532.

[103] Tennyson, S.A., N.K. Mital, and A.I. King. Electromyographic signals of the spinal musculature during +Gz impact acceleration. *Orthopedic Clinics of North America*, 8:97–119, 1977.

[104] Thunnissen, J.G.M. Unpublished data, in preparation for submission to Journal of Biomechanics, 1996.

[105] Thunnissen, J.G.M., J.S.H.M. Wismans, C.L. Ewing, and D.J. Thomas. Human volunteer head-neck response in frontal flexion: a new analysis. In *Proceedings of the 39th Stapp Car Crash Conference*, pp. 439–460, 1995. SAE Paper No. 952721.

[106] Tien, C.S. and R.L. Huston. Biodynamic modeling of the head/neck system. In *Field Accidents Data Collection Analysis, Methodologies and Crash Injury Reconstruction*, pp. 359–364, 1985. SAE Special Publication P-159. Paper No. 850438.

[107] TNO Crash-Safety Research Centre, Delft, The Netherlands. *MADYMO User's Manual, Version 5.1*, 1994.

[108] Tominaga, T., C.A. Dickman, V.K.H. Sonntag, and S. Coons. Comparative anatomy of the baboon and the human cervical spine. *Spine*, 20:131–137, 1995.

[109] Walker Jr., L.B., E.H. Harris, and U.R. Pontius. Mass, volume, center of mass, and mass moment of inertia of head and head and neck of human body. In *Proceedings of the 17th Stapp Car Crash Conference*, pp. 525–537, 1973. SAE Paper No. 730985.

[110] White III, A.A. and M.M. Panjabi. *Clinical Biomechanics of the Spine*. J.B. Lippincott Company, 2nd edition, 1990.

[111] Wilke, H.-J., S. Wolf, L.E. Claes, M. Arand, and A. Wiesend. Stability increase of the lumbar spine with different muscle groups: a biomechanical *in vitro* study. *Spine*, 20:192–198, 1995.

[112] Williams, J.L. and T.B. Belytschko. A three-dimensional model of the human cervical spine for impact simulation. *Journal of Biomechanical Engineering*, 105:321–331, 1983.

[113] Winters, J. M. and L. Stark. Analysis of fundamental human movement patterns through the use of in-depth antagonistic muscle models. *IEEE Transactions on Biomedical Engineering*, BME-32:826–839, 1985.

[114] Winters, J.M. Hill-based muscle models: A systems engineering perspective. In *Multiple Muscle Systems: Biomechanics and Movement Organization*, edited by J.M. Winters and S.L-Y. Woo, pp. 69–93. Springer-Verlag, 1990.

[115] Winters, J.M. and J.D. Peles. Neck muscle activity and 3-D head kinematics during quasi-static and dynamic tracking movements. In *Multiple Muscle Systems: Biomechanics and Movement Organization*, edited by J.M. Winters and S.L-Y. Woo, pp. 461–480. Springer-Verlag, 1990.

[116] Winters, J.M. and L. Stark. Estimated mechanical properties of synergistic muscles involved in movements of a variety of human joints. *Journal of Biomechanics*, 21:1027–1041, 1988.

[117] Winters, J.M. and S.L-Y. Woo, editors. *Multiple Muscle Systems: Biomechanics and Movement Organization*. Springer-Verlag, 1990.

[118] Wismans, J., E. van Oorschot, and H.J. Woltring. Omni-directional human head-neck response. In *Proceedings of the 30th Stapp Car Crash Conference*, 1986. SAE Paper No. 861893.

[119] Wismans, J., M. Philippens, E. van Oorschot, D. Kallieris, and R. Mattern. Comparison of human volunteer and cadaver head-neck response in frontal flexion. In *Proceedings of the 31st Stapp Car Crash Conference*, 1987. SAE Paper No. 872194.

[120] Wismans, J.S.H.M., W.E.M. Bruijs, E.G. Janssen, M. Beusenberg, W.P. Koppens, and H.A. Lupker. *Injury Biomechanics*. Course Notes. Eindhoven University of Technology, Eindhoven, The Netherlands, 1993.

[121] Wismans, J.S.H.M. and C.G. Huijskens. Incidentie & preventie van het "whiplash" trauma (Incidence and prevention of the 'whiplash' trauma. In Dutch.). TNO-report 94.OR.BV.041.1/JW, TNO Road-Vehicles Research Institute, Delft, The Netherlands, 1994.

[122] Wittenburg, J. *Dynamics of Systems of Rigid Bodies*. Teubner, Stuttgart, 1977.

[123] Woo, S. L-Y., M.A. Gomez, and W.H. Akeson. The time and history-dependent viscoelastic properties of the canine medial collateral ligament. *Journal of Biomechanical Engineering*, 103:293–298, 1981.

[124] Xu, R., M.C. Nadaud, N.A. Ebraheim, and R.A. Yeasting. Morphology of the second cervical vertebra and the posterior projectioon of the C2 pedicle axis. *Spine*, 20:259–263, 1995.

[125] Yamada, H. *Strength of Biological Materials.* Williams and Wilkins, Baltimore, 1970. Editor: F.G. Evans.

[126] Yoganandan, N., J.B. Myklebust, G. Ray, and A. Sances Jr. Mathematical and finite element analysis of spine injuries. *CRC Critical Reviews in Biomedical Engineering*, 15:29–93, 1987.

[127] Yoganandan, N., F. Pintar, J. Butler, J. Reinartz, A. Sances Jr., and S.J. Larson. Dynamic response of human cervical spine ligaments. *Spine*, 14:1102–1110, 1989.

[128] Yoganandan, N., F.A. Pintar, P. Arnold, J. Reinartz, J.F. Cusick, D.J. Maiman, and A. Sances Jr. Continuous motion analysis of the head-neck complex under impact. *Journal of Spinal Disorders*, 7:420–428, 1994.

[129] Zajac, F.E. Muscle and tendon: properties, models, scaling, and application to biomechanics and motor control. *CRC Critical Reviews in Biomedical Engineering*, 17:359–411, 1989.

Whiplash op de computer: 50 botsingen per uur

een populair-wetenschappelijke samenvatting van het proefschrift
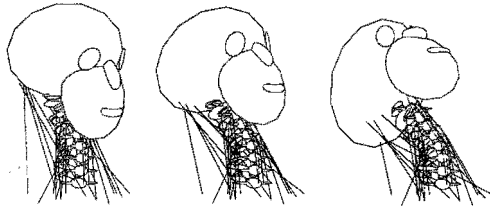
Whiplash is een letsel van de nek dat vaak tot langdurige klachten leidt. Meestal is whiplash het gevolg van een achteraanrijding, maar de precieze oorzaak van het letsel en van de bijbehorende klachten wordt nog slecht begrepen. Aan de Technische Universiteit Eindhoven is een computermodel gemaakt dat nabootst wat de nek bij een botsing te verduren krijgt. Dit model geeft inzicht in het ontstaan van nekletsel bij botsingen en helpt ontwerpers bij het ontwikkelen van veiliger auto's.

Achteraanrijdingen komen veel voor in files en voor verkeerslichten. Zo'n botsing kan al bij lage snelheden leiden tot nekletsel doordat hoofd en nek snel naar achter bewegen en daarna soms nog naar voren. Dit heen-en-weer slingeren wordt aangeduid met whiplash en werd lang gezien als de (enige) oorzaak van whiplash-letsel. Inmiddels is duidelijk dat het letsel ook kan volgen uit andere botsingen of bijvoorbeeld een ongelukkige val in huis of op het sportveld.

Whiplash leidt tot klachten als een pijnlijke stijve nek, hoofdpijn, vergeetachtigheid, duizeligheid en tintelingen in de vingers. Een groot probleem is dat deze klachten 'vaag' zijn: ze zijn moeilijk aan te tonen. Een arts vindt zelden beschadigingen in de nek, zelfs niet met de modernste hulpmiddelen zoals MRI (magnetic resonance imaging). Hierdoor wordt whiplash nog slecht begrepen en dat maakt het bepalen van een goede behandeling moeilijk.

Meer inzicht is dringend gewenst omdat whiplash ernstige sociale en financiële gevolgen kan hebben. Jaarlijks komen er in Nederland 15.000 tot 30.000 whiplash-slachtoffers bij door verkeersongevallen. Buitenlandse studies stellen dat de meeste patiënten in 2 tot 3 maanden genezen, maar dat eenderde deel klachten houdt die tot volledige arbeidsongeschiktheid kunnen leiden. Uitkeringen aan whiplash-patiënten

voor schadeloosstelling (genoegdoening) en arbeidsongeschiktheid zijn hoog en de laatste jaren sterk in aantal toegenomen. De totale maatschappelijke kosten ten gevolge van whiplash werden voor Nederland in 1994 geschat op ruim 600 miljoen gulden.

Computermodel
De nek — of halswervelkolom — bestaat uit zeven wervels (botten) die verbonden worden door diverse structuren opgebouwd uit zachte weefsels, zoals een tussenwervelschijf, bindweefselbanden en spieren. Al deze onderdelen kunnen schade oplopen. Het hoofd speelt hierbij de hoofdrol vanwege zijn grote 'gewicht' (ruim 4 kg voor een volwassen man): bij een botsing oefent het zware hoofd grote krachten uit op de beweeglijke nek en dat maakt de nek kwetsbaar.

Er zijn diverse mogelijkheden om meer over nekletsels te weten te komen, zoals patiëntenonderzoek, dierproeven en computersimulaties van botsingen. In samenwerking met de Rijksuniversiteit Limburg in Maastricht en TNO-Botsveiligheid in Delft, is aan de Technische Universiteit Eindhoven een computermodel van de menselijke nek gemaakt. Dit is een wiskundige beschrijving van de vorm en mechanische eigenschappen (sterkte, stijfheid e.d.) van de nek, waarmee de computer kan berekenen welke krachten er op de nek inwerken en welke bewegingen de nek maakt bij een botsing. Het model is gerealiseerd met het computerprogramma MADYMO van TNO dat speciaal geschikt is voor botsveiligheidsanalyses van voertuigen en inzittenden. Dit programma wordt door de meeste autofabrikanten gebruikt bij het ontwerpen van veiliger auto's zodat het model direct toepasbaar is voor de industrie.

In het onderzoek is ervoor gekozen eenvoudig te beginnen en later de complexiteit van het computermodel te vergroten. Omdat iedere nek anders is, is noodgedwongen een soort gemiddelde nek 'nagebouwd'. Eerst is een zeer eenvoudig model gemaakt dat bestaat uit zeven onvervormbare wervels waartussen een flexibele verbinding zit die het mechanische gedrag nabootst van de zachte weefsels van de nek. Dit model is voor te stellen als een opeenstapeling van zeven sjoelschijven verbonden door rubberen balkjes.

Botsproeven
Omdat het model een sterke vereenvoudiging van de werkelijkheid is, moet de betrouwbaarheid ervan getoetst worden. Daarvoor is gebruik gemaakt van botsproeven die tussen 1980 en 1985 in de Verenigde Staten zijn uitgevoerd. Met mannelijke vrijwilligers zijn bij lage, veilige snelheden botsproeven gedaan waarbij nauwkeurig de bewegingen van het hoofd en de nek zijn gemeten. Frontale botsingen van zo'n 35 km/u bleken voor deze mannen nog veilig te zijn, maar achteraanrijdingen zijn niet uitgevoerd omdat dit te gevaarlijk werd geacht. Dit geeft gelijk een beperking aan van de toetsmogelijkheden voor dergelijke modellen: botsproeven bij 100 km/u kunnen nu eenmaal niet met mensen gedaan worden. Het computermodel is getoetst door dezelfde frontale botsing van 35 km/u na te rekenen en de bewegingen van model en vrijwilligers te vergelijken: de bewegingen blijken redelijk goed overeen te komen.

Omdat het model eenvoudig is, kan de computer er snel mee rekenen. Het leent zich daardoor uitstekend voor toepassing in computermodellen van bijvoorbeeld een auto met chauffeur. Bij het ontwerpen van veilige auto's is het namelijk gewenst dat
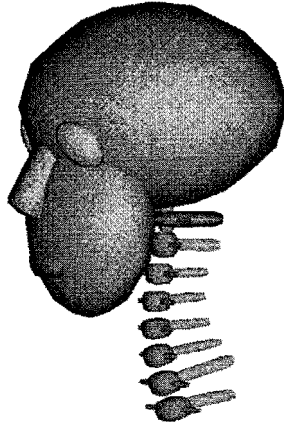
Schematische weergave van het eenvoudige computermodel van de menselijke nek.
Afgebeeld zijn de eerste borstwervel (onderaan), de zeven nekwervels en het hoofd.

de afzonderlijke onderdelen van zo'n samengesteld model eenvoudig zijn opdat de computer zo snel mogelijk kan rekenen. De ontwerper kan dan in korte tijd vele ontwerpvarianten laten doorrekenen om te bepalen welke airbag of hoofdsteun de passagier de meeste bescherming biedt bij botsingen. Dit gaat sneller en goedkoper dan met echte botsproeven in het laboratorium. Computermodellen vervangen zo een deel van het experimentele werk. Uiteindelijk hoeven nog slechts enkele experimenten uitgevoerd te worden om de computerberekeningen te bevestigen. Internationale regelementen eisen bovendien dat auto's aan diverse botsproeven moeten voldoen alvorens ze de weg op mogen.

80 ms   100 ms   120 ms   140 ms   160 ms   180 ms
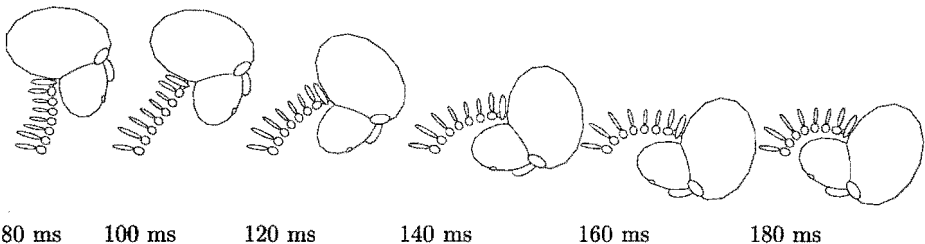
Computersimulatie van een frontale botsing van zo'n 35 km/u met het eenvoudige model.
Afgebeeld is de vorm van het model vanaf 80 milliseconden (ms) na de botsing in stapjes van 20 ms. De bewegingen van het model komen redelijk goed overeen met de bewegingen van vrijwilligers zoals die bij botsproeven gemeten zijn.

Gedetailleerd

Het eenvoudige model is ongeschikt om de precieze oorzaak van letsels te achterhalen. Daarvoor is het nodig dat de onderdelen van de nek die beschadigd kunnen worden als afzonderlijke elementen in het model zijn opgenomen. Pas dan kan de computer de krachten op en vervormingen van deze onderdelen berekenen en ze vergelijken met toelaatbare grenzen om te bepalen of letsel optreedt. Als tussenstap naar zo'n gedetailleerd nekmodel is eerst een model van een bewegingssegment van de nek gemaakt.

Een bewegingssegment is een stukje nek gevormd door twee wervels en alle tussenliggende weefsels. De nek kan gezien worden als een aaneenschakeling van bewegingssegmenten. Het gedrag van een enkel segment is karakteristiek voor de nek, net zoals het gedrag van twee schakels dat is voor een ketting. Vanwege die karakteristieke eigenschappen worden bewegingssegmenten veel gebruikt in experimenten waardoor er veel gegevens beschikbaar zijn om een model te maken en te toetsen. Het gedrag van het gemaakte model blijkt goed met de experimentele gegevens overeen te stemmen. Een aantal van deze modellen zijn daarna aaneengeschakeld tot een gedetailleerd model van de hele nek.

Dit gedetailleerde model bestaat uit wervels verbonden door tussenwervelschijven, bindweefselbanden, facetgewrichtjes en spieren. Facetgewrichtjes zijn kleine 'scharnieren' tussen de wervels waar de wervels met elkaar in contact komen. De sjoelschijven zijn nu uitgebreid met glijvlakjes voor de facetgewrichten en worden bijeengehouden door rubberen balkjes (tussenwervelschijven), elastiekjes (bindweefselbanden) en koorden die kunnen samentrekken (spieren). Dit model bevat alle onderdelen die van belang zijn voor een goede beschrijving van de beweging van hoofd en nek en behoort daar-
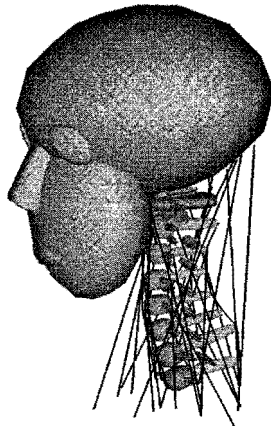

Schematische weergave van het gedetailleerde computermodel van de menselijke nek.
Afgebeeld zijn de eerste borstwervel (onderaan), de zeven nekwervels, het hoofd de
facetgewrichtjes, de bindweefselbanden en de spieren. De facetgewrichtjes lijken te zweven
maar zijn in het model vast verbonden met de wervels; deze verbinding is niet te zien.

mee tot de meest gedetailleerde hoofd-nekmodellen. Het heeft als voordeel dat het met een efficiënte (multibody) techniek ontwikkeld is, terwijl de andere modellen met een (eindige-elementen) techniek ontwikkeld zijn die veel meer rekentijd vergt, waardoor die modellen minder praktisch en duurder in gebruik zijn. Bovendien ontbreken bij die modellen de spieren.

Het gedetailleerde model is getoetst door een zijdelingse en een frontale botsing na te bootsen. Voor de zijdelingse botsing blijken de bewegingen van het model zeer goed overeen te stemmen met de hoofd-nekbewegingen van de vrijwilligers. Tevens blijven de krachten op de bindweefselbanden en tussenwervelschijven binnen veilige grenzen, wat moet aangezien de vrijwilligers geen letsel hebben opgelopen. Voor de frontale botsing komen de bewegingen redelijk overeen, maar hoofd en nek slaan te ver door: het model is te slap. Vanwege noodzakelijke vereenvoudigingen in de weergave van de spieren, blijken de spieren van model niet in staat de hoofd-nekbewegingen voldoende tegen te houden bij deze frontale botsing. Voor een verdere vervolmaking van het model moet hier aandacht aan besteed worden. Bij de zijdelingse botsing functioneren de spieren wel goed omdat de buiging van de nek niet te groot wordt. De verwachting is dat de spieren ook goed werken bij botsingen waarbij de voor/achterwaartse beweging van het hoofd beperkt wordt door een airbag of hoofdsteun.

| 80 ms | 100 ms | 120 ms | 140 ms | 160 ms | 180 ms |
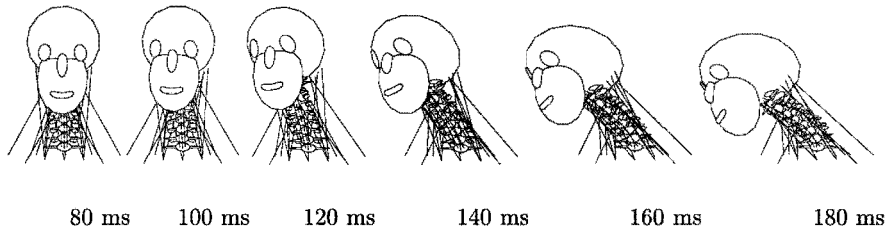
Computersimulatie van een zijdelingse botsing van zo'n 15 km/u met het gedetailleerde model. De bewegingen van het model lijken goed op de bewegingen van vrijwilligers zoals die bij botsproeven gemeten zijn.

Diagnose

Het gedetailleerde model kan, net als het eenvoudige model, gebruikt worden voor het veiliger maken van auto's. Het model geeft meer informatie maar rekent langer. Aan te raden is het model te gebruiken voor een nauwkeurige evaluatie van de meestbelovende ontwerpvarianten die eerder met het eenvoudige model gevonden zijn. Bovendien geeft het gedetailleerde model inzicht in het ontstaan van nekletsel omdat het nauwkeurig kan nagaan welke weefsels het zwaarst belast worden bij verschillende botsingen. Uiteindelijk kan deze kennis gebruikt worden bij het narekenen van een echt ongeluk om de arts te helpen bij de diagnose van nekklachten van (whiplash)patiënten. Omdat hiervoor aanvullend experimenteel onderzoek noodzakelijk is, wordt binnenkort een vervolgproject opgestart tussen de TU Eindhoven, Rijksuniversiteit Limburg en TNO.

Acknowledgements

I thank all who contributed to this thesis research. In particular: